NICKEL HYDROXY-CARBONATE PRECIPITATION IN A PELLET REACTOR

DAMIEN GUILLARD

Nickel hydroxy-carbonate precipitation in a pellet reactor

Damien Guillard

Environmental Processing Research Group
Department of Chemical Engineering
University of Cape Town
Rondebosch, 7700
South Africa

10th of July 2001

A thesis submitted for the degree of Master of Science at the University of Cape Town.

Acknowledgements

I wish to thank all the people who have contributed directly and indirectly to the good realisation of this project:

Dr. A.Lewis my supervisor for the time she spent on this project and her availability, and the advice she gave me to stay on the right track.

Pr G.Von Rosmalen and Dr.M. Seckler for their advice on the pellet reactor precipitating systems.

Pr D.Chalton for his "statistical contribution", and his precious help in analysing the experimental data.

Pr D.Lowenthal for his advice on aquatic chemistry and especially his precious knowledge on the carbonate system.

The member of the Green Group who understood my situation of foreign student and gave me the support I needed far from my home country.

Finally the financial support of the Environmental Processing research group is gratefully acknowledged.

Synopsis

Recently environmental release standards of waste streams have become much tighter, especially in the Mineral and Mining sector regarding the levels of metals and heavy metals of the effluent. Recovery of such metals from waste streams will become an environmental priority, coupled with an economic obligation when dealing with valuable metals. Metal recovery techniques are numerous, but the most widely used technique is precipitation, which covers a broad range of metals and is suitable for large flows.

Precipitation in pellet reactors was developed primarily for water softening purposes, and then extended in the Netherlands in a research context to heavy metal recovery from stream concentrations varying from 10 to 10 000ppm. The metals include copper, iron, lead, manganese, nickel and zinc. The potential for effluent treatment is broad and covers a range of mining industries metal-containing effluents.

The process using carbonate precipitation in a pellet reactor to recover nickel has several advantages over the more commonly used hydroxide sludge process. As a seeded precipitation, no sludge is formed, instead, there is a dense precipitate with good de-watering properties, permitting easy solid-liquid separation. The metal is easily recovered and can be reused by dissolving the pellets. No expensive and environmentally unfriendly disposal in waste landfill is needed. Furthermore, carbonate precipitation occurs at a lower pH than hydroxide precipitation, thus reducing post-neutralisation costs.

A laboratory scale fluidised bed was used for the purposes of this study in order to establish the mechanisms of nickel carbonate precipitation in such reactors using a synthetic nickel sulphate waste flow in concentration ranging from 50 to 150ppm of nickel. The study was structured around two main areas.

The first one was the study of precipitation processes occurring in the pellet reactor. Different profiles of the bed were established to determine the relative importance of various precipitation phenomena. The rapid kinetics of nickel carbonate nucleation were driven by high local supersaturation, the liquid-solid equilibrium being reached only a few seconds after mixing of the reactants. In general, the nickel removal efficiency was not only solubility dependant but largely influenced by fines nucleation, and thus by the supersaturation profile of the reactor. The nickel hydroxy-carbonate solubility model was established using literature based solubility constants, has therefore to be cautiously used for removal efficiency predictions. Agglomeration of the fines did not play an important role in the nickel removal efficiency of the reactor.

The second part of the study aimed at the minimisation of the total ($Ni_{tot\ out}$) and dissolved ($Ni_{dis\ out}$) nickel concentrations in the outlet stream of the pellet reactor taking five parameters into account. They were the pH (taken over a range between 9.5 and 10.5), the nickel concentration of the feed (between 50 and 150ppm), carbonate to nickel feed ratio (between 1 and 4), the number of carbonate feed inlets (between 1 and 3) and the re-circulation rate of the stream (between 0.66 to 1.66 of the waste stream flow rate). The experimental plan was designed using a Response Surface Methodology and the two different response surfaces were analysed with the SAS analytical package.

The results of the analyses showed that the most influential parameters were the pH, the nickel feed concentration and its ratio, while the re-circulation rate and the multiple inlet points were of secondary importance. The minor influence of the agglomeration on the nickel removal was again demonstrated.

The point of minimum response was a saddle point on each surface investigated, which means that no absolute minimum was found within the boundaries of the experimental surface. Further experiments are needed in order to isolate the process response minimum. In addition, the steepest descent analysis was blurred by an uncontrolled variability of the nickel outlet concentrations. 17.2% of the $Ni_{tot\ out}$ and 12.9% of the $Ni_{dis\ out}$ values were unpredicted by the second order model fitted to the data points with the five parameters as variables. The factors inducing variations in the response were the random experimental and analytical errors, the dynamic behaviour of the fluidised bed reactor, the lack of steady state conditions and the cyclical steady state behaviour of the pellet reactor. The temperature of the reaction did not significantly influence the responses in the range observed in the laboratory during the experiments. 4.3% of the variability observed in the $Ni_{tot\ out}$ response was due to fines formation mechanisms.

The $Ni_{tot\ out}$ response appears more relevant for industrial purposes, as the minimum occurred at lower pH than that for $Ni_{dis\ out}$, consequently reducing the amount of post neutralisation chemical needed. The fines concentration was also much lower around the predicted minimal $Ni_{tot\ out}$ response point thus avoiding problems associated with filtration of the effluent.

Contents

List of figures

List of tables

Nomenclature

a	= surface area of a solute entity in a cluster surface	(m^2)
a_i	= activity of ion i	$(mol.L^{-1})$
$a_{eq}I$	= activity of ion i at equilibrium	$(mol.L^{-1})$
A	= fluidised bed cross section	(m^2)
$\hat{A}$	= second order model matrix	(-)
B_0	= secondary nucleation rate	$(nuclei.m^{-3}.s^{-1})$
C_B	=	$(kmol.10^{-3})$
C_i	= actual concentration of ion i	$(mol.L^{-1})$
C^*_i	= equilibrium concentration of ion i	$(mol.L^{-1})$
C_T	= total concentration of carbonic species	$(mol.L^{-1})$
d	= particles diameter	(μm)
g	= gravity acceleration	$(m.s^{-2})$
g_f	= interfacial free energy	(J)
G	= growth rate	$(m.s^{-1})$
ΔG	= Gibbs free energy	(J)
ΔG^*	= critical Gibbs free energy	(J)
H	= depth of fluidised bed	(m)
$J(t)$	= nucleation rate	$(nuclei.m^{-3}.s^{-1})$
K_a	= shape factor related to the particle surface	(-)
K_s	= solubility constant	$(g.L^{-1})$
K_{sp}	= solubility constant of the nickel hydroxy carbonate	$(mol.L^{-1})$
K_v	= shape factor related to the particle volume	(-)
K_w	= water dissociation constant	$(10^{-14}g.L^{-1})$
$K_{1,2}$	= acidity constant of carbonic acid	(-)
L	= particle lenght	(m)

L_c	= length of cluster	(m)
L_{ij}	= average of the particle size	(m)
m_{pb}	= particle mass in the bed	(kg)
m_i	= i^{th} moment of the particle size distribution	(-)
m_p	= particle mass	(kg)
MF	= multiple feed inlet points of the reactor	(-)
M_T	= crystal mass of slurry	(kg)
N*	= critical number of particle in a critical cluster	(-)
N	= stirrer rotational rate	(rpm)
$Ni_{dis\ out}$	= dissolved nickel concentration in the outlet stream	(ppm)
Ni_{feed}	= nickel feed of the reactor	(ppm)
$Ni_{tot\ out}$	= total nickel concentration in the outlet stream	(ppm)
N_{sc}	= number of supercritical clusters	(-)
N(0)	= number of particles at time 0	(-)
N(t)	= number of particles at time t	(-)
ΔP	= pressure drop in the fluidised bed	(Pa)
r	= radius of cluster	(m)
r*	= critical radius of a cluster	(m)
R	= gas constant per mole	($8.31439 J.deg^{-1}.mol^{-1}$)
Ratio	= molar ratio carbonate to nickel feed to the reactor	(-)
RF	= re-circulation flow	($L.min^{-1}$)
RR	= re-circulation ratio	(-)
t	= time	(s)
t_i	= induction time	(s)
T	= temperature	($^{\circ}K$)
V_{absp}	= absolute volume of particle	(m^3)
V_b	= volume of the bed	(m^3)
V_{hp}	= hydrodynamic volume of particle	(m^3)
V_m	= molecular volume	($m^3.mol^{-1}$)
WF	= waste water flow	($L.min^{-1}$)
X_1	= pH coded value for RSM purpose	(-)
X_2	= Ratio carbonate to nickel coded value for RSM purpose	(-)
X_3	= RR re-circulation ratio coded value for RSM purpose	(-)

X_4	= MF multiple feed points coded value for RSM purpose	(-)
X_5	= Ni_{feed} coded value for RSM purpose	(-)
X_6	= temperature coded value for RSM purpose	(-)
y	= first order model response function	(ppm)
y_f	= average response of the 2^k factorial design runs	(-)
y_c	= average response of the 2^k factorial design centre points	(-)

β	= saturation ratio	(-)
β_t	= coefficients for the 1st and 2nd order models	(-)
β_{agg}	= overall agglomeration rate	($m^3.s^{-1}$)
β_{coll}	= collision rate	($col.s^{-1}$)
ε	= power input	(w)
ε_s	= statistical error on the first order model	(ppm)
ε_b	= voidage of the particles bed (porosity)	(-)
ε_{mf}	= voidage of the fluidisation onset	(-)
Φ	= wetting angle of the particle	(rad)
γ	= activity coefficient	(-)
Γ	= shear rate	(s^{-1})
η	= true response function of the first order model	(-)
φ	= fines concentration	(%)
φ_0	= $kv.N.L^3$	(-)
λ	= eigenvectors coefficients	(-)
μ	= ionic force	($J.kmol^{-1}$)
μ_f	= fluid viscosity	($Ns.m^{-2}$)
ρ_{abs}	= particles absolute density	($kg.m^{-3}$)
ρ_b	= bed density	($kg.m^{-3}$)
ρ_f	= fluid density	($kg.m^{-3}$)
ρ_p	= particles density	($kg.m^{-3}$)
σ	= relative supersaturation	(-)
ξ_i	= natural variables used for the first order model	(-)
ψ	= efficiency factor	(-)

(ion)	= "ion" activity	($mol.L^{-1}$)
[ion]	= "ion" concentration	($mol.L^{-1}$)

Chapter I

Introduction

1.1 Background

The concept of sustainable development has recently achieved prominence by the realisation that human development and biophysical environment needs are interdependently connected. A full integration of the natural, economic and social needs would induce a "development that meets the present generation's needs in an equitable way without compromising that of future generations to meet their own needs" (World Commission of Environment and Development, 1987). Environmental concerns are today placed on the same level as economic priorities and social well being and different industrial sectors publish health and environmental reports, which highlight their progress and "green" attitude towards the environment.

The Mineral and Mining sector has played a major role in the social, economic and infrastructural development of the Southern Africa but is still commonly seen as a heavily polluting industry, because of its history of release of massive quantities of pollutants. As environmental standards and economic constraints become tighter, this industry is placing greater emphasis on treating pollution containing effluents, with particular attention on the recovery of metals and heavy metals from effluent streams.

Several techniques have been developed to recover metals, such as evaporation, ion exchange, cementation, reverse osmosis and electrolysis (McAnally and Benefield, 1984). The most commonly used process is precipitation (Mishra, 1999) as it offers a cost-effective solution applicable to large operating units. For metals and heavy metals such as zinc, copper, manganese, lead and nickel, hydroxide precipitation is generally used for large scale plants, although it has many environmental drawbacks and is not always cost-effective.

Considerable effort is being expended to develop more efficient precipitation processes. The development of heavy metal precipitation in pellet reactors is one proposed method to improve metal recovery at lower cost. Pellet reactors are fluidised bed reactors where the product is obtained on the fluidised particles. This pellet reactor technology has been developed for softening of drinking water (Schöller et al, 1987) as well as for removal of phosphates from waste water (Seckler, 1994). Recently, this technique has been extended to the removal of heavy metals (Wilms, 1988; Zhou *et al*, 1999) using carbonate as a precipitating agent. The treated concentration ranges from 10 to 100 000ppm of metal from various waste streams such as acid mine drainage, rinsing, plating and drag-out effluents, and thus finds a direct application in the mining industry.

1.2 Waste effluent composition and treatment

Effluents containing heavy metals originate from mining and industrial wastes. Acid Mine Drainage (AMD) is a common metal-containing stream in South Africa due to the extensive mining activity in the country. Runoff from waste piles or working shafts is usually the origin of AMD, which forms when sulfide minerals in rocks are exposed to oxidizing conditions. Iron sulfides, pyrite and marcasite are the predominant AMD producers.

Table 1.1 details various world-wide AMD compositions. Other possible origins for the waste streams are base metal refining effluents and metal finishing effluents. These streams contain the process metals as well as other impurities (see Table 1.2).

	Concentration (mg/L)			
Location	*South Africa*	*USA*	*Ireland*	*Norway*
	Grootvlei	*Anaconda Copper*	*Avoca*	*Wallenberg*
pH	6.25	2.5	2.7	5.52
SO_4^{2-}	1383	3510	10579	2940
Fe_T	187	300	1031	139
Zn		155	362	34
Cu		29	243	2
Ni	3			
Al		125		1
Mn	5	88		14
Mg		225		350

Table 1.1: AMD composition (Moosa, 2000)

	Concentration (mg/L)		Concentration (mg/L)
pH	7.5	**SO_4^{2-}**	1420
Ni	55	**Na**	300
Fe	1	**Zn**	1.2
Cu	7	**t-NH_3**	670
Se	< 2	**Cl**	0.028
Te	< 2	**Co**	4

Table 1.2: Base metal refining waste water composition (Impala Platinum Limited, 2000)

Nickel is seldom the primary production of mining companies (Habashi, 1997) as it is found during gold and platinum-mining processes as a secondary product and special interest has been developed around this product for its valuable use in stainless steel and alloys. The principal uses are for domestic and automobile products, construction and machinery and the chemical industry.

Six primary chemicals have been used to treat AMD in a bulk process depending on the characteristics of the effluent. They are limestone, hydrated lime, pebble quicklime, soda ash, caustic soda and ammonia (Skousen *et al*, 1997). The principal action of the chemical used is to raise the water pH to such a level where the metal hydroxides precipitate out of the stream and a settleable sludge is formed.

The choice of a precipitating system is strongly linked to the features of the AMD (type of metals, concentrations, various dissolved ions)(Baltpurvins *et al* , 1997) as well as the quality of the desired final water. As the solubility of the different metal carbonates varies as a function of the pH (minimum solubility between a pH of 6 and 11 for most of the metals)(Brooks, 1991; Jenkins *et al*, 1964), the optimal treatment also varies greatly as a function of which metals are contained in the effluent. Finally the optimal hydroxide treatment is different for each AMD quality (Skousen *et al*, 1997).

Three major drawbacks directly linked to the nature of the hydroxide treatment can be isolated. The metal is firstly recovered as a sludge without any commercial or industrial value. It also has poor de-watering properties (Patterson *et al*, 1977) and produces a voluminous sludge that must be stored in waste landfills (Van Dijk *et al*, 1986). Also, the optimum precipitation occurs at relatively high pH, around 10.5-11 (Tunay *et al*, 1992), which increases the cost of post neutralisation of the streams.

1.3 Carbonate precipitation in pellet reactor advantages

The pellet reactor using carbonate precipitation presents several advantages over metal hydroxide precipitation in a bulk process. Formation of carbonate salts occurs at lower pH than the hydroxide salts of the same metal, though a mixture of metal hydroxy-carbonate is generally produced. The cost of post-neutralisation agent used decreases exponentially with the reduction of the precipitating pH.

The second advantage is linked to the nature of the precipitation within the pellet reactor, where a compact precipitate is formed instead of the large amount of sludge produced within the hydroxide bulk process. The seeds facilitate nucleation and provide a surface for growth and agglomeration. Using this technology, a dense precipitate of metal carbonate is obtained directly on to the large surface area provided by the pellets within the fluidised bed of the reactor. The de-watering and filtration problems of the metal hydroxide sludge are avoided, whilst the compact pellets are simply separated from the stream and dried. The fluidised bed reactor allows controlled operation, easy handling and a high mixing rate which optimises mass transfer between the continuous phase and the particles.

With hydroxide sludge precipitation, the product is seldom recovered as an industrially exploitable form (large amount of sludge containing water) and has to be expensively disposed of in waste landfills. An additional advantage of the pellet reactor technology is

therefore that the metal salt covering the seeds can be recovered in concentrated solution by dissolving the pellets in strong acid as follows:

$$MeCO_3 + 2H_3O^+ \longrightarrow Me^{2+} + 3H_2O + CO_2 \quad (1.1)$$

The carbonate escapes as carbon dioxide and the nickel is recovered in a concentrated form that can easily be reused in industry. The seeding material can also be reused in the reactor. The system has both economic and environmental advantages.

1.4 Objectives and outlines of this study

Nickel precipitation from synthetic waste streams of concentration between 50 and 150 ppm is the core focus of this research. For experimental study purposes a laboratory scale pellet reactor was used. The main control variables of the process were the reactor nickel feed rate and concentration, the carbonate to nickel molar ratio, the re-circulation rate, the pH and the number of carbonate feed inlets. The aim of the study was twofold: It firstly consisted of the development of understanding and description of nickel carbonate precipitation and removal mechanisms from the stream. The second interest was in the optimisation of the process through a Response Surface Methodology (RSM) experimental design and analysis.

The first part of this dissertation encompassing Chapters II, III and IV, consists of a background presentation, giving an overview on the basic precipitation phenomena and the specifics of pellet reactors. Chapter IV deals with solubility concepts and aims to establish a nickel hydroxy-carbonate solubility model as a function of the carbonate concentration and the pH.

The experimental procedure is thereafter described in Chapter V, with a description of the experimental set up used in the laboratory together with the methodology used for the reactant preparation, the runs and the analysis of samples.

A first set of experiments was run aiming at a description of the precipitation phenomena occurring in the pellet reactor. The parameters influencing the process were established and the essential results are described in Chapter VI.

The second set of the experiments was carried out using a Response Surface Methodology (RSM), which aimed to optimise the nickel removal from the wastewater stream. Five main influencing parameters were identified: the nickel load of the column, the carbonate to nickel inlet ratio, the pH, the re-circulation rate of the effluent and the number of feed points for the carbonate. Two different responses were measured, the total and the dissolved nickel concentration of the outlet stream. A first order model was fitted to the collected data, and the response surface analysed in Chapter VII.

Chapter VIII analyses the fitting of a second order model to the surface of investigated data points, and a general discussion is carried out on the optimisation of the process of nickel removal by carbonate precipitation in pellet reactor.

Chapter II

Precipitation theory

This chapter consists of an overview of basic precipitation concepts. The main terms and principles described in this section are directly related to the later study of precipitation mechanisms within the pellet reactor. After a brief introduction and definition of precipitation and its general uses, the concepts of supersaturation, nucleation, crystal growth and finally agglomeration are discussed.

2.1 Definitions

Precipitation is defined as reactive crystallisation. As the solubility of precipitates are low, typically in the range of 10^{-3}-1kg/m^3 (instead of 10-300 kg/m^3 in crystallisation), common evaporative and cooling crystallisation processes cannot usually be used (Söhnel and Garside, 1992; Kind, 1999). Precipitation is achieved by the mixing of two reactants, which form a third compound with a low solubility. In this study, soluble nickel and carbonates react together, forming sparingly soluble nickel carbonate salt. The stoichiometry of the process is changed as a function of the supersaturation, changing the product composition, and the precipitation process is controlled by the mixing rate (Söhnel and Garside, 1992).

A direct consequence of the low solubility of the precipitate is the development of high supersaturation, which ensures a high primary nucleation rate. Therefore, a large number of crystals are produced. This reduces the average size of the crystal population (Walton, 1967).

Crystallisation processes are divided into two categories: primary and secondary processes. The primary processes include mixing, chemical reaction in solution, nucleation and growth (Söhnel and Garside, 1992). Generally, these processes have very high rates depending on the local supersaturation. The secondary processes encompass agglomeration phenomena and ageing processes, including Ostwald ripening, re-crystallisation and polymorphic transitions, which occur at lower rates. A clear differentiation between primary and secondary processes is difficult, as growth and agglomeration operate with the same range of time constants. A distinction based on the change in shape of the PSD (particle size distribution) is often not possible.

Precipitation is mostly used in industry in two kinds of processes: the removal of unwanted species from process and effluent streams (as in the softening of drinking water or the recovery of metals from synthetic streams using pellet reactors, Seckler, 1994), and the production of solids with specified particulate properties.

In both of these processes, attention must be paid to the properties of the precipitate. The physical properties of the particles, i.e., the crystal size distribution, the particle surface area and the particle morphology have a great impact on the precipitate processing characteristics, for example: the drying rate, the density of the formed phase and the ease of solid/liquid separation. Secondly, the chemical nature of the precipitate, such as the degree of crystallinity or its amorphous or polymorphous nature, is of critical importance for its future use (Söhnel and Garside, 1992, Randolph *et al*, 1988).

The use of pellet reactors for precipitation has many advantages. They allow the removal of species from dilute or concentrated solutions, whilst producing a solid phase with desirable features: a dense, easily separable precipitate, which can either be disposed of or reused (Seckler, 1994; Van Dijk *et al*, 1986).

2.2 Supersaturation

2.2.1 Definition and influence

Crystallisation occurs when the concentration of a solute exceeds its solubility. The solution is then said to be supersaturated, and this supersaturation acts as the driving force for crystallisation (Mullin, 1972). Supersaturation can be generated by several means: cooling the solution below the saturation point, evaporating the solvent, adding a 3rd miscible component that changes the solubility of the solute or introducing a reactant that creates with the solute a product of very low solubility. In this case, the interest is only in reactant addition.

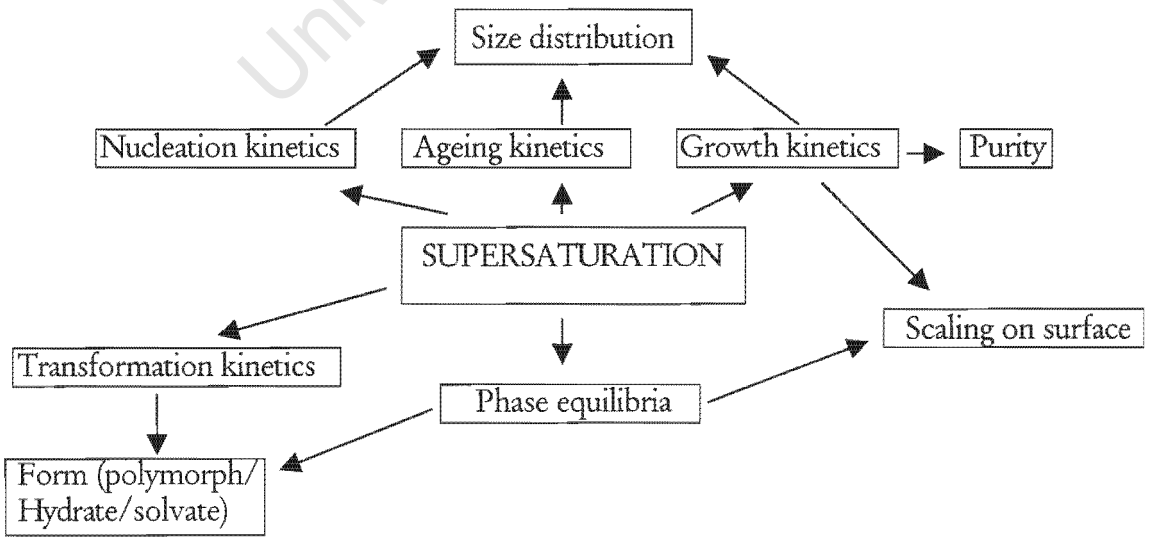

Figure 2.1: Influence of supersaturation on the precipitation process (Söhnel and Garside, 1992)

It is important to note that, for precipitation, supersaturation must exist, but the supersaturation state alone does not ensure phase change by nucleation, nor crystal growth. The level of supersaturation, as well as the hydrodynamic conditions and the presence of other materials in suspension or in solution affect the form and degree of growth. Supersaturation drives all the crystallisation processes as illustrated in Figure 2.1.

2.2.2 Mathematical definitions

In practice, the supersaturation represents the concentration difference between the actual concentration, C and the equilibrium concentration, C*. It is defined by the relationship (Mullin, 1972):

$$\Delta C = C - C^* \tag{2.1}$$

The driving force for precipitation is given by equation 2.2 (Söhnel and Garside, 1992).

$$\Delta\mu = RT\ln(\frac{a}{a_{eq}}) = RT\ln(\frac{\gamma c}{\gamma c^*_{eq}}) = RT\ln(\frac{\gamma}{\gamma c_{eq}}).(1+\sigma) \tag{2.2}$$

Where $a = \gamma.c$

$\sigma = \Delta C / C^*$

The supersaturation of the solution is thus defined in terms of ion activity. Since the rate of precipitation is determined by the supersaturation level, it is a critical parameter to monitor and control.

The supersaturation can also be defined in terms of saturation ratio, β (Mullin, 1972):

$$\beta^{\nu} = \frac{\prod_i a_i^{\nu i}}{K_{sp}} \tag{2.3}$$

Where: $\nu = \sum_i \nu i$

For the nickel hydroxy-carbonate, in order to calculate the supersaturation in the pellet reactor, the following equilibrium is considered:

$$Ni^{2+} + XOH^- + YCO_3^{2-} \quad \Leftrightarrow \quad Ni(OH)_X(CO_3)_Y \tag{2.4}$$

Combined with the electro-neutrality equation:

$$X + 2Y = 2 \tag{2.5}$$

Equation 2.4 was used to calculate the supersaturation within the reactor. Using the solubility of this salt, the saturation ratio, β (equation 2.3) can be calculated as a function of the composition of the precipitate, which is only obtainable by analysis of the pellets, as it varies with pH, carbonate to nickel ratio, and some secondary vectors:

$$\ln \beta = \frac{1}{1+X+Y} \cdot \ln\left(\frac{(Ni^{2+}).(OH^{-})^{X}.(CO_3^{2-})^{Y}}{Ksp}\right) \qquad (2.6)$$

In this case K_{sp} is obtained graphically as a function of the pH, from the Patterson *et al* (1982) model.

2.2.3 Mixing and supersaturation

Three different scales of mixing can be determined for any reactor where two solutions or fluids are mixed (Baldyga *et al*, 1993). The scale of mixing is defined as the average distance between centres of maximal difference in properties (Uhl, 1966). Macro-mixing occurs at a scale equivalent to the size of the reactor, meso-mixing at the scale comparable to size of the reagent feed pipe, and micro-mixing at the Kolmogorov scale (size of the smallest eddy). All of the scales influence the precipitate features, their relative influence depending on the particular system (Torbacke and Rasmuson, 2001).

Figure 2.2 gives an overview of the different supersaturation zones obtained when mixing two compounds A and B in the bulk of a solution. Each of the different numbered zones corresponds to different precipitation phenomena, which occur related to increasing supersaturation levels. The zones are numbered from 1 (undersupersaturation) to 6 (highest supersaturation): Zone 1 is situated under the saturation limit, or solubility curve. Zone 2 represents a supersaturated area where only secondary nucleation can occur. In Zone 3, heterogeneous nucleation occurs. In Zone 4, supersaturation drives the homogeneous nucleation. Colloid precipitation occurs in Zone 5 and gel formation occurs in Zone 6.

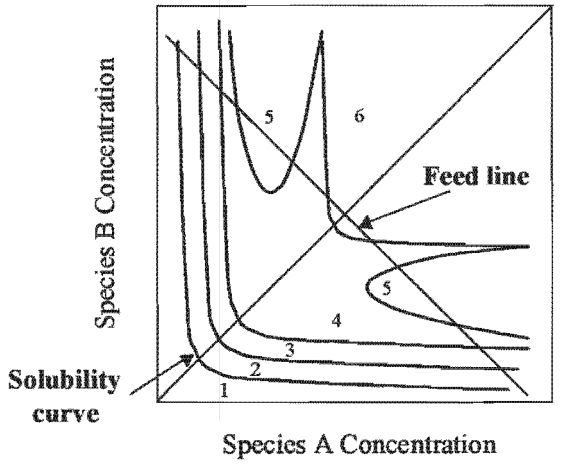

Figure 2. 2: Mixing and supersaturation: precipitation zones (Nielsen, 1979)

Figure 2.2 also shows the influence of mixing on the supersaturation profile of the solution. The "feed line" represents all the supersaturation values that can be reached when mixing two equi-molar solutions. The supersaturation at the mixing point is likely to be in any of the six zones previously described. It is the nature of the mixing that determines in which of the zones the supersaturation will occur. Noting that all precipitation phenomena are dependent on the supersaturation conditions highlights the major importance of the mixing.

2.3 Nucleation

The study of nucleation is generally difficult. Nuclei are too small to be measured and crystal growth occurs simultaneously. There are two different types of nucleation: primary and secondary nucleation. The nucleation principle can then be summarised in Figure 2.3:

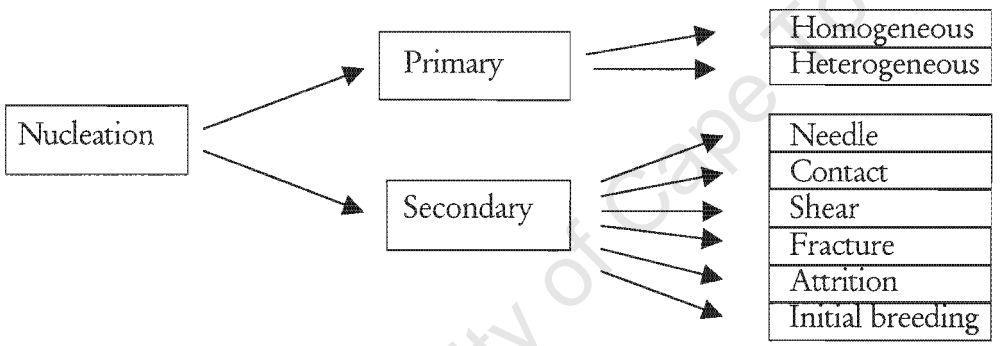

Figure 2.3: Nucleation principle (Randolph and Larson, 1988)

2.3.1 Primary nucleation

Primary nucleation is not influenced by the precipitate phase already present. Primary nucleation can either be homogeneous, i.e. presence of solute only, or heterogeneous, i.e. the nucleation is initiated by the presence of a foreign solid phase such as sand seeds, dust or reactor walls. In a pellet reactor, as in most precipitation processes, nucleation is heterogeneous, as the formation of new solid phase particles is catalysed by the presence of the solid-liquid interface provided by the foreign solid. Secondary nucleation is initiated by the presence of the crystal phase itself.

In a solution containing a solute, there is the formation of solute clusters within a reversible process. Single solute entities form clusters by attaching to each other. The number of these clusters remain stable and constant in undersaturated solutions whereas in supersaturated solutions clusters of a critical size are formed and are able to become nuclei that grow further. Every time a particle is added to a cluster there is a resultant Gibbs free energy change linked to the variation of volume area and surface of the

particle (Mullin, 1972). This change is illustrated in equation 2.7 where the negative part of the right hand side of the equation represents the gain in Gibbs free energy linked to the change in volume, and the positive part, the loss of surface energy:

$$\Delta G = \Delta G_{volume} + \Delta G_{surface} = \frac{-K_v L_c^3}{V_m} \Delta\mu + K_a L_c^2 g \tag{2.7}$$

If K_a and K_v, which are shape factors of the particle, are related to a spherical nucleus, equation 2.7 becomes:

$$\Delta G = \frac{-4\pi r^3}{3V_m} + 4\pi^2 r g_f \tag{2.8}$$

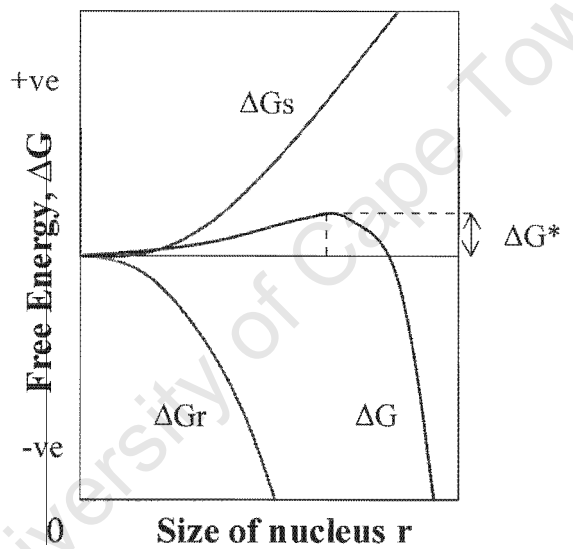

Figure 2.4: Critical Gibbs free Energy (Kurz *et al*, 1989; Mullin, 1972)

Figure 2.4 represents the Gibbs free energy of a cluster as a function of the size of a nucleus radius. The size of the critical nucleus as well as the critical free energy can be determined graphically, the critical number of particles can then be calculated:

$$r^* = \frac{2\gamma V_m}{\Delta\mu} \tag{2.9}$$

$$n^* = \left(\frac{2a\gamma}{3\Delta\mu}\right)^3 \tag{2.10}$$

For example, the critical number of particles for an easily soluble compound is around 200 to 300 molecules for a critical nucleus, and only 3 or 4 molecules for a slightly soluble compound, which indicates a high probability of the phenomenon occurring.

The nucleation rate is defined as the change in the number of supercritical clusters, N, in a time and volume unit value (Mullin, 1972):

$$J_{hetero}(t) = \frac{1}{V} \cdot \frac{dN}{dt} \tag{2.11}$$

A similar relationship can be developed for the homogenous nucleation rate, J_{homo}. A comparison between the two relationships shows that at low supersaturation J_{hetero} is always greater than J_{homo}, whereas at much higher supersaturation, where J_{homo} increases, it can be greater than J_{hetero}, but this case is seldom found in practice. The ratio between heterogeneous and homogenous nucleation thus depends greatly on the supersaturation level of the solution (Kind, 1999) as illustrated in Table 2.1.

Supersaturation ratio	*Interfacial energy*	*Nucleation*	*Growth*	*Morphology*
1 to 2	High	None	None	
	Low	Heterogeneous	Slow, dislocation	Well formed crystals
2 to 5	High	Heterogeneous	Slow, surface	no agglomeration
	Low	Heterogeneous	Dendritic	Poorly formed crystals
10 to 50	High	Heterogeneous	Dendritic	no agglomeration
	Low	Homogeneous		Stability dependent
> 1000	High	Homogeneous		agglomeration
	Low	Homogeneous		Colloidal

Table 2.1: Dependence of precipitate nucleation growth and morphology upon supersaturation (Walton, 1967)

An important parameter for heterogeneous primary nucleation is, ϕ, the wetting angle of the substrate surface. This parameter indicates if the presence of the substrate will facilitate nucleation. It can be considered for seeded precipitation, as is the case in the pellet reactor, to see the influence of various seeds on type of nucleation. The critical Gibbs free energy relationship, between heterogeneous and homogeneous nucleation is then:

$$\Delta G^*_{hetero} = \phi \Delta G^*_{homo} \tag{2.12}$$

For any supersaturated solution, nucleation is not spontaneous within a zone called the metastable zone (Figure 2.5). The solubility limit of the solute on one side and the metastable limit on the other delimit this zone (Coulson and Richardson, 1991). The metastable limit represents the maximum supersaturation of solute for which the system

can stay stable long enough to be measured. For any point of the metastable zone, the ability of the system to stay in a metastable equilibrium is determined by a parameter called the induction time, t_i, which represents the period before the formation of any measurable solid phase.

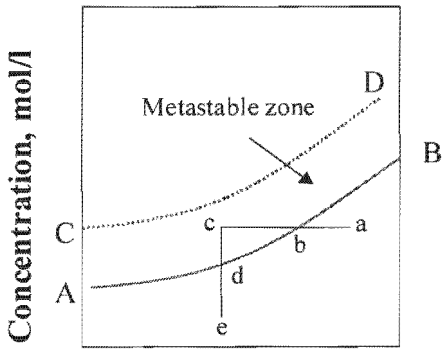

Figure 2.5: Metastable zone as a function of the concentration and temperature (Coulson and Richardson, 1991)

In Figure 2.5, the curve AB represents of the solubility limit of a compound, as a function of the temperature. The cd segment is a representation of the supersaturation of the compound at the concentration c. The metastable limit is represented by the CD curve which is roughly parallel to AB, and thus the metastable zone lies between the two curves.

2.3.2 Secondary nucleation

Secondary nucleation represents the birth of nuclei at the interface of the pre-existing precipitate. This birth can occur at much lower supersaturations than for primary nucleation. There are several different types of secondary nucleation: initial breeding, dendritic or needle breeding, fracture breeding, contact nucleation or attrition breeding, and fluid shear breeding (Figure 2.3).

The most common type of secondary nucleation is attrition breeding. The attrition of the precipitate is due to collisions of the precipitate particles with other particles, with the walls of the reactor and with the impeller. In the case of the pellet reactor, the influence of secondary nucleation on fines formation can be relatively important (Seckler, 1994) depending on the operating conditions. Two sources of nuclei for attrition breeding have been identified: surface breeding and mechanical breeding. Surface breeding is the production of secondary nuclei by attrition of surface entities, and mechanical breeding is the attrition of portions of the parent crystal, which become a possible nucleus (Coulson and Richardson, 1991). Attrition breeding is known to occur in a three-step process. The first step is the formation of attrition fragments by one of the two former means. The second is the removal of the fragment from the original precipitate surface, and the last step is the survival and the growth of the fragment.

The secondary nucleation rate by attrition breeding, B_0, is the most important to be studied in the case of a pellet reactor, and can be calculated by the empirical power law (Bardsley *et al*, 1973):

$$B_0 = k_N^1 \sigma^b \varepsilon^k M_T^{\ j} \tag{2.13}$$

Where: $1<b<3$
$0.6<k<0.7$
j=1 for dominating crystal-impeller collision
j=2 for dominating crystal-crystal collision

The parameters influencing this relationship are the growth rate, the mixing rate and the crystal concentration. The design of the reactor, the scale of operation and the design of the mixing device are also of primary importance. Several ways to achieve modelling of secondary nucleation are possible: using the power law, from the attrition behaviour of the parent crystal and using a method based on a physical attrition model.

2.4 Crystal growth

Crystal growth occurs in two stages: the diffusion of solute to the crystal surface and the surface integration reaction (Randolph and Larson, 1988), and depends both on the temperature and general concentration of solute in the liquid. In the pellet reactor, the mixing rate is sufficient to eliminate diffusion resistance, and to have surface integration controlled precipitation, i.e. the growth rate of the pellets depends on the supersaturation and the mechanism of solute integration onto the crystal surface. Although the supersaturation is relatively high in precipitation processes due to the low solubility of the product, the growth rate of crystals is generally low. Figure 2.6 describes the different steps in the growth of the precipitate.

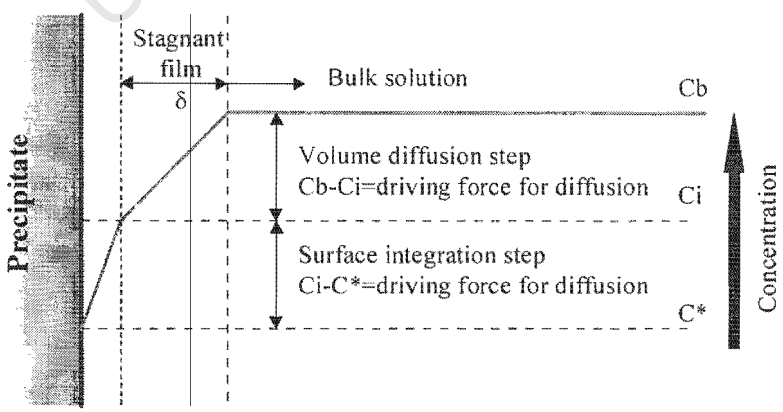

Figure 2.6: Concentration profile perpendicular to the crystal surface during growth (Van Rosmalen, 1998; Kurz *et al*, 1989)

The growth rate G is generally defined as the linear growth rate R_{lin}, in a relationship that links the overall linear growth rate to the increase in mass of the crystal with time:

$$G = \frac{dL}{dt} = 2\,\overline{R_{lin}} \tag{2.14}$$

The growth rate on the crystal faces determines the shape of the precipitate as well as the precipitate structure and purity (Mullin, 1972). The structure is also influenced by several other factors such as the binding energies between atoms, the nature of the solvent and the temperature. In addition, the presence of impurities in solution influences the growth rate, and is likely to even inhibit growth or dissolution of the solid phase.

2.5 Agglomeration

Properties of precipitates and their suspensions are strongly dependent on the extent to which secondary processes, like agglomeration, have modified the initial suspension (Söhnel and Mullin, 1987). Agglomeration is an important part of every kind of precipitation process. There are in fact very few precipitation processes in which agglomeration does not occur. This is a phenomenon where the particles collide and adhere together and eventually cement together to form an agglomerate (Söhnel and Garside, 1992). This phenomenon occurs parallel to crystal growth, and is responsible for rapid enlargement of the particle size. Agglomeration and crystal growth are both strongly dependent on supersaturation and solution composition (Hatakka *et al*, 1999; Hounslow *et al*, 1999), and a high level of supersaturation will favour agglomeration of particles over crystal growth. Even with a study of the particle with Scanning Electron Microscopy (SEM), it is difficult to distinguish visually whether size enlargement has occurred via growth or agglomeration.

Figure 2.7 describes the different processes leading to agglomeration of particles. Usually, agglomeration occurs through the following steps:

1. Transport and collision with another particle
2. Attachment of the particles
3a. Either disruption of aggregate (loose bound)
3b. Or cementing of the particles by growth

The first process is the reversible formation of aggregates, with aggregation and break up rates depending on the movement of the particles within the fluid. Inter-particle forces like Van der Waals forces contribute largely to the attachment process of the particles. The agglomerates are then formed by cementing, which is the creation of a solid bridge between aggregates. The rate of bridge formation is directly linked to the growth rate of the precipitate in the space between the touching particles.

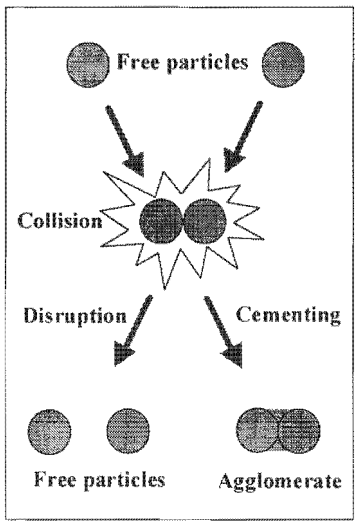

Figure 2.7: Agglomeration principle

Three kinds of collision mechanisms can be identified: perikinetic collisions, only valid for small particles (<1μm) represent the collisions generated by thermally induced motion of particles and is also influenced by the zêta-potential of the particles (Söhnel and Garside, 1992). For larger particles, two kind of collisions can be distinguished: orthokinetic collisions if the motion of the particles is influenced by the movement of the surrounding liquid (Brownian motion) and inertial collisions if gravitational and inertial forces dominate the movement of the particles (Randolph and Larson, 1988). The disruption of aggregates is directed by the same kind of processes.

The resulting equation governing agglomeration due to the collisions in the system is then:

$$N(t) = N(0)\exp\left[-4\varphi_0 . \Gamma . t / \pi\right] \tag{2.15}$$

Where: $\varphi_0 = k_v N L^3$

$\beta_{coll} = 4/3 . \Gamma . L^3$

Figure 2.8 shows the effects of the shear rate and more generally the mixing rate for laminar flow, on particle agglomeration.

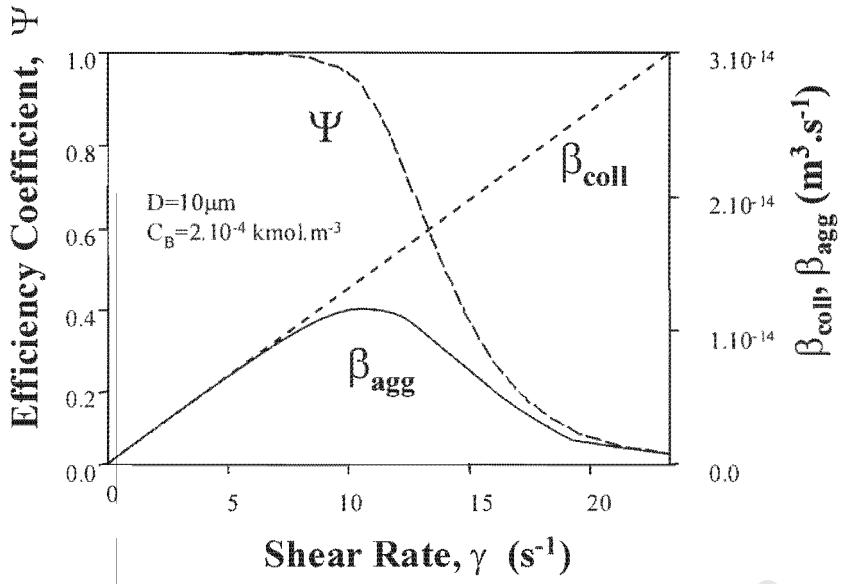

Figure 2.8: Overall agglomeration rate β_{agg} and efficiency coefficient Ψ as a function of the shear rate Γ (Van Rosmalen, 1998).

The overall agglomeration rate can be described as a combination of the collision, the breakage and the cementing rates. With the introduction of an efficiency coefficient, ψ, the relationship is then:

$$\beta_{agg} = \psi . \beta_{coll} \tag{2.16}$$

Figure 2.8 shows that the overall agglomeration rate reaches a maximum, for a specific shear rate, and then decreases as the shear rate increases. This phenomenon is due to the rapid increase of the breakage rate at high stirring speeds, and therefore, the agglomeration rate does not benefit from the increase of the collision rate. After a while, the cementing of the aggregates prevents any disruption. The cementing is due to the growth of the crystalline phase and thus the cementing rate is proportional to growth rate.

Chapter III

Pellet reactor

A pellet reactor, where the process reaction occurs directly on the seeds or pellets, has many advantages over other industrial precipitation processes for metal removal. A small quantity of dense precipitate is produced on the pellets with a potential of reuse, whereas in hydroxide bulk precipitation a large amount of sludge is generated and this must be disposed of in hazardous waste sites. The process also needs minimum supervision and maintenance; the investment costs are low because of the simplicity of the equipment involved, and the cost of chemicals and sludge disposal are also very low (Van Dijk *et al*, 1986). In this chapter, an overview of fluidised beds is firstly given, with a focus on the specificity of pellet reactors. The general precipitation process principles are subsequently described, followed finally by a discussion of efficiency in the metal removal area.

3.1 Fluidisation fundamentals

The pressure loss in the bed is due to frictional resistance of the fluid passing upwards through a bed of particles and this increases with increasing fluid flow. At the point where the drag force exerted by the fluid on the particle is equal to the apparent weight of the particles; the particles are lifted by the fluid and the bed becomes fluidised. Then, the pressure drop can be calculated as the quotient of the particle weight minus the up-thrust on particles, on the bed cross section area. In other terms, (Rhodes, 1998; Coulson and Richardson, 1991)

$$\Delta P = \frac{HA(1-\varepsilon_b)(\rho_p - \rho_f)g}{A} \tag{3.1}$$

or,

$$\Delta P = H(1-\varepsilon_b)(\rho_p - \rho_f)g \tag{3.2}$$

This relation applies from the initial expansion of the bed until transport of solid takes place. The pressure loss across the bed as a function of superficial fluid velocity is plotted in Figure 3.1. In the OA region, the response of the bed is that of a packed bed, and the

pressure drop increases steadily with fluid velocity increase. The pressure loss is then given by the Carman-Kozeny equation in laminar flow, and the Ergun equation in general (Rhodes, 1998).

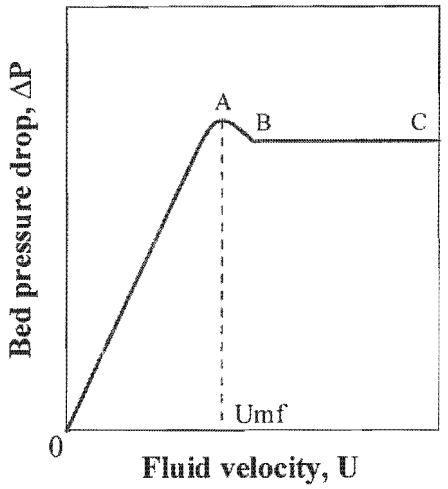

Figure 3.1: Pressure drop vs fluid velocity for fluidised beds (Rhodes, 1998)

BC corresponds to the fluidisation of the bed, where equation 3.2 applies and the pressure drop is constant with increasing fluid velocity. The bed depth increases with the velocity. In general, the pressure loss through a uniformly fluidised bed is a function of the bed height (at zero flow) and particle density, and is independent of particle size (Othmer, 1956). There is a peak in the pressure drop at point A, at the limit of fluidisation. This peak is generally associated with the extra force required to overcome inter-particle attractive forces. This limit of fluidisation is also characterised with a minimum fluidisation velocity of the fluid, U_{mf}. U_{mf} increases with particle size and density, and varies with the fluid properties. The Reynolds number for the minimum fluidisation velocity, is then:

$$\mathrm{Re}_{mf} = \left(\frac{U_{mf} d \rho_f}{\mu}\right) \tag{3.3}$$

For Reynolds number values less than about 2 (Coulson 1991), the flow is laminar, and for values greater than 100, it is turbulent. The change from complete streamline to complete turbulent flow is very gradual because flow conditions are not the same in all fluid interstices between the particles. Thus, the flow starts to become turbulent in the larger pores, and subsequently in successively smaller interstices as the value of Re increases. It is probable that the flow never becomes completely turbulent, since some of the passages may be so small that streamline conditions prevail even at high flowrates.

The corresponding U_{mf} is then:

$$U_{mf} = 0.0055 \frac{\varepsilon_{mf}^3 d^2 (\rho_p - \rho_f) g}{(1 - \varepsilon_{mf}) \mu} \tag{3.4}$$

In practice, the voidage of the bed at the onset of fluidisation, ε_{mf}, is not known accurately but is estimated to be 0.4. The fluid velocities employed are generally intermediate between U_{mf} and the velocity which will sweep the bed out of the container. Thus the reactor must be operated in a relatively narrow range of velocities, between packed bed conditions on the one hand and pneumatic transport on the other (Othmer, 1956).

Different parameters defining the powder and the particles constituting the fluidised bed are of primary importance (Zeng, 1960). The first is the particle density (Rhodes, 1998):

$$\rho_p = \frac{m_p}{V_{hp}} \tag{3.5}$$

For porous particles, the particle density (also called apparent or envelope density) is not easy to measure. The absolute density ρ_{abs} which takes into account the material of which the particle is made, can be also used:

$$\rho_{abs} = \frac{m_p}{V_{absp}} \tag{3.6}$$

Finally, the bed density can be expressed in the following terms:

$$\rho_b = \frac{m_{ph}}{V_b} \tag{3.7}$$

Where V_b represents the volume occupied by the bed at zero flow. It encompasses the volume of the particles and the voids between them.

An appropriate particle size definition to be used in equations when accurate results are needed, is the hydrodynamic diameter (Kunii, 1991). However, in practice, the sizing of the particles' diameter was achieved by mechanical sieving.

The particle size and the fluid properties have a great effect on the expansion of the bed. A bed composed of particles greater than 100μm will expand much less than one with a particle size of 30 to 80μm. The shape of the particle also plays an important role as irregularly shaped particles are more difficult to fluidise. Extremely non-spherical particles, such as needles or flakes may not fluidise at all (Othmer, 1956).

3.2 The pellet reactor

The pellet reactor provides an ideal environment for controlled crystallisation of the nickel carbonate in a very stable continuous process. The high active surface area provided by the pellets favours heterogeneous nucleation on the seeds (Heffels and

Kind, 1999), and allows operation with a slightly supersaturated solution that avoids homogeneous nucleation of fines that are not easily separated from the stream. The relatively high fluid velocity in the reactor, typically in the range of 40 to 120m/h (Scholler *et al*, 1987), prevents the cementing of the pellets by allowing their fluidisation, or suspension. Very good mixing of the reactants is also provided. Theoretically the sedimentation velocity of the sludge is also a limiting factor for the heavy metal surface load of the reactor. In the case of pellet reactors, the nickel carbonate precipitate density is much higher than in other precipitation processes. Consequently the sedimentation velocity of the grains is much greater than that of $NiCO_3$ flocs. A greater surface load of 20 to 100 times that of a sludge process is therefore possible. Pellet reactors are generally modelled as plug flow reactors, even if this assumption is not acurate, because of a partial classification of the crystals in the bed (Wojcik, 1999). The model closest to the actual physical phenomena, appears to be the axial dispersion model developed by Toyokura *et al* (1973) and Wojcik (1999).

3.3 Principles of the pellet reactor

The bases of the precipitation process within a pellet reactor lies in the coating of the precipitate on the pellets either directly by heterogeneous primary nucleation and precipitate growth or in a secondary process involving agglomeration of clusters formed in the bulk of the solution on the pellet. The unwanted species are then removed from the main stream, concentrated and compacted on the surface of the pellets. The formation of fines is obviously undesirable, since they are prone to being washed from the bed with the outlet stream. After a sufficient growth of the pellets, they are easily separated from the solution by filtration techniques.

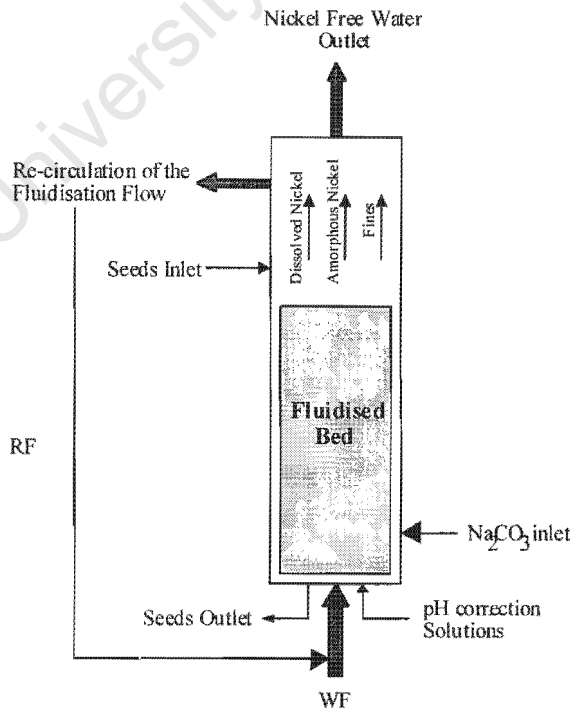

Figure 3.2: Schematic fluidised bed principle (Seckler, 1994)

Figure 3.2 is a schematic representation of the basic principle of the pellet reactor. The major control parameters of the reactor are the feed rate, the feed temperature, the re-circulation rate, the rate of removal of the nuclei, and the height of the bed at zero flow.

3.3.1 Re-circulation rate

The fluidisation was achieved mainly through the re-circulation flow, RR, which is defined as the quotient of the re-circulation flow over the waste stream flow (equation 3.8). The re-circulation flow also increases the residence time of the nickel in the reactor, and provides dilution of the waste stream, which therefore prevents any over-supersaturation effects. Finally the re-circulation flow introduces a buffering and thus stabilising effect over the whole process. The process is then operated with easy handling.

$$RR = \frac{RF}{WF} \tag{3.8}$$

3.3.2 Supersaturation profile influence

All the precipitation processes within the fluidised bed depend on the supersaturation profile of the bed. The supersaturation level is not constant through the bed (Seckler, 1994). A gradient is observed with a high supersaturation at the bottom of the bed, decreasing with the bed height and precipitate formation.

The control of supersaturation in the study of nickel hydroxy carbonate precipitation is linked by definition to the concentration, or dilution, of three species: nickel, hydroxide, and carbonates (equation 2.6, Van Rosmalen, 1998):

$$\ln \beta = \frac{1}{1+X+Y} \cdot \ln\left(\frac{(Ni^{2+}).(OH^{-})^{X}.(CO_3^{2-})^{Y}}{Ksp}\right) \tag{2.6}$$

The important parameters to control the overall supersaturation are the concentrations of the waste nickel and the carbonate streams, the pH and the re-circulation flow.

Some local high supersaturation can also develop at the reactant inlets. The mixing of inlet flows has to maintain a slight supersaturation at the bottom of the column. The supersaturation acts as a driving force for the very fast nickel carbonate precipitation on the seeds. The local supersaturation level determines the nature of the crystalline phase and the kinetics of nucleation growth and aggregation (Söhnel and Garside, 1992).

As a result of the differences in supersaturation over the bed, a mixture of various crystalline and amorphous materials with slightly different solubilities and elemental compositions comprise the precipitate product. However for the purposes of this work, it is assumed that the product is composed of only one single compound, with

characteristics independent of the bed position. This assumption was partly supported by the analysis of the precipitate described in Chapter VI.

The two unwanted processes are spontaneous primary nucleation and the abrasion of the mineral coating of the pellets. Both processes lead to the formation of colloidal particles and fines, which are not retained by the bed, and therefore contribute to the nickel that is not recovered in the reactor. Too high a local supersaturation is undesirable as it may cause spontaneous primary nucleation to occur.

Maintaining a constant low supersaturation through the bed is moreover of primary importance, as agglomeration of the fines on the pellets cannot occur at zero supersaturation (Söhnel and Garside, 1992). The supersaturation level also drives other secondary phenomena, such as pellet dissolution and attrition.

3.3.3 Influence of pH

Controlling the pH during operations is obviously essential as the hydroxide concentration plays a major role in the supersaturation level in the reactor. Figure 3.3 indicates the influence of the pH on the overall nickel removal efficiency, the nickel conversion, and on the fines generation.

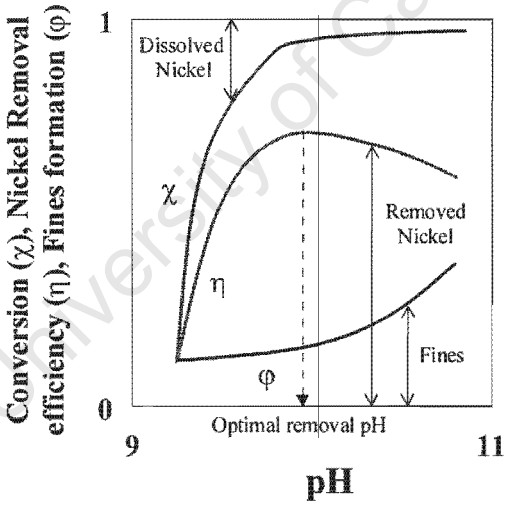

Figure 3.3: Nickel conversion, removal efficiency and fines formation as a function of the precipitation pH (Seckler, 1994)

The curves presented on Figure 3.3 are defined by the three following relationships.

Nickel removal efficiency: $$\eta(\%)=\frac{Ni_{intro}-Ni_{tot-out}}{Ni_{intro}}\times 100 \quad (3.9)$$

Nickel conversion: $$\chi(\%)=\frac{Ni_{intro}-Ni_{dis-out}}{Ni_{intro}}\times 100 \quad (3.10)$$

Fines concentration: $$\varphi(\%) = \chi(\%) + \eta(\%) \quad (3.11)$$

3.3.4 Seeding material and particle size profile

The seeding material is chosen in such a way as to avoid any bubbling phenomenon in the bed that causes changes in the height of the bed as well as in the pressure loss. In general, no bubbling is observed with fluid fluidised systems (Rhodes, 1998). Any channelling of the bed has also to be avoided to maximise the residence time of the fluid through the bed, as well as the interface between fluid and solid.

The movement of the particles observed in the bed is free but not totally random. They rise through the centre of the bed where the velocity is high, and fall on the sides of the vessel where the velocity is the lower and sometimes even negative (Zenz *et al*, 1960).

The coating of the pellets by the precipitate is responsible for a change in the particle size distribution of the pellets as well as a change in their density. Related to this phenomenon, the great mobility of the particles through the fluidised bed establishes a particle size gradient within the height of the bed. The heaviest particles, which are less entrained by the fluid, settle at the bottom of the bed, while the lightest float over it. The biggest particles can then be easily removed from the bottom of the reactor, and new seeding material introduced at the top, while operating in a continuous process. The axial position of the particles can be related to the residence time of the effluent in the plug flow type reactor (Seckler, 1994).

3.3.5 Active surface of the pellet

The active total surface of the pellets influences the general efficiency of the whole process (Wang and Anderson, 1992). Therefore, the precipitation mechanisms such as heterogeneous nucleation, crystal growth and agglomeration are all surface-dependant, and very sensitive to the number and nature of sites provided (Randolph and Larson, 1988). The total surface available on the pellets is characterised by the bed height at zero flow, the voidage in the bed, the particle size distribution of the pellets and their shape.

In order to draw a simple model relating the particle size diameter to the total active surface available in the bed (Figure 3.44), some assumptions were made: the height of the bed at zero flow was assumed constant, with a constant voidage of 0.4; the particles were approximated as spheroids and the particle size distribution was considered as mono-dispersed (which was not the case during the operation of a pellet reactor).

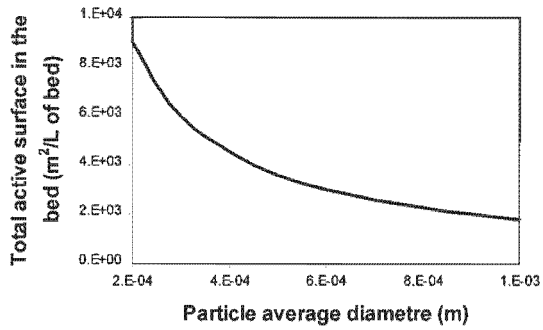

Figure 3.4: Active surface of pellets in the bed = F(particle average diameter) at constant bed volume

Figure 3.4 shows the asymptotic decrease of the active surface when increasing the average particle diameter.

When considering the size of the reactor as a limiting parameter of the pellet volume, the average size of the pellet has to be kept small, usually less than 1 mm (Wilms, 1988), to optimise the reactor operation at steady state. Moreover, the particle size distribution is considered to be constant when running the reactor at a steady state. The biggest pellets are removed from the bottom of the column and replaced by new seeds.

During start up experiments, the active surface area provided at the beginning is very large and slowly decreases when the pellets are removed because of the enlargement of the bed. In order to reach a steady state, a frequency of pellet removal has to be defined. Seckler (1994) estimated an average pellet residence time of 10^6s.

3.3.6 Pellet composition

The pellets are obtained as a relatively pure, low water, nickel hydroxy-carbonate precipitate salt. In general, impurities like suspended mater and other ions have a relatively low incorporation rate in the high-density product (Walton, 1967). They can nevertheless generate the nucleation of fines in the bulk of the solution. This kind of seeded precipitation represents a major advantage over bulk precipitation processes, where the sludge-like precipitate incorporates large amounts of impurities and water (Wilms, 1988). The hydrodynamic conditions in the reactor induce high collision rates and favour attrition of any branching on the precipitate surface and are a possible explanation for differences in density and appearance of the precipitate between the two processes. It is interesting to note that no scientifically established theory exists to acount for the different aspects of the precipitate (Kramer, 2001).

Analysis of the nickel carbonate pellets shows that they consist of: 99.8% Ni and 0.2% of other metals for a solution prepared with tap water, (Van Dijk *et al*, 1987). Van Dijk also showed that under their operating conditions, 50-60% of the ligands were CO_3^{2-}, and the rest mainly constituted of hydroxides.

3.3.7 Dissolving the pellet

The nickel on the pellets can be reused by dissolving the pellets in strong acids, HCL, H_2SO_4 or H_3PO_4 (Jeffery *et al*, 1989) and recovered in concentrated solutions (Wilms, 1988). The carbonate is released as carbon dioxide, and the seeding material can be reused in the reactor after abundant washing.

$$2nYH_3PO_4 + nYCO_3^{2-} \longrightarrow 2nYH_2PO_4^- + nYCO_2 + nYH_2O$$

$$nXH_3PO_4 + nXOH^- \longrightarrow nXH_2PO_4^- + nXH_2O$$

$$2nH_3PO_4 + nXOH^- + nYCO_3^{2-} \longrightarrow 2nH_2PO_4^- + n(X+Y)H_2O + nYCO_2 \quad (3.12)$$

3.3.8 Start-up effect

During start-ups of the reactor new seeding material with a very small average particle size is used in the column. Although the surface provided for precipitation is far larger than during the operation at steady state, the removal efficiency is relatively poor and improves with time. Steady state is reached after few days of continuous operation. Zhou *et al* (1999) have demonstrated poor lattice compatibility between the SiO_2 of the sand particles and the nickel hydroxy-carbonate precipitate. The sand surface is therefore initially inappropriate for metal coating, and heterogeneous nucleation, crystal growth and fines-pellet agglomeration probability are less likely. This problem disappears when the first layer of precipitate covers the pellet. Metal removal reaches a steady state with the increased ability of nucleation and agglomeration of precipitate on precipitate. Some co-plating agents such as calcium chloride can be added to the waste stream during start ups in order to accelerate the formation of the first layer (Zhou *et al*, 1999). Steady state is reached when the pellet average size remains relatively constant balanced between the precipitate growth, the removal of the largest pellet and the introduction of new seeding material.

3.4 Process efficiency

In practice, very good results can be achieved, and waste nickel effluent streams of a range of concentrations from 10 up to 100 000ppm can be treated to up to 99.95% metal removal (Van Dijk *et al*, 1987). In the case of effluents of low concentration, small or no re-circulation of the stream is needed, whereas for flow of higher concentration. The efficiency of the nickel removal is improved by increasing the re-circulation flow rate.

The main problem encountered is due to the carry over of nickel containing fines or amorphous nickel. Although most of the nickel precipitates onto the seeds, the presence of local high supersaturation zones due to poor meso-mixing at the reactant inlets, or to partial channelling of the bed, causes the formation of nickel carbonate and hydroxide primary nucleates.

Controlling the pH during operation is obviously essential as the hydroxide concentration plays a major role on the supersaturation. Figure 3.3 indicates the influence of pH on overall nickel removal, the nickel conversion, and on fines generation, and can be used to estimate regions of optimum process efficiency.

Abrasion of the pellets can also trigger the presence of fines of amorphous nickel in the upward flow. As the precipitation of nickel carbonate is time limited within the fluidised bed, most of the amorphous nickel formed does not have the opportunity to aggregate onto the seeding material, and is recovered in the outlet flow of the column. Pellet attrition generally occurs at the bottom of the column (Seckler, 1994) and just above the input nozzle for the fluidisation flow. Therefore, the flow re-circulation rate has to be optimised to enhance the process efficiency.

The precipitation of nickel carbonate causes the pellet size to increase. As the efficiency of the nickel removal depends on the active specific surface of the seeds, the pellet size has to remain very small, usually below 1 millimetre. Therefore the biggest seeds are removed periodically from the bottom part of the bed where they automatically concentrate, while new seeding material is added from the top of the reactor. Keeping a small average seed size also prevents an increase of fines formation by pellet abrasion.

In general if nickel removals greater than 80% are needed a filtration step must be added after the reactor (Seckler, 1994; Wilms, 1988). Using sand filters after industrial scale columns is the commonly used process, as the backwash water of the filters can be diluted with the inlet effluent and the nickel re-dissolved, and recovered within the column (Van Dijk, 1987). Nickel removal efficiencies of up to 99.95% can be expected when using the post-filtration stage. This process can be extended with similar efficiencies to other heavy metals such as Zn, Cu, Co, Cd, Mn, Ba, Sr, Ag, Pb and Hg. Chromium does not form carbonate salts (Patterson *et al*, 1982).

Chapter IV

Nickel hydroxy-carbonate solubility

Solubility diagrams are commonly used in order to predict solubility of a product under specific experimental conditions. As the determination of all the species present in solution is generally impossible, the concept of a "solubility domain" has to be defined, instead of having a precise solubility model for each species (Tunay *et al*, 1995; Baltpurvins *et al*, 1996). This solubility domain is constructed through interpretation of thermodynamic and kinetic constants found in the literature. The solubility domain of nickel has to be defined for a solution containing numerous ions, as nickel carbonate precipitation never occurs alone, but in competition with nickel hydroxide precipitation. The final solubility domain will be determined from a superposition of the hydroxide and carbonate solubility diagrams.

For metal hydroxy-carbonate precipitation, the construction of the solubility diagram has been approached as follows:

1. Determination of the known and potential hydroxide, carbonate and mixed compounds.
2. Determination of the solubility products from the literature. Corrections can be made for ionic strength and temperature.
3. Determination of the solubility system (hydroxide or carbonates), under specific operating conditions (pH, carbonate concentration).
4. Definition of zone of lower solubility by the construction of phase diagrams.

4.1 Solubility of nickel hydroxides

4.1.1 Solubility diagram

The solubility of nickel hydroxide is defined by its equilibrium equations. These relations describe the equilibrium between the nickel hydroxide solid and soluble species. The most important ligand is OH^- ion, which may form various hydroxy complexes with nickel. The mononuclear hydroxy complex species that have been mentioned in the literature are: $Ni(OH)^+$, $Ni(OH)_2^0$, $Ni(OH)_3^-$ (McAnally *et al*, 1984), and the composition of the solid phase is then: $Ni(OH)_2(s)$. Usually the polynuclear polyhydroxy species

involving several nickel atoms are transition forms, and form very slowly. Their formation constant depends on the dilution and on the experimental conditions of their determination. The polynuclear forms, as transition species, are difficult to use for the representation of the solubility diagram and in any event do not provide more useful information in this case. The equilibrium relationships for literature given hydroxy complexes, are:

$$Ni(OH)_2\ (s) \Leftrightarrow Ni^{2+} + 2OH^- \quad (4.1)$$

pK_{S0}= 14.7 for fresh precipitate
17.2 for aged precipitate

$$Ni(OH)_2\ (s) \Leftrightarrow Ni(OH)^+ + OH^- \quad (4.2)$$

pK_{S1}= 11.3

$$Ni(OH)_2\ (s) \Leftrightarrow Ni(OH)_2^0 \quad (4.3)$$

pK_{S2}= 4.5

$$Ni(OH)_2\ (s) + OH^- \Leftrightarrow Ni(OH)_3^- \quad (4.4)$$

pK_{S3}= 1.7

Solubility product constants:

$$K_{S0} = [Ni^{2+}].[OH^-]^2 \quad (4.5)$$

$$K_{S1} = [Ni(OH)^+].[OH^-] \quad (4.6)$$

$$K_{S2} = [Ni(OH)_2^0] \quad (4.7)$$

$$K_{S3} = [Ni(OH)_3^-] / [OH^-] \quad (4.8)$$

The previous equations can be transformed into logarithmic form:

$$\text{Log}\,[Ni^{2+}] = -pK_{S0} - 2pH + 28 \quad (4.9)$$

$$\text{Log}\,[Ni(OH)^+] = -pK_{S1} - pH + 14 \quad (4.10)$$

$$\text{Log}\,[Ni(OH)_2^0] = -pK_{S2} \quad (4.11)$$

$$\text{Log}\,[Ni(OH)_3^-] = -pK_{S3} + pH - 14 \quad (4.12)$$

These solubility products found in the literature are generally for zero corrected ionic strength (Jenkins *et al*, 1964). In general the solubility product decreases with ageing, (McAnally *et al*, 1984). This decrease is due to the ordering of the crystal structure. With time and ageing larger and more ordered crystal structures are developed, ordered crystals being less soluble than disordered structures. The negative logarithms of the solubility products, pKs, of common heavy metals are presented in Table 4.1.

Metal	*Precipitate*	*pKs0*	*pKs1*	*pKs2*	*pKs3*	*pKs4*	*pH of min solubility*
Nickel	fresh	14.7	11.3	4.5	1.7		10.5
	aged	17.2					
Cadmium	fresh	13.7	9.5	5.3	4.6	4.9	10.5
	aged	14.4					
Lead	fresh	14.9	9.1	4.1	1		10
	aged	15.3					
Zinc	fresh	16	11.9	5.9	1.8	0.5	9.8
	aged	17					

Table 4.1: Common heavy metal solubility products (Patterson *et al*, 1982)

The plot of logarithmic equations 4.9 to 4.12 as a function of the pH is shown in Figure 4.1. On the resultant curve the solubility domain of the nickel hydroxide system can be identified, and the total soluble nickel concentration can be defined for any given pH. Similar graphs can be drawn for any of the metals given in Table 4.1 with their solubility constants.

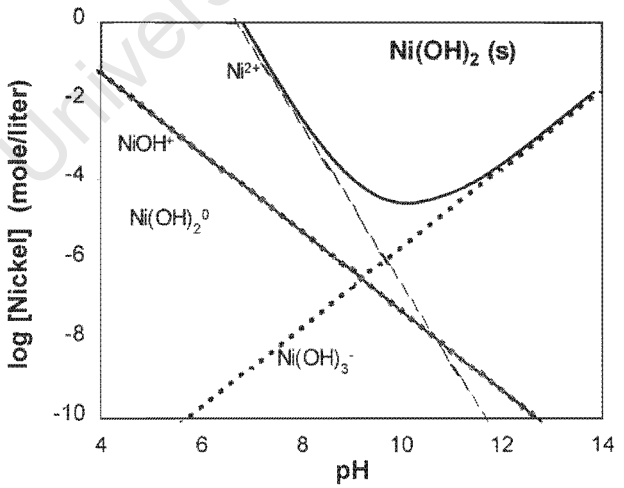

Figure 4.1: Theoretical nickel hydroxide solubility curve

The species of importance can be identified as: Ni^{2+}, $Ni(OH)_2^0$, $Ni(OH)_3^-$; The domain of the minimum solubility for the nickel hydroxide is around pH 10.5.

4.1.2 Theoretical versus experimental solubilities

Figure 4.1 shows the theoretical hydroxide solubility curves, calculated from the nickel solubility products. Patterson *et al* (1977) and McAnally *et al* (1981 and 1984) studied the discrepancies between theoretical and actual solubilities of the nickel hydroxides.

Patterson *et al* (1982) demonstrated that the experimental pH of the best precipitation for the nickel hydroxide was at pH 11, rather than pH 10.5. This result has been disputed by McAnally *et al.* (1984) who demonstrated that the lowest solubility hardly changed in the pH range 10-11. The transition point between low precipitation (pH 6-8) and high precipitation (pH 10-11) appeared to be pH 9.

Deviations from the theory are observed for several reasons. The major discrepancy sources are the different range of solubility constants found in the literature, the presence of other insoluble metal hydroxides, the lack of equilibrium conditions, ionic strength effects, analytical inability to precisely separate the colloidal precipitate and the presence of impurities and complexing agents (Patterson *et al* (1982); McAnally *et al* (1984)).

McAnally *et al* (1981 and 1984) also suggested that the species $Ni(OH)_2^0$ does not play an important role in the nickel hydroxide solubility. The experiments aimed to compare theoretical and experimental soluble nickel concentrations after precipitation. The results of the study showed that the theoretical curve without considering the ion pair $Ni(OH)_2^0$ is more representative of the actual nickel solubility in the range of pH 8-11. The different models are plotted in Figure 4.2.

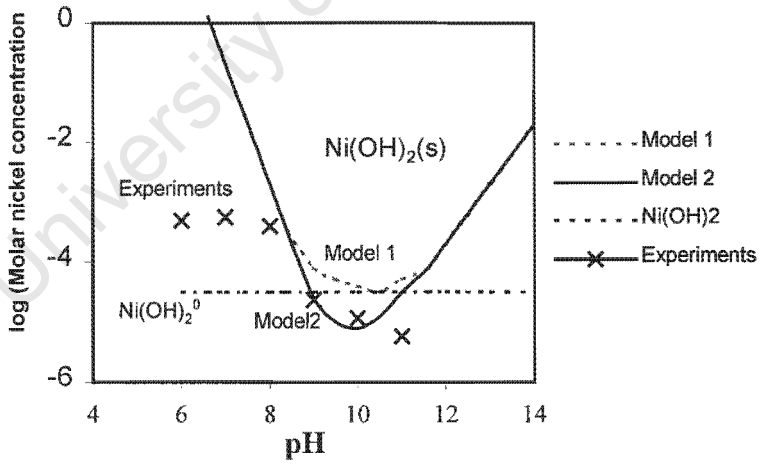

Figure 4.2: Comparison of the nickel solubility diagram models and experimental results (McAnally *et al.*, 1984)

Model 1 takes the $Ni(OH)_2^0$ species into consideration, while Model 2 does not. The data points represent the experimental values obtained by McAnally *et al* (1984), for fresh precipitates. While both models estimate the lower solubility pH to be between pH 10 and 10.5, model 2 more accurately describes the experimental results. The concentrations tend to be lower at pH 11 than predicted in both models. This discrepancy could be attributed to the reasons given previously.

In another study Baes *et al* (1976) aimed to describe the behaviour of aged precipitate. He proved that $Ni(OH)_2^0$ species are of great importance in the aged solubility system and that Model 1 describes these experimental results better. For industrial precipitation, the precipitate will not reach an aged state in the reactor and the second model will be used for this study.

4.2 Nickel carbonate solubility

The carbonate system in a water solution is represented by different ions, depending on the pH of the medium. Furthermore, the carbonates will not be the only available ligands for metal precipitation, especially at high pH values. With the high concentration of OH^- ions, there will be a competition between several precipitation systems. The following describes the carbonate solubility mechanism by means of the construction of the solubility diagram.

4.2.1 Carbonate chemistry

In a system containing carbonates, the inorganic carbon in solution has four forms: dissolved CO_2, carbonic acid (H_2CO_3), bicarbonate (HCO_3^-) and carbonate ions (CO_3^{2-}). As the two first forms cannot be distinguished separately by analysis, they form a single composite species $H_2CO_3^*$ in a pH dependent equilibrium with atmospheric carbon dioxide (in the case of open systems).

The carbon system can be defined by two systems. The first one is open to the atmosphere and considers the carbon dioxide uptake or release to the atmosphere as the metal carbonates precipitate or dissolve. The second system, closed to atmosphere, does not allow any carbon dioxide exchange and the initial C_T value, which corresponds to the total carbonate concentration in solution, remains relatively constant. Carbonate precipitation generally involves high C_T values. For a closed system like the pellet reactor:

$$C_T = [CO_2 + H_2CO_3] + [HCO_3^-] + [CO_3^{2-}] = \text{constant} \qquad (4.13)$$

The carbonate dissociation equilibrium has to be considered (carbonate can be described as a weak dibasic acid, H_2CO_3) in order to do an approximation of the different carbonate species concentrations:

$$H_2CO_3 \quad \Leftrightarrow \quad 2H^+ + CO_3^{2-} \qquad (4.14)$$

The dissociation constants of the carbonic acid are:

$$K_1 = [H^+] \cdot [HCO_3^-] / [H_2CO_3] \qquad (4.15)$$

$$K_2 = [H^+] . [CO_3^{2-}] / [HCO_3^-] \qquad pK_1 = 6.3 \qquad pK_2 = 10.3 \tag{4.1}$$

The water dissociation constant:

$$K_w = [H^+] . [OH^-] \qquad pK_w = 14 \tag{4.2}$$

A plot of the log species concentration of the predominant species of carbonic acid versus pH is illustrated in Figure 4.1.

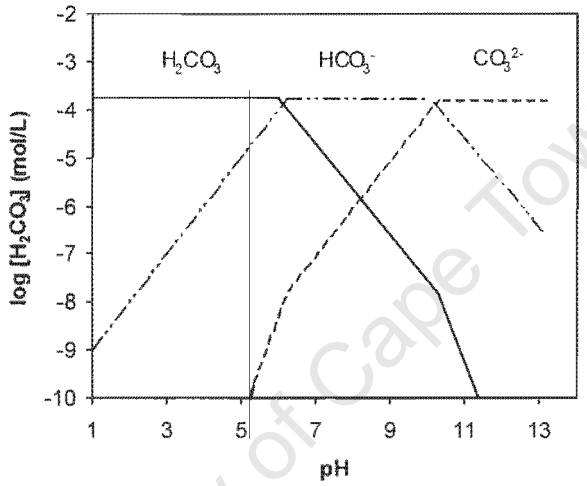

Figure 4.1: log species concentration vs pH for C_T ($C_T = 10^{-3.8}$)

Figure 4.3 allows a good approximation of the concentration of the different carbonate species for any given pH.

4.2.2 Solubility diagram

The nickel carbonate solubility diagram is defined similarly to the nickel hydroxide one, i.e. by the solubility products of the metal salts and by the equations relating soluble and solid species. Two other factors have to be considered, which are the carbonic acid dissociation and the hydrolysis of the metal ion to form metal hydroxides. The latter factor helps to have a more complete review of all the soluble metal species present in the medium for a given pH and a constant C_T. Different pH zones have to be considered for the construction of the diagram. These zones are related to the inorganic carbon system and predominating species. C_T is considered constant, and the following approximations are made:

$$pH < pK_1 \quad \Rightarrow \quad [H_2CO_3] = C_T \tag{4.3}$$

$$pK1 < pH < pK2 \quad \Rightarrow \quad [HCO_3^-] = C_T \tag{4.4}$$

$$pK_2 < pH \quad \Rightarrow \quad [CO_3^{2-}] = C_T \tag{4.5}$$

The following equilibrium equations relate nickel hydroxide and carbonate species.

4.2.2.1 pH zone 1: $pH<pK1 \Rightarrow C_T = [H_2CO_3]$

$$NiCO_3 + 2H^+ \quad \Leftrightarrow \quad Ni^{2+} + H_2CO_3 \tag{4.6}$$

$$pK_3 = -8.4$$
$$\text{Log}\,[Ni^{2+}] = \log K_3 - \log C_T - 2pH \tag{4.7}$$

$$NiCO_3 + H^+ + H_2O \quad \Leftrightarrow \quad NiOH^+ + H_2CO_3 \tag{4.8}$$

$$pK_4 = 4.7$$
$$\text{Log}\,[NiOH^+] = \log K_4 - \log C_T - pH \tag{4.9}$$

$$NiCO_3 + 3H_2O \quad \Leftrightarrow \quad Ni(OH)_3^- + H_2CO_3 + H^+ \tag{4.10}$$

$$pK_5 = 23.1$$
$$\text{Log}\,[Ni(OH)_3^-] = \log K_5 - \log C_T + pH \tag{4.11}$$

4.2.2.2 pH zone 2: $pK1<pH<pK2 \Rightarrow C_T = [HCO_3^-]$

$$NiCO_3 + H^+ \quad \Leftrightarrow \quad Ni^{2+} + HCO_3^- \tag{4.12}$$

$$pK_6 = -2.1$$
$$\text{Log}\,[Ni^{2+}] = \log K_6 - \log C_T - pH \tag{4.13}$$

$$NiCO_3 + H_2O \quad \Leftrightarrow \quad NiOH^+ + HCO_3^-$$

$$pK_7 = 11$$
$$\text{Log}\,[NiOH^+] = \log K_7 - \log C_T \tag{4.14}$$

$$NiCO_3 + 3H_2O \quad \Leftrightarrow \quad Ni(OH)_3^- + 2H^+ + HCO_3^- \tag{4.15}$$

$$pK_8 = 29.4$$
$$\text{Log}\,[Ni(OH)_3^-] = \log K_8 - \log C_T + 2\,pH \tag{4.16}$$

4.2.2.3 pH zone 3: pH>pK2 $\Rightarrow C_T = [CO_3^{2-}]$

$$NiCO_3 \quad \Leftrightarrow \quad Ni^{2+} + CO_3^{2-} \tag{4.17}$$

$$pK_9 = 8.2$$
$$\text{Log}\,[Ni^{2+}] = \log K_9 - \log C_T \tag{4.18}$$

$$NiCO_3 + H_2O \quad \Leftrightarrow \quad NiOH^+ + CO_3^{2-} + H^+ \tag{4.19}$$

$$pK_{10} = 21.3$$
$$\text{Log}\,[NiOH^+] = \log K_{10} - \log C_T + pH \tag{4.20}$$

$$NiCO_3 + 3H_2O \quad \Leftrightarrow \quad Ni(OH)_3^- + CO_3^{2-} + 3H^+ \tag{4.21}$$

$$pK_{11} = 39.7$$
$$\text{Log}\,[Ni(OH)_3^-] = \log K_{11} - \log C_T + 3pH \tag{4.22}$$

The final solubility diagram, which considers both hydroxide and carbonate precipitate formation is different from both the hydroxide one and the carbonate one, which neglect hydrolysis. The diagram is constructed by the superposition of the hydroxide and carbonate solubility diagrams. Different solid phases may form alternatively, and the one with the lowest solubility will appear as the thermodynamically stable phase.

The construction of an activity diagram (Figure 4.2) may be useful to determine the thermodynamic solid phase, which will precipitate for a given C_T as a function of the pH. On this diagram are plotted the relative activities of the different solids and soluble species present in the solution. The solid phase with the higher relative activity will precipitate as $Ni(OH)_2$ at pH 11 and $Ni(CO_3)$ at pH 8 ($C_T = 10^{-2}$).

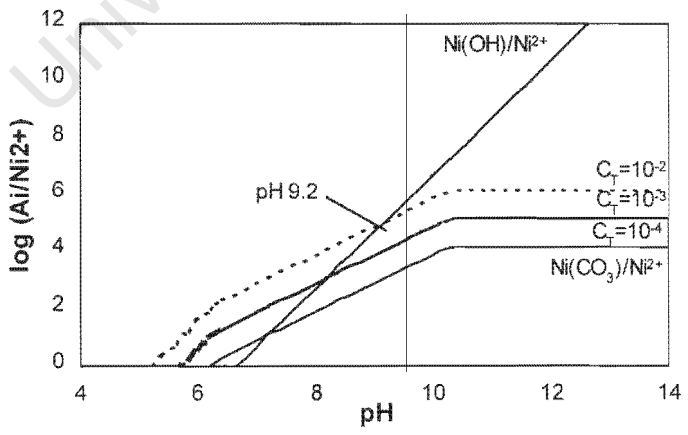

Figure 4.2: Nickel hydroxy-carbonate activity diagram (Stumm and Morgan, 1997)

The different solid solubility controlling domains are then determined on the solubility diagram (Figure 4.5), which is drawn at a constant C_T value of 10^{-3}mol/L. The solubility domains are easily delimited. The principal use of this diagram is to determine the pH for the lower solubility and thereafter the solid phase predominating at this certain pH. The solubility domain is highly dependent on the C_T concentration. Different diagrams can be drawn for different C_T values to illustrate the effects of an increase in the carbonate concentration.

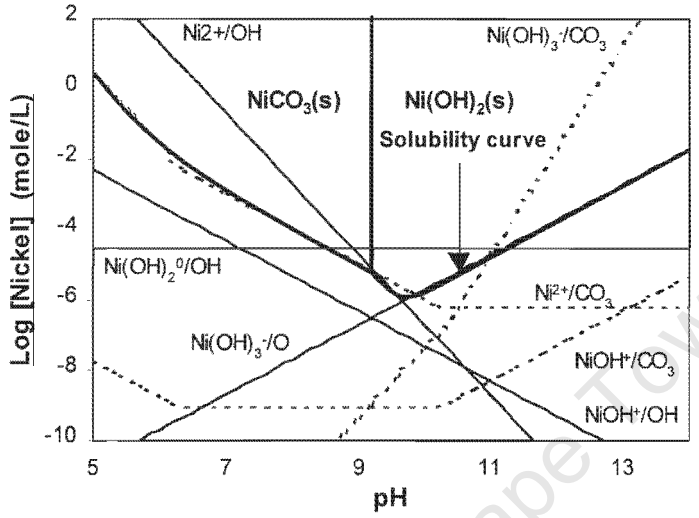

Figure 4.5: Nickel hydroxy-carbonate diagram. $C_T = 10^{-3}$ mol/L

Again it is assumed that the $Ni(OH)_2^0$ species does not have a great influence on the fresh precipitate system. For a C_T of 10^{-2} mol/L the lower solubility is obtained for a pH around 10.5 and the solid system, which appears to control the solubility is the hydroxide one.

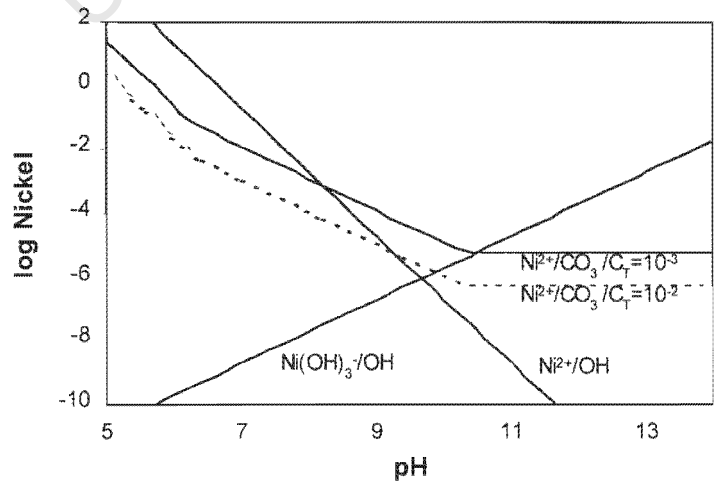

Figure 4.6: Nickel carbonate solubility comparison for different C_T values

Figure 4.6 shows that an increase in the carbonate concentration from 10^{-3} to 10^{-2} mol/L tends to lower the solubility of the metal species from 10^{-4} to 10^{-5}mol/L of soluble nickel. The minimum solubility pH also decreases with the increase of C_T. Moreover the pH limit between the carbonate and the hydroxide solid controlling zone varies as a function of the C_T. There is a broadening of the pH bandwidth of the carbonate solubility control domain with an increase of C_T in the concentration range studied. The first solid nickel hydroxide appears at pH 9.4 for a C_T of 10^{-2}mol/L, and pH 8.4 at 10^{-3}mol/L C_T.

Chapter V

A view from the laboratory

This chapter consists of an overview of the operating process on a laboratory scale. First, the general experimental set-up is described, followed by a description of the reactor design and the process control parameters. Thereafter experimental procedure is given together with observations made on the reactor operation. Finally reagent preparation and analytical methods are described.

5.1 Experimental set-up

Figure 5. 1 shows a schematic diagram of the experimental set up. The major control parameters of the reactor are the feed rate, the re-circulation rate, the operating pH, the height of seeds at zero flow and the number of feed points.

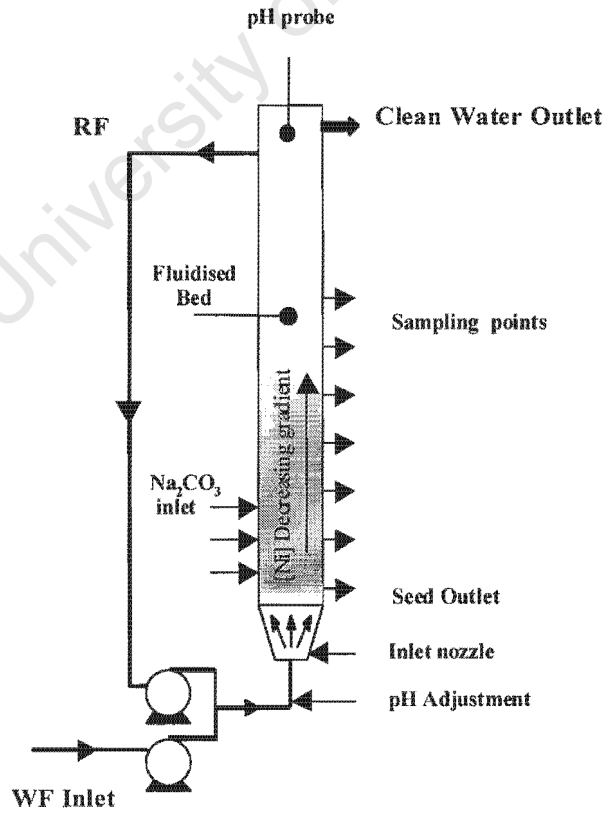

Figure 5.1: Schematic representation of the pellet reactor

A detailed description of the experimental equipment is given Table 5.1.

Re-circulation pump	Watson Marlow 505S, Masterflex tubing 16
Nickel stream pump	Masterflex, Console drive, 6-600RPM, tubing 16
Carbonate stream pump	Masterflex, Console drive, 6-600RPM, Masterflex tubing 14
pH control pump	UCT custom made peristaltic pump
Electric stirrer (carbonate tank)	Heidolph, with 5cm impeller
pH meter	Microprocessor Hanna pH212, with a HI 1131 probe

Table 5.1: Experimental equipment

5.1.1 Reactor design

The pellet reactor consisted of a vertical cylindrical glass vessel, 1m high and 0.025m ID (Table 5.2) sealed from the atmosphere (Figure 5.1). The inlet flow distribution mechanism at the bottom of the column consisted of a conical glass fitting incorporating a plastic nozzle with large holes. The sealing of this fitting onto the column was assured by two grippers and was further reinforced by a silicon gel joint. This fitting was filled with glass beads of decreasing diameters that allowed uniform distribution of the upward flow, avoiding any unwanted phenomenon of channelling through the bed, and thus any short-circuiting in the reactor. Plug-flow conditions are obtained in the reactor (Van Weert *et al*, 1993).

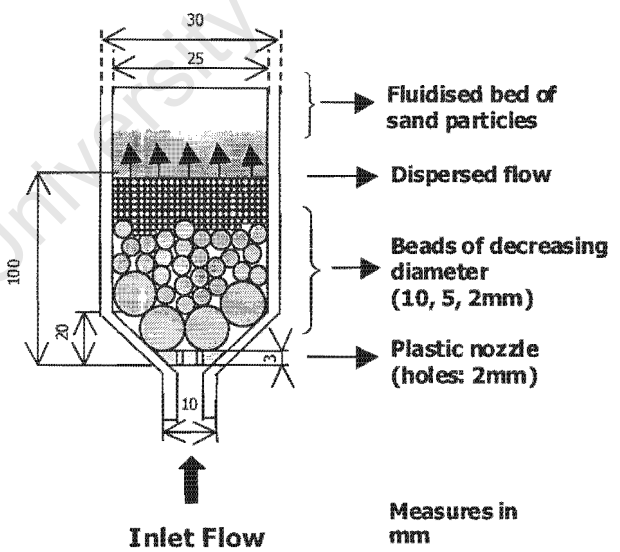

Figure 5.2: Pellet reactor inlet nozzle

The bed of beads also acts as a buffer to regulate the dissipation energy of the aqueous flow entering the reactor. As a result, the pellet abrasion at the foot of the column is reduced when compared with the effect of a nozzle with spaced holes, or the side blow inlet used by Seckler, 1994. The mesh of glass beads also provides a support for the seeds (Figure 5. 2) when the bed is not operated. A crushed glass mesh of 0.5mm porous size

was formerly used, but presents major drawbacks: the flow was not dispersed enough and channelling of the bed was observed. Therefore the scaling of the mesh was rapid due to its large surface area available for nucleation, crystal growth and agglomeration of the precipitate. A significant pressure drop through the mesh was recorded, and was increasing rapidly as it blocked. Finally, the use of such a glass mesh was not practical for a continuous operation of the reactor.

Column	Height (m)	1
	Diametre (m)	2.50E-02
	Surface XS (m^2)	4.91E-04
Bed at 0-flow	Height (m)	0.6
	Volume (m^3)	2.95E-04
	Mass (kg)	4.22E-01
	Bed Density (kg/m^3)	1434
Quartz	Absolute Density (kg/m^3)	2643
	Particles size ave. (mm)	250
Pellet at Steady state	Absolute Density (kg/m^3)	2300
	Particles size ave. (mm)	500

Table 5.2: Reactor and bed properties

The reactor was filled with sand of a narrow particle size distribution ranging from 50 to 70 mesh, which corresponds to a range from 210 to 290µm. The average surface provided by the seeds at steady operation was relatively large, estimated at around 3600m^2 per litre of bed. As a result of the small particle size of the pellets the surface area on the pellet was quite large. The shape of the sand particles was assumed to be spherical. The composition was white quartz sand mixed with calcite and aragonite (XRD analysis). The height of the bed at rest was 60±5cm, and reached a maximum of 87cm when operated. This height corresponds to the maximal depth of the bed without blowing the seeding material out of the bed (pneumatic transport of the particles). The characteristics of the bed are presented in Table 5.1.

Up to three possible inlets existed for the carbonate solution on the side of the column. Each inlet was controlled with a separate valve, and consisted of a steel tube, 1mm ID. The inlets were spaced every 10cm starting 15cm from the bottom of the bed. The major aim of this dispersal was to lower the supersaturation level at each inlet point, and to disperse the supersaturation effect.

Seven sampling points (10mm OD) were spaced every ten centimetres from the bottom of the column (Figure 5. 1). The outlet points allowed the withdrawal of solution as well as pellets from the reactor at different heights. At the top of the column, there were two similar outlets (glass tube of 10mm OD), that were used for the re-circulation flow and the reactor outlet.

5.1.2 Mixing and re-circulation

Two peristaltic pumps were operated separately, one for the re-circulation flow and the other for the waste stream (Figure 5.1). The re-circulated flow consisted of a part of the clean effluent separated before the final outlet mixed with the waste stream flow before re-circulating it on the plug flow reactor. The mixing point of the two flows was situated just before the "inlet flow" point located on Figure 5.2 and the mixing was achieved by a "T" mixer (Figure 5.3) in order to improve the mixing of the two flows at a meso scale. Thereafter dispersion in the bed of glass beads and the fluidisation effect provided micro-mixing by allowing a mixing of the incoming solutions at a molecular scale. Moreover the fluidising flow had two important characteristics, which were the composition homogeneity on the radial axis and the regular dispersion in the reactor.

The distance between the T-mixer and the entrance to the reactor was reduced to its minimum to prevent an excess of fines precipitating before the presence of seeding material in the bed. This phenomenon was induced by the presence of carbonates and hydroxides in the re-circulated flow that consequently generated a high supersaturation before the inlet of the mixed flow in the reactor when mixed with the waste nickel stream.

The minimum fluidisation velocity was calculated for pellets of 500µm volume diameter measured with a Scanning Electron Microscope (SEM) technique, and their absolute density was measured after 10 days continuous operation (lower than the pure quartz density, Table 5. 2). Using equations 3.3 and 3.4, U_{mf} and Re_{mf} are calculated:

$$U_{mf} = 0.0055 \frac{\varepsilon_{mf}^3 d^2 (\rho_p - \rho_f) g}{(1-\varepsilon_{mf})\mu} = 0.188 cm/s$$

$$\mathrm{Re}_{mf} = \left(\frac{U_{mf} d \rho_f}{\mu}\right) = 0.94$$

with: $d=500.10^{-6}$m, $\varepsilon_{mf}=0.4$, $\rho_p=2300$kg/m^3, $\rho_f=997$kg/m^3, $\mu = 10^{-3}$kg/m^3/s

The corresponding minimum fluidisation velocity Reynolds number (Re_{mf}) has a value of 0.94 and the flow is laminar (Re below 2). The U_{mf} value is less than those recorded in the literature (Scholler *et al*, 1987) for sand fluidisation, as a result of the small particle size of the seeds used, and the drop of density due to the coating of the pellet.

The experimental flowsheet is drawn in Figure 5.3 and shows the operating conditions. During the operating of the reactor the waste stream flow rate was set as a constant and the re-circulation stream controlled the variations in the upward flow velocity. The characteristics of the flows have been calculated in Table 5.3 for the different re-circulation ratios that were used during operations. In any case the calculated Reynolds numbers indicate a laminar flow.

Fluidisation was achieved mainly through the re-circulation flow rate (RR), which is defined as the quotient of the re-circulation flow over the waste stream flow (equation 3.8). The maximum RR used was 1.66 to the inlet stream corresponding to the maximal experimental depth of the bed. The minimum experimental RR was 0.7, corresponding to an upward flow of 4.6mm/s. This flow rate was the bottom limit for proper operating

of the column. A phenomenon of intense scaling and even cementing of the pellets at the bottom of the reactor was observed when operating at smaller RR. The mixing intensity was then insufficient to break the agglomerates of pellets especially at high supersaturation (high pH, nickel load and carbonate ratio). Severe channelling of the bed was related to the blockage of the column. In the worse case the pressure before inlet can increase to a level at which all the inlet systems can be damaged.

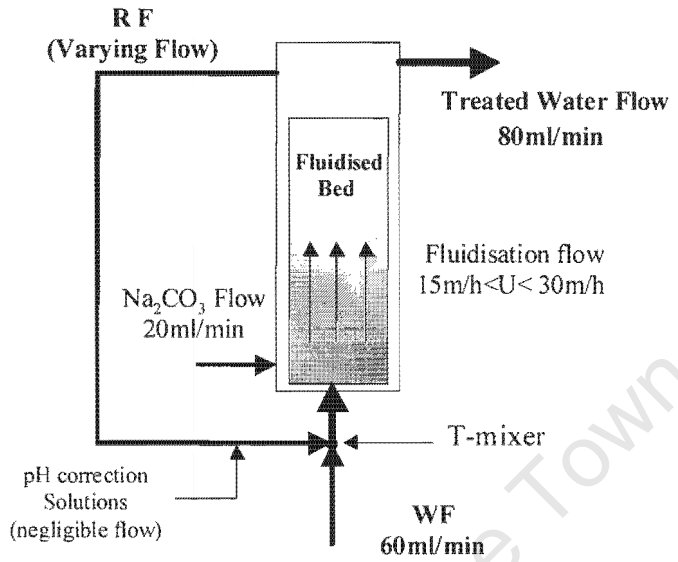

Figure 5.3: Experimental flowsheet

WM pump* grad	*RR flow rate* ratio	*RR flow rate* mL/min	*Total flow in column* mL/min	*Upward velocity* m/s	*Bed height* m	*Residence time in bed* min	*Re*
0	0	0	80	0.0027			1.35
30	0.7	55	135	0.0046	0.71	2.57	2.29
50	1.1	91	171	0.0058	0.79	2.27	2.89
70	1.6	129	209	0.0071	0.86	2.02	3.54

*Watson Marlow 505s

Table 5.3: Experimental flow characteristics

5.1.3 Particle size profile

During reactor operation, the coating of the pellets by the precipitate was responsible for a change in the particle size distribution of the pellets as well as a change of their density. A gradient in the particle size was observed through the height of the bed, while operating the bed under continuous condition, as the heaviest particles, which were less lifted by the fluid, settle at the bottom of the bed. The biggest particles were then removed from the reactor and new seeding material added. The average particle size distribution of the pellet reached a relative steady state, estimated around 500µm diameter (measured using SEM) as a result of the combined effects. It was then possible

to evaluate the total active surface of the pellets in the reactor to be 3 600m^2 per litre of bed.

5.1.4 pH control

The operating pH varied between 9 and 11 and was maintained by addition of hydrochloric acid or sodium hydroxide base in the re-circulation loop in order to allow an instantaneous mixing of the pH liquors with the bulk of the solution. A pH probe (Hanna HI 1131, Table 5.1) was situated at the top of the column allowing continuous monitoring of the system pH (pH-meter Hanna Microprocessor pH212, Table 5.1). The pH measured at the top of the reactor was of primary importance for the interpretation of the precipitation mechanisms. It corresponded to the equilibrium pH of the solid phase with the soluble nickel still in solution in the experimental condition. Some overall pH profiles of the bed were also established in order to study the evolution of the pH during the precipitation process. The pH pump was a UCT custom-made pump (Table 5.1) tuned by hand that allowed very small flow rates. The pH adjustment solutions were 0.01 to 0.1 molar of hydrochloric acid and sodium hydroxide (diluted with distilled water to avoid precipitation of metal hydroxides in the case of the base solution). The pH was considered constant when it fluctuated over a range of 0.05pH units around the desired value. Under normal operating conditions the operating pH was very stable because of the buffering effect of the carbonates and the re-circulation flow. Some problems of stability of the measurement and interference were encountered when using a BNC extension cable for the probe.

5.2 Experimental procedure

5.2.1 Background

The different parameters of importance investigated during the runs were: pH, re-circulation ratio, nickel concentration of the stream, carbonate to nickel ratio (by adjusting the carbonate mother solution concentration) and the influence of multiple feed points to the column. The other parameters like the nickel and carbonate solution flow rates were kept constant. The reactor was operated at a pH ranging from 9 to 11, corresponding to the lower solubility of the product (Figure 4.5). The temperature during operation was monitored, but not controlled and the operating range was 25 ± 4°C.

For each experiment the same mass load of pellet was used in a continuous process, where the five different variables were set and the bed given half an hour to stabilise after the stabilisation of the pH (maximum 0.05pH unit away from the desired value), before taking any measurements. Thereafter the samples were taken either from the points on the side of the column (for the profiles) or from the outlet in order to measure the process removal efficiency. During the runs the following values were monitored at each sampling time: temperature of effluent, height of the bed and the addition of acid or base. The pH of the solutions of nickel and carbonate were monitored with each experiment. Tap water analysis aiming at monitoring the concentration of carbonate, nickel and various ions were carried out every week. The nickel concentration of the tap water used was always below 0.1ppm, the detection limit of the AA technique.

The aim of the successive continuous runs was therefore primarily to establish bed profiles (total and dissolved nickel concentration, pH, carbonates, supersaturation), and to develop an understanding of the precipitation phenomena within the reactor, as a function of the five parameters influencing the process efficiency (listed above). Subsequently an experimental Response Surface Methodology (RSM) was designed and carried out in order to evaluate the relative influence of the parameters on the optimisation of the nickel recovery.

5.2.2 Start-up and shut down

When operating with new sand particles for the first time, a "start up" was run for at least 48H of continuous operations, to allow a first layer of nickel hydroxy-carbonate to cover the seeds. The total and dissolved nickel concentration in the outlet was monitored to confirm that the process had reached a steady state. During start up the increase of the particle size coupled with bed expansion was monitored and some of the initial seeds were regularly removed to maintain the bed height in the operating range. The decrease of the pellet surface within the reactor was important before reaching steady state.

Some runs were also operated to evaluate the reactor behaviour after shut down of the reactant concentration inlets. The carbonate and nickel solution feeds to the reactor were replaced by pure water in order to prevent any changes in the upward flow velocity in the reactor. The pH control pump was tuned to maintain a constant pH. Some samples were then taken from the outlet stream over a period of two hours, to analyse the changes in concentration induced. These runs allow an approximation of the response time of the reactor as well as an indication of the pellet attrition during the process.

5.2.3 Multiple start effect

At certain times between two different sets of experiments the reactor was not used for a relatively long time (often a week), without changing the seeding material and operating a new whole start up experiment when re-starting the reactor. When the re-circulation and feed flows were shut for a sufficient time, a white sludge precipitate was formed in the unseeded solution above the bed, and settled on top of the bed on an uncompacted sludge layer. This formation proves that equilibrium conditions were not entirely met through the bed depth and that very slight supersaturation still existed above the bed and was sufficient to induce growth of the precipitate present in the liquid medium. Another further precipitation phenomenon was observed on the walls of the reactor where a fine layer of dense and solid precipitate grew over the time. When starting up the reactor again these two phenomena were a source of problems. The fine sludge was blown upwards by the current, and parts of the wall-covering precipitate were detached and reduced to small "plates" with the abrasion effect of the fluidised pellets (Figure 5.4). The plates, depending on their densities, were either expelled to the re-circulation or the outlet, or settled on the top of the bed where they were slowly reduced to finer plates eventually transported by the flow. This phenomenon could be called the "multiple starts effect", and caused the outlet nickel concentration to be widely variable until all plates and sludge had disappeared from the reactor. The process then reached steady state, and new experimental runs could be carried out. Note, that the formation of plates and interference with the removal process, was due to a large "wall effect" of the laboratory

scale reactor. In industrial operations, where the ratio wall surface to bed surface is much smaller this multiple start effect would not have the same impact on the efficiency of the process. A filtration stage would also limit it.

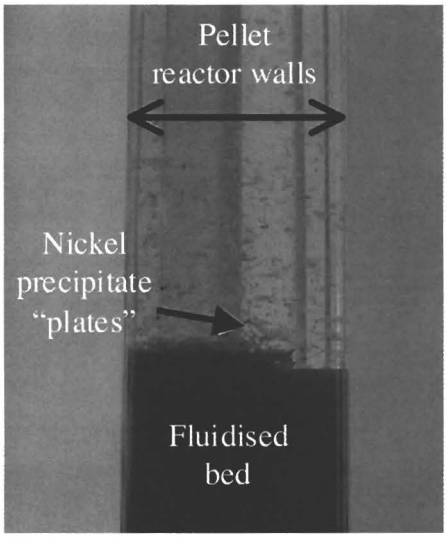

Figure 5.4: Illustration of the multiple start-up effect

5.3 Reagents

Precipitation was achieved by mixing a pure nickel sulphate solution with sodium carbonate.

The synthetic nickel solution fed to the reactor had a concentration of 50-150ppm of nickel ($8.5*10^{-4}$ - $2.6*10^{-3}$mol/L) depending on the experiment. This corresponded to a nickel load of 367 -1098g/h/m^2 reactor XSA. The solution was prepared with nickel sulphate hexa-hydrate (MM=262.8g/mol) grade 1 or hepta-hydrate (280.88g/mol) grade 2 accurately weighed in the laboratory (Balances Instrulab Precisa 205A and 3100C) before dissolving with tap water containing less than 0.1ppm of nickel and 8.10^{-4}mol/L of carbonates. The concentration of nickel in the mother solution was measured with Atomic Adsorption technique for every run, using a Spectrophotometer Varian SpectroAA30 and 110. Regarding the relatively high nickel concentration of the solution the pH of the mother solution was adjusted and maintained below 7.5 in order to prevent any hydroxide precipitation before operating. Two tanks of 100L and 25L were used depending on the duration of the run. Intense stirring was applied (electric stirrer Heidolph, Table 5.1, 300RPM) when preparing the liquor to ensure homogeneity.

The carbonate solution had a concentration of $2.8*10^{-3}$ - $3.4*10^{-2}$ mol/L of carbonate. This corresponded to a relative carbonate to nickel ratio of 1:1 to 1:4 when fed to the reactor. The carbonate used was anhydrous sodium carbonate (MM=105.99g/mol). A 20L tank was used during the operation, and continuous stirring was provided to avoid excessive decrease of concentration via re-crystallisation of the sodium carbonate. The mother solution tank was sealed from the atmosphere to prevent any carbon dioxide exchange. The carbonate concentration of the mother solution was measured for every run using titration techniques (described in Appendix 5). The carbonate concentrations

of the effluent and of the tap water were checked in order to carry out an approximate carbonate mass balance over the process, and thus to monitor the amount of carbonate consumed in the precipitation reaction. The balance was then:

$$C_{mother\_CO3} \times Q_{CO3} + C_{tap\_water\_CO3} \times Q_{Ni} = n_{CO3\_ppt} + C_{effluent\_CO3} \times (Q_{CO3} + Q_{Ni}) \quad (5.1)$$

The flow rates of the nickel and carbonate solutions were constant: Q_{Ni}=3.6L/h and Q_{CO3}=1.2L/h. The calibration of the peristaltic pumps (Masterflex Consoledrive 6-600RPM, with pump heads 14 and 16) were checked every two months and occasionally the tubing replaced.

The pH solutions were prepared 1 litre at a time. The concentrated hydrochloric acid 30% in mass was diluted in distilled water, and the sodium hydroxide pellets were approximately weighed and dissolved in distilled water. Standard solutions with very precise concentrations were only used for titration purposes.

All the chemicals were furnished by the Associated Chemical Enterprise (ACE) (PTY) ltd. The chemical safety data sheets can be found in Appendix 2.

5.4 Analysis

5.4.1 Sampling

Samples were taken from the side of the bed and from the top outlet. These were used to determine the nickel removal efficiency as well as to establish concentration and pH profiles of the fluidised bed. For every sample drawn from the column half the volume was filtered using a 0.45µm filter syringe just after the catchment, thus reducing the filtering time to a minimum. The other half was left as drawn. A comparison of the total and dissolved nickel was then possible with the equation 5.2 linking the total nickel, dissolved nickel and fines concentrations.

$$Ni_{tot\_out} = Ni_{dis\_out} + Ni_{fines\_out} \quad (5.2)$$

The two half samples were thereafter acidified with 5 drops of hydrochloric acid 0.1 M to prevent further precipitation and to allow the re-dissolution, or digestion of the fines.

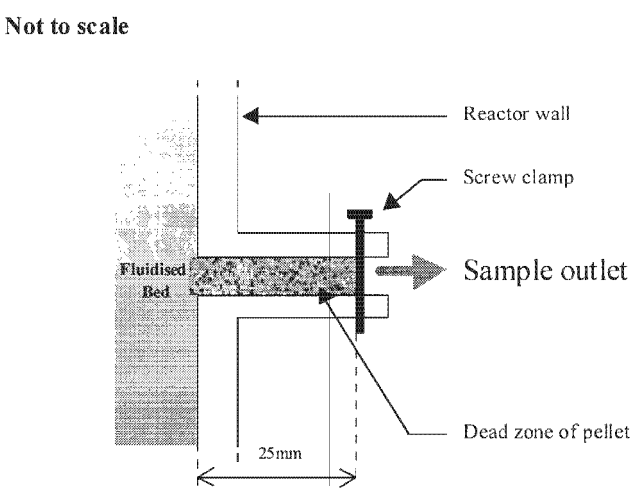

A description of the sampling points on the side of reactor is given in Figure 5.5. The sampling outlet was controlled by a screw clamp that can be operated manually. The pellet "dead zone" corresponds to a volume of pellet that was never fluidised in the bed and not in contact with the bulk solution. The scaling was important in this section. A volume of solution equivalent to two times the dead zone volume was drawn from the column before taking any sample.

Figure 5.5: Sampling points description

Before taking any readings and sample, the reactor was operated for at least half an hour at constant parameters (including pH) in order to reach steady state. Four times two samples (four filtered and four non filtered) were then taken for every setting of parameters, spaced every 10 minutes and the analytical results averaged. The same sampling procedure was maintained during all the runs. For each sample, the temperature of the effluent was measured together with the exact pH and the height of the fluidised bed.

5.4.2 Analytical methods

The analysis of the nickel samples was carried out using Atomic Adsorption Spectrophotometry (AAS). The carbonate concentrations were determined by two different titration techniques: colourimetric titration with a 0.1N hydrochloric acid standard solution combined with a mixed indicator (methyl orange – indigo carmine); and a pH-metric method using the same titration standard. The analyses of the pellets were carried out using XRD, XRF and SEM techniques, as well as a titration technique developed experimentally.

5.4.2.1 Carbonate Titration

The carbonate pH-metric titration technique is described in Appendix 5. The procedure used a 0.1 molar hydrochloric acid standard titration aiming at measuring the total alkalinity of the solution (Lowenthal, 2000). A Hanna pH-metre pH212 was used in correlation with a mixed pH indicator (methyl orange – indigo carmine). This method gave very accurate results in comparison with the quick and simple colorimetric titration, as the equivalent point volume was measured as the result of five different pH measurements, and not related to the subjectivity of a pH-indicator colour change.

Carbonate titration was carried out mainly to check the mother liquor concentration. It was also measured as an indicator of the precipitation of nickel carbonate, when carrying out the carbonate molar balance of the system (considered closed to the atmosphere). The calculations are shown in Appendix 5.

5.4.2.2 Pellet composition

Qualitative Analysis

The determination of the pellet composition was relatively complex. The analyses were first conducted qualitatively to determine the nature of the precipitate phase and its crystalinity as well as the nature of the impurities. X-ray diffraction and fluorescence (XRD and XRF) techniques were used (spectra in Appendix 7). A blank sample composed of the sand used as seeding material was firstly analysed to prevent later misunderstandings of the origin of the impurities present in the precipitate. The precipitate preparation implicated its complete drying (24h in an EcoTherm oven, 150°C) grinding and sieving (80µm sieve). A fine powder was obtained, which was used for analysis. It is important to notice the presence of some sand fines in this powder as a consequence of the grinding process of the pellets. XRD and XRF techniques provided an accurate determination of the powder qualitative composition.

Quantitative analysis

The Scanning Electron Microscope (SEM) analyses were carried out on the dry whole pellets, in order to determine the qualitative composition of the pellet and to provide information on the quantitative ratio between the metallic nickel and the other metallic impurities. A measurement of the thickness of the precipitate layer was also possible.

A method to analyse the precipitate composition was developed by coupling AA spectroscopy and the titration of phosphoric acid used to dissolve the precipitate (Clesceri *et al* (1998); Jeffery *et al* (1989)). The experimental procedure was based on the dissolving reaction of nickel hydroxy-carbonate by phosphoric acid (equation 5.3):

$$2nH_3PO_4 + nYCO_3^{2-} + nXOH^- \longrightarrow 2nH_2PO_4^- + nYCO_2 + n(X + Y)H_2O \qquad (5.3)$$

The procedure described in Appendix 6 was followed and gives relatively reproducible results, but the accuracy of the method was low. Only approximate compositions could be obtained.

Other techniques

The above analytical technique gave a rough approximation of the precipitate composition. If a greater accuracy is needed, Packter *et al*, 1975, have described different analytical techniques for nickel hydroxy-carbonate that encompasses thermogravimetric, differential calorimetry and infra-red spectrophotometry analyses.

Chapter VI

Precipitation mechanisms in the pellet reactor

The aim of this study is to improve understanding of the different precipitation mechanisms that occur in the pellet reactor, as well as identifying a direction for the optimisation of the process by describing the effects of each parameter of importance on the process efficiency. The study was carried out using the laboratory scale reactor described in Chapter V. This chapter presents the results obtained during a first set of experiments, which aim at a general description of the precipitation mechanisms in the pellet reactor, as well as defining the parameters of importance for the overall nickel removal efficiency. The results obtained encompass different important aspects of the process, such as the operation of the reactor, the solubility and composition of the product and the description of the precipitation mechanisms by the establishment of pH and concentration profiles of the reactor.

6.1 Start-up

Several experiments have been carried out in order to characterise the start-up and stabilisation conditions of the pellet reactor. Figure 6.1 and Figure 6.2 are plots of the nickel outlet total and dissolved concentrations versus time. The experiments were run continuously under steady conditions for 48hours, using new seeding material. The conditions under which the two start-ups were carried out were different. They are shown in Table 6.1.

	Experiment number	
Variable	*SU01*	*G01*
pH	10	9.15
Ni_{feed}, ppm	100	50
Ratio	2.5	2
RR, rpm	50	50
MF	2	1

Table 6.1: Experimental conditions of the Start-up runs

In both experiments, $Ni_{dis\ out}$, which had a slightly higher value during the first 10 minutes of the run, rapidly stabilised, and was almost constant during the whole run. The $Ni_{dis\ out}$ concentration was directly linked to the solubility of the product and the equilibrium conditions established in the bed. The solubility changed only slightly with pH during the start-ups and the response stabilised at a value around 5ppm for the run at pH 10, and around 1.5ppm for the run at pH 9.15.

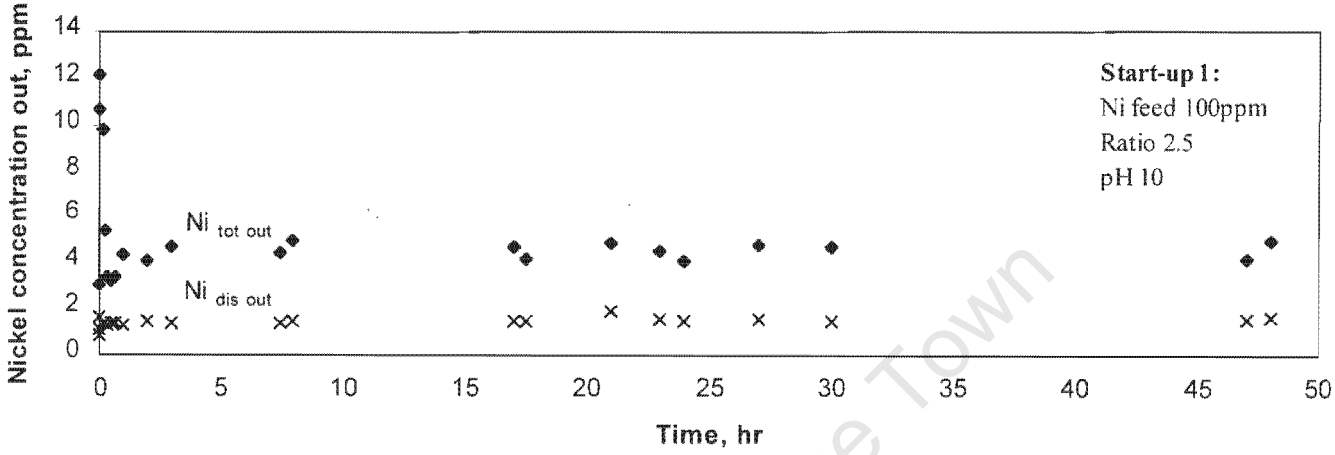

Figure 6.1: Experiment Start-up 1 (SU01) of the pellet reactor, $Ni_{dis\ out}$ and $Ni_{tot\ out}$ versus time (hr)

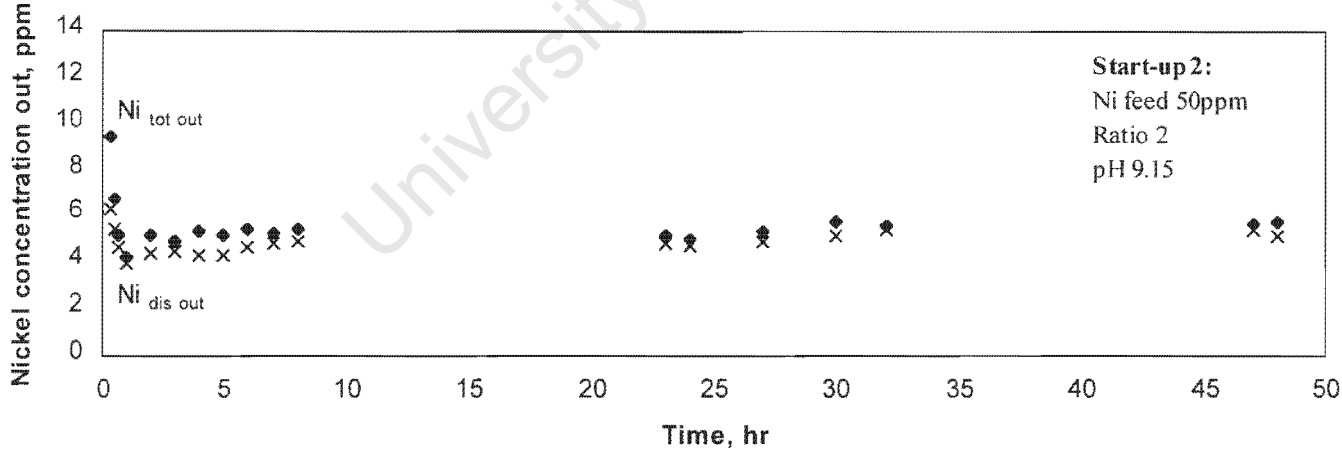

Figure 6.2: Experiment Start-up 2 (G01) of the pellet reactor, $Ni_{dis\ out}$ and $Ni_{tot\ out}$ versus time (hr)

The $Ni_{tot\ out}$ concentration encompassed the $Ni_{dis\ out}$, as well as the fines in the outlet (equation 5.2). In both runs, the $Ni_{tot\ out}$ concentration within the first 20 minutes was high starting at 9.41 (experiment SU01) and 12.2ppm (experiment G01) respectively from their initial concentration. The nickel fines tended to block the filter when taking the $Ni_{dis\ out}$ sample. The total outlet concentration rapidly decreased after the first 20

minutes to reach steady state after 1 hour of experimentation. No major variations were noticed until the end of the runs. During the first start-up, the $Ni_{tot\ out}$ concentration stabilised around 5.5ppm, and around 4.5ppm for the second start-up. A large difference in the fines concentration during the 2 start-ups was observed: 0.5ppm of nickel fines for the run at pH 9.15, and 3ppm for the one at pH 10.

During the two start-ups the height of the bed was also measured. The runs were operated under constant conditions, and no pellets were removed during the 48 hours of the experiment. A linear increase of the bed depth was recorded as shown in the Figure 6.3.

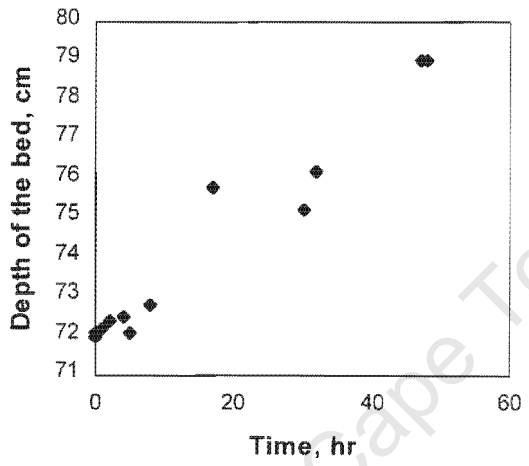

Figure 6.3: Depth of the bed (cm) versus time (Hr) during the experiment G01.

During the 48 hours of the start-up, the width of the precipitate layers remained small (<5μm). The bed depth increase cannot only be linked to the overall increase of the pellet size. The other phenomenon observed was the pellet density change, related to the increasing width of the precipitate coating layer (from 2643kg/m^3 for raw quartz to 2300kg/m^3 for the nickel hydroxy-carbonate pellet). The particles of lower density were therefore more entrained by the fluid.

6.2 Feed shut down

In order to measure the influence of the pellet attrition on the process the nickel and carbonate feed were shut down at time t=0, and the feeds were replaced by pure tap water in order to keep the same flow rate through the reactor. The pH was kept constant by adding sodium hydroxide via the pH control pump. In Figure 6.4, two "nickel attrition" runs are plotted: $Ni_{dis\ out}$ and $Ni_{tot\ out}$ versus time, after shutting the reagent inlets. One experiment was recorded after the experiment S34, while the second one after the experiment SC14 (Table 6.2).

Variable	Experiment number S34	SC14
pH	10.5	10
Ni_{feed}, ppm	150	100
Ratio	4	2.5
RR, rpm	70	50
MF	1	2

Table 6.2: Experimental conditions of the feed shut down runs

A relatively constant, slowly decreasing dissolved nickel concentration was observed during the two experiments, reaching a value of 0.5ppm after 2 hours of blank run. This value was likely to correspond to the equilibrium solubility of the precipitate, and thus to the re-dissolution of the pellet because of the introduction of pure water into the column.

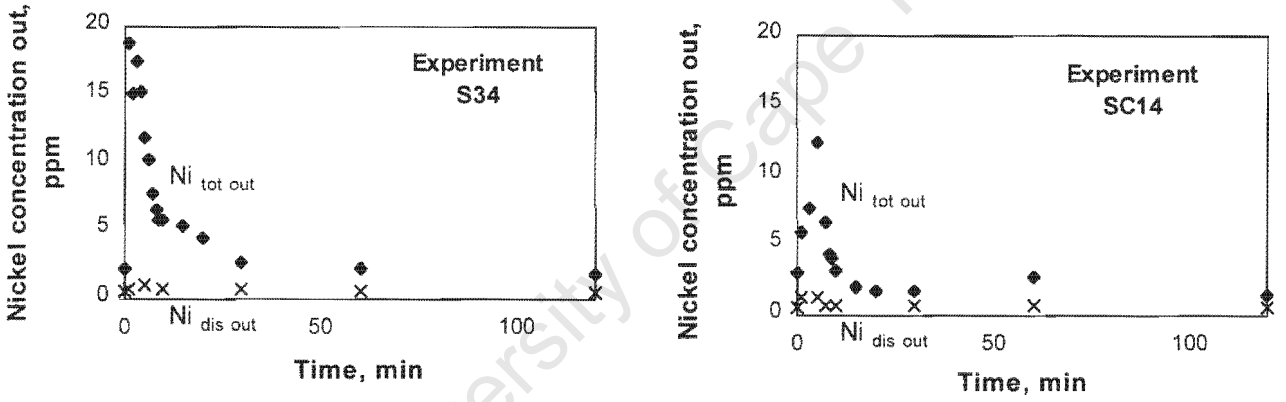

Figure 6.4: Nickel concentrations out versus time after shut of nickel and carbonate outlet. Experiments S34 and SC14

In both cases, a large peak of total nickel was observed. Both peaks reached a maximum within 4 minutes after the shutting off of reagent feed. The response to the reactant shut down was firstly not instantaneous, due to the draining time of the nickel and carbonate pipes. On average, the draining time of the nickel pipe (3m, 1cm ID) was 1min 40s, whereas that of the carbonate pipe (1.2m, 1cm ID) was 40s. According to these simple calculations, the responses to the inlet shut off were not synchronised: the nickel's feed lasting one minute longer than the carbonate. Although a large increase in the total nickel outlet was observed, the extra one minute addition of nickel in the reactor did not appear to influence the dissolved nickel outlet. This phenomenon could be interpreted by the fact that a large amount of sodium hydroxide was introduced into the reactor through the pH regulation pump, in order to balance the rapid carbonate concentration drop and keep the pH constant. The nickel then precipitated with the hydroxide, forming a large amount of fines not likely to agglomerate on the pellets.

The $Ni_{tot\ out}$ then rapidly decreased and reached a steady level after 30 minutes of blank run. The stabilisation value was below 2ppm of total nickel in the outlet. This amount was composed of 0.5ppm of dissolved nickel, and the balance of fines. A difference of 0.6ppm was observed between S34 and SC14. As the dissolved nickel concentration was low, no or extremely low supersaturation occurred, and the formation of the fines by spontaneous primary nucleation was negligible. The fines formed after nickel shut off were thus produced mostly by attrition, and the difference between the nickel total and dissolved gave a measurement of the attrition magnitude in the pellet reactor under the specific operating conditions.

6.3 Comparison of theoretical versus observed solubility

Figure 6.5 and Figure 6.6 show a comparison of the theoretical Paterson *et al* (1982) model (Figure 4.5) and actual nickel carbonate solubilities.

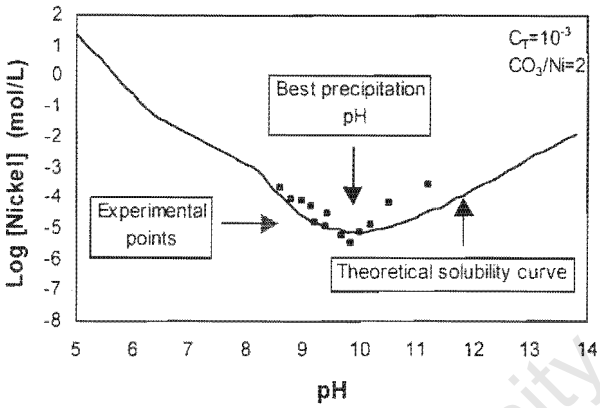

Figure 6.5: Solubility for – $C_t=10^{-3}$mol/L and CO_3 to Ni mole ratio = 2

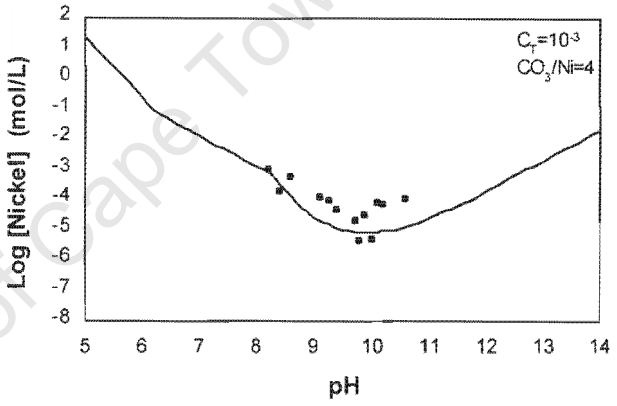

Figure 6.6:$C_t=10^{-3}$mol/L and CO_3 to Ni mole ratio = 4

These data were collected for CO_3 to Ni ratios 2 (Figure 6.5) and 4 (Figure 6.6). It can be seen that, for a ratio of 2, there was relatively good agreement between the experimental points and the theoretical solubility curve from pH ≈ 8 until pH ≈ 10.5. Above a pH of 10.5, the experimental points lay significantly above the theoretical solubility curve. For the experimental points collected for a ratio of 4, a discrepancy with the theory was observed over a much larger pH range, starting at a pH of 8.5. The optimal removal was obtained at a pH of 9.8 irrespective of the C_T to nickel ratio.

6.4 Optimal precipitating pH

Figure 6.7 and Figure 6.8 show the effect of pH on nickel removal efficiency (equation 3.9), nickel conversion (equation 3.10) and fines formation (equation 3.11) during two sets of experiments at carbonate to nickel ratio: 2 (Figure 6.7) and 4 (Figure

6.8). The fines concentration is plotted on the figures as percentage of introduced nickel (equations 3.9 to 3.11)

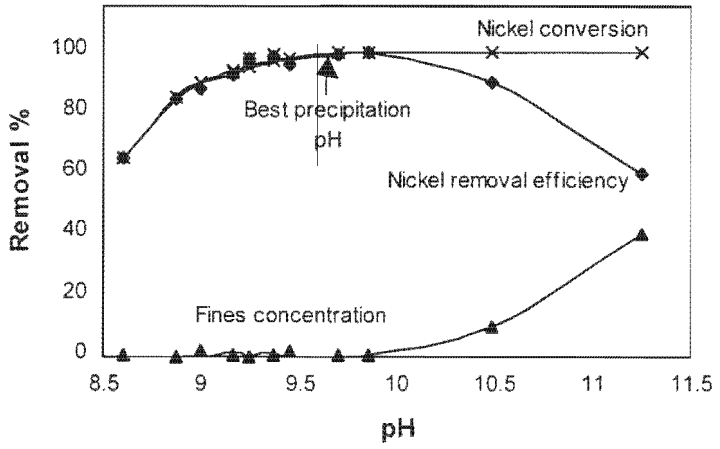

Figure 6.7: Process efficiency as a function of pH– $C_t = 10^{-3}$ mol/L and Ratio = 2

From the Figures 6.7 and Figure 6.8, it is apparent that nickel conversion increased steadily with increasing pH until pH ≈ 9.8 and then levelled out at a value of 100% for both ratios. The curve for the nickel removal reached a maximum at pH ≈ 9.8 for both experiments. Firstly, the removal increased with increasing pH and thus increasing nickel conversion, and reached a peak of 99.6% (ratio 2) and 97.2% (ratio 4) at pH ≈ 9.8. Thereafter, the efficiency decreased again with increasing pH, and the fines appeared in the outlet. The fines concentration was minimal until pH ≈ 9.8, whereafter it began to increase, reaching its maximum value of 40% (ratio 2) and 20% (ratio 4) coinciding with the maximum measured pH value. In contrast to ratio 2, fines remained in the outlet over the whole pH range of the ratio 4 experiment.

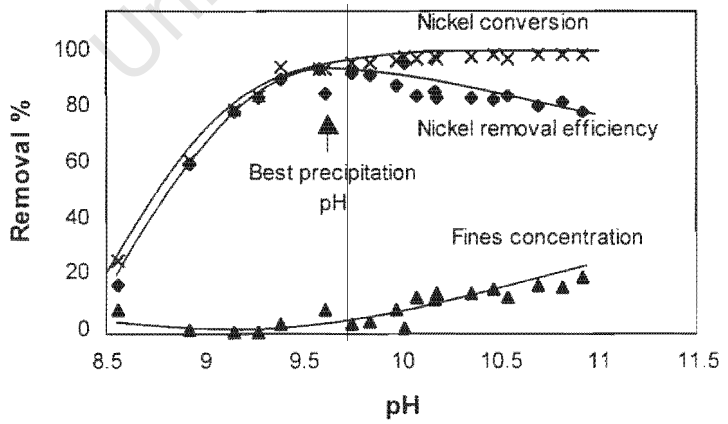

Figure 6.8: Process efficiency as a function of pH – $C_t = 10^{-3}$ mol/L and Ratio = 4

6.5 Bed profiles

6.5.1 Dissolved Nickel profile

Figure 6.9 shows a plot of the $Ni_{dis\ out}$ reactor profile. Each line was measured during a different experiment, working at fixed outlet pH's of 9.15, 9.75 and two runs at 10.5 respectively. In each case, the decrease in the dissolved nickel concentration occurred within the first 20cm of the bed after which the concentration reached a relatively steady level as the soluble nickel reached its solubility limit. The dissolved nickel concentration stabilised at: 4.6ppm at pH 9.15, 0.85ppm at pH 9.75, and an average of 0.5ppm for the 2 runs at pH 10.5. The steeply negative slopes of the dissolved nickel concentration curves show the fast kinetics of the precipitation reaction. For this case, the slopes were very similar for the 2 runs at pH 9.15 and 9.75 and the 2 runs at pH 10.5.

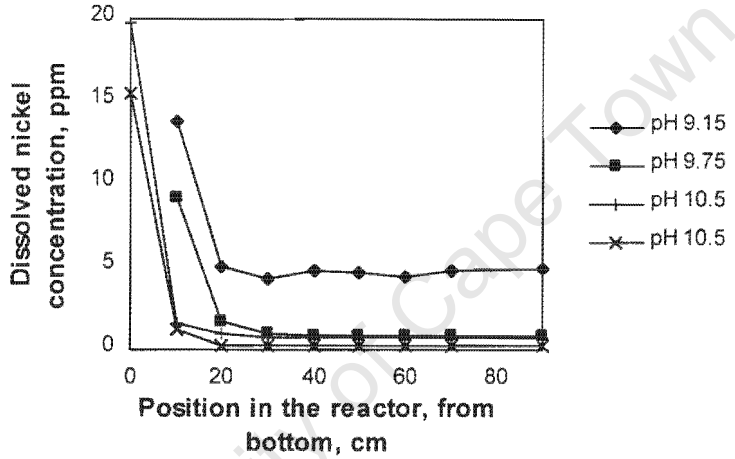

Figure 6.9: [Ni] dissolved profile within the fluidised bed

The average of the runs at pH 9.15 and 9.75 was a loss of 0.81ppmNi per centimetre of bed and 1.62ppmNi/cm for the runs at pH 10.5. The equilibrium with the solid phase was reached a few seconds after the mixing of the reactants, and no further significant conversion was measured upwards in the bed.

6.5.2 Total nickel profile

Similarly to the previous profile plot, each curve represents on Figure 6.10, a depth profile drawn for a different experiment with different operating conditions. The $Ni_{tot\ out}$ profiles were taken at different pH: 9.15; 9.2; 9.7; 9.75 and 10.5. Although the general shape was the same for every curve, some deviations occurred. The $Ni_{tot\ out}$, high at the bottom of the bed (up to 60ppm, for the experiment at pH 10.5) rapidly decreased through the first 30cm of the reactor with the fast nucleation and growth of the precipitate on the pellets. Then the concentrations stabilised and decreased slowly upwards in the reactor, with the agglomeration of the fines on the pellets. The rate of

decrease of the total nickel was different in the different runs, and the $Ni_{tot\ out}$ concentration ranged from 0.8ppm (pH 9.2) to 9ppm (pH 10.5), varying with pH.

The profiles drawn were less regular than the $Ni_{dis\ out}$ ones and a large increase in the concentration was noted for 2 runs (pH 9.7 and 10.5) at the top outlet of the reactor. The total nickel concentration therefore appeared more fluctuating throughout the reactor, as it is linked to many more parameters, such as the local supersaturation and the mixing, attrition of the pellet and agglomeration, as well as the dissolved nickel concentration. Also, the total nickel concentration was more difficult to sample and more subject to operating errors.

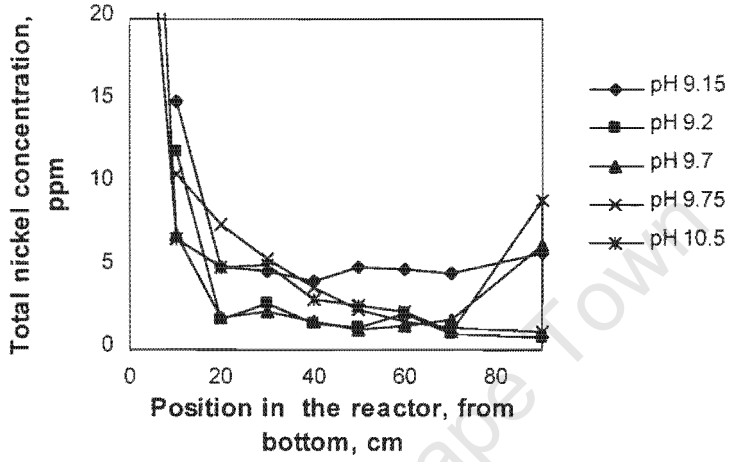

Figure 6.10: [Ni] total concentration within the fluidised bed

Figure 5.5 describes the sampling points used to establish the reactor profiles. The "dead zone" consisted of a 25mm wide layer of pellet that was placed inside the outlet pipe just before the sample outlet. When taking the samples two simultaneous phenomena could occur: attrition of pellets in the dead zone and filtration of the largest fines present in the bulk of the solution by the layer of pellets. Both could lead to a change in the total nickel concentration, but not in the dissolved nickel. The filtration of the fines by the pellet dead zone could explain the reason why, in the runs at pH 9.7 and 10.5, the total nickel concentration suddenly increases at the top of the reactor where the sample was taken directly from the outlet stream without any filtration phenomenon. Another sampling technique should be developed for further study of the total nickel profiles of the bed, or any study on the fines through the bed such as a particle size distribution study.

6.5.3 Nickel profile summary

Figure 6.11 was plotted to give an overview of the importance of the different precipitation mechanisms in the reactor. It describes the dissolved nickel profile, the nickel on pellet profile (which represents the nickel removal efficiency), and the fines concentration profile observed during the experiments S28 (similar profiles were established for the experiment SC11). The nickel introduced has been plotted as a reference. This graphic nevertheless only gives a rough idea of the precipitation

mechanisms since errors could have been introduced due to the lack of reliability of the total nickel concentration sampling method.

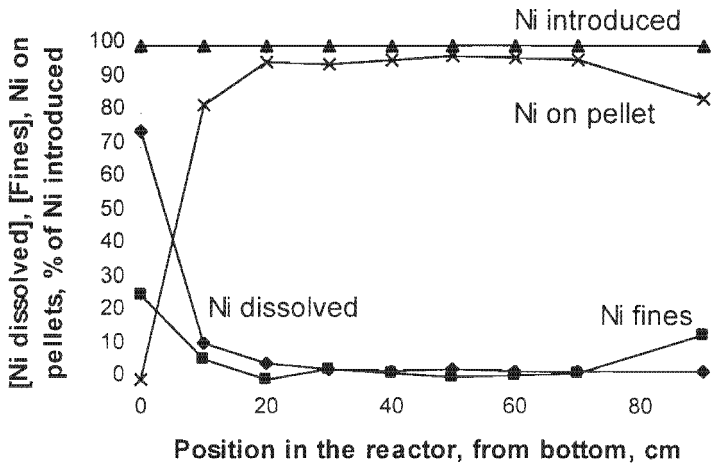

Figure 6.11: Nickel concentration profiles of the reactor (experiment S28)

The carbonate was injected 15cm from the bottom of the bed. The precipitation of the nickel occurred in the first 20 centimetres of the bed (disappearance of the dissolved nickel), and remained constant thereafter, indicating that the dissolved and solid species were in equilibrium. The nickel on pellet curve rapidly increased at the bottom of the bed, and then stabilised around the removal efficiency of the process. A peak in the fines concentration curve was observed at the reactor inlet. Thereafter it decreased and remained constant through the column. The peak in the fines curve corresponded to a fast spontaneous nucleation of particles in the bulk of the solution linked to the supersaturation between the T-mixer and the reactor inlet. The fines concentration thereafter increased again at the top outlet of the reactor and consequently the nickel on pellet curve decreased. This phenomenon was linked to the sampling problem described in paragraph 6.5.2. According to Figure 6.11, the agglomeration of fines played a role in the nickel removal only within the first 20cm of bed, as more than 12% of the nickel precipitated as fines agglomerates on the pellets before the outlet. Through the height of the bed, agglomeration did not seem to play an important role in nickel removal, especially after the carbonate inlet where a peak in the fines concentration was expected, but not observed. In conclusion agglomeration did not seem to play a major role in nickel removal from the waste stream, in comparison to the nucleation and growth of the precipitate on the pellet. The identification and localisation of the agglomeration mechanisms remained nevertheless difficult because of the sampling problem.

6.5.4 pH profile.

Each of the lines drawn on Figure 6.12 represents a different pH set point, which is monitored and controlled through the pH probe at the top of the column. The set points were pH 9.75, 9.4, 9.2, 9.15 and 8.4. For all but one of the set points, the pH values are the lowest at the bottom of the bed. For the set points of 9.75, 9.4, 9.2 and 8.4, the pH profiles experienced a peak at the carbonate injection point, as the incoming carbonate

solution causes the pH to increase. Thereafter, the pH steadily decreases an average of 0.2 pH units through the bed height, due to carbonate consumption by the nickel carbonate precipitation reaction. Contrary to previous observations, this phenomenon indicates that agglomeration does play a role, as supersaturation is gradually consumed up the length of the bed. A corresponding decrease in nickel concentration would be barely detectable over this pH range (see Figure 5.6). For the set point of 9.15, the increase in pH over the height of the bed is much more gradual, with the highest pH value occurring at sample point 4.

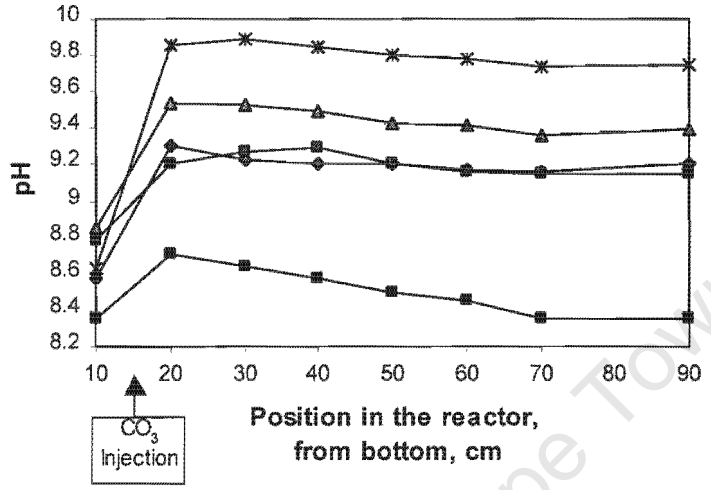

Figure 6.12: pH profile of the reactor. Outlet pH 8.4, 9.15, 9.2, 9.4, 9.75

6.5.5 Carbonate profile

The carbonate concentration profiles were established for three different experiments (Figure 6.13), for the purposes of establishing supersaturation profiles. The experimental conditions were different during these runs, and are displayed in Table 6.3.

	Experiment number		
Variable	*G07*	*G09*	*S34*
pH	9.75	9.15	10.5
Ni_{feed}, ppm	60	60	150
Ratio	4	2	4
RR, rpm	50	50	70
MF	1	1	1

Table 6.3: Experimental conditions of the G07, G09 and S34 runs

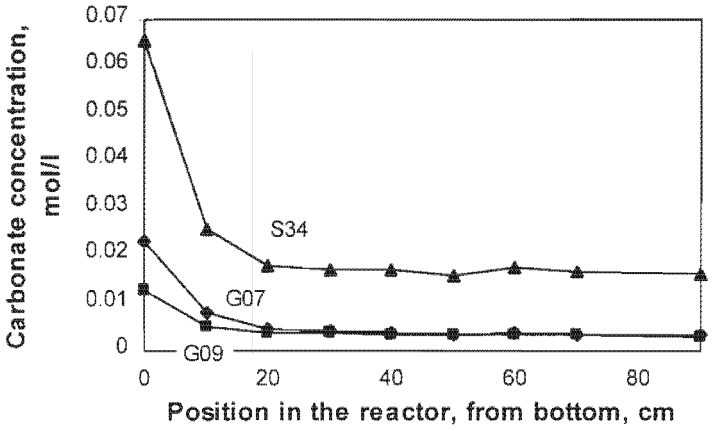

Figure 6.13: Carbonate profile of the bed. Experiments G07, G09 and S34

The point at 0cm corresponded to the concentration at the feed inlet of the reactor. The general shapes of the curves were similar to the nickel concentration profiles. The concentrations decreased rapidly in the first 20 centimetres of the bed, and then stabilised upwards in the bed. The outlet values varied as a function of the different concentrations and ratios reacting in the reactor: $3.4.10^{-3}$mol/L of carbonate in the outlet during experiment G07, $3.1.10^{-3}$mol/L during experiment G09, and $16.3.10^{-3}$mol/L during the experiment S34.

The titration of the carbonates, and an example of the calculations of the carbonate balances calculated are described in Appendix 5.

6.5.6 Supersaturation profile

The supersaturation in the bed is calculated using equation 2.6:

$$\ln \beta = \frac{1}{1+X+Y} \cdot \ln\left(\frac{(Ni^{2+}).(OH^{-})^{X}.(CO_3^{2-})^{Y}}{Ksp}\right) \qquad (2.6)$$

The brackets represent the activity of the ions, but for simplification purposes, activities are replaced by concentrations (low concentrations). The composition of the precipitate (calculated in paragraph 6.6.2) is: $Ni(OH)_{0.67}(CO_3)_{0.67}$, and the K_{sp} solubility constant is calculated for each data point as a function of the pH, using the Patterson *et al* (1982) solubility model (Figure 4.5). The supersaturation profiles of the reactor for the experiments G07 and G09 are presented in Figure 6.14.

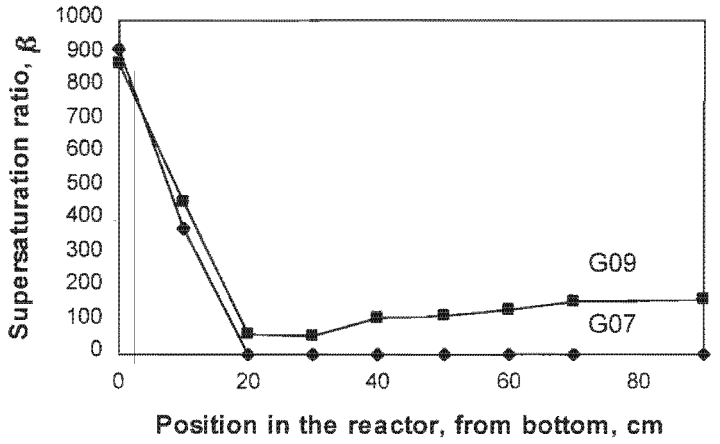

Figure 6.14: Supersaturation ratio profile of the bed. Experiments G07 and G09

During the two experiments, the high supersaturation at the bottom of the reactor rapidly decreased in the first 20 centimetres of the bed, where the precipitation mechanism rates are the fastest. The supersaturation ratio then stabilised, at two very different values: 0 in G07, and 150 in G09.

6.6 Pellet analysis

6.6.1 Qualitative analysis

XRD, XRF and SEM techniques were carried out on the pellets drawn from the bottom of the bed after a 48 hour run.

The following figures show the surface of pellets chosen randomly from the pellets withdrawn from the bed after the run. The pellet was totally coated with green nickel hydroxy-carbonate (Figure 6.15) and the general shape of the sand seeds still apparent, as the layer of precipitate was only 5µm thick (Figure 6.21), measured in a fissure of the precipitate. The precipitate was very dense and the surface of the pellets was smooth (Figure 6.16), probably the result of friction and attrition between the pellets. The layer of precipitate cracked when dried. The precipitate layer surface showed several different aspects from one pellet to another and from one location on a pellet to another. The precipitate on the pellet was identified as mixture of amorphous and crystalline material (Figure 6.17, 6.18, 6.19 and 6.20), and was likely to have slightly different chemical compositions and solubilities. This difference of composition could be linked to different operating conditions in the reactor, pH, supersaturation, hydrodynamics (Seckler, 1994).

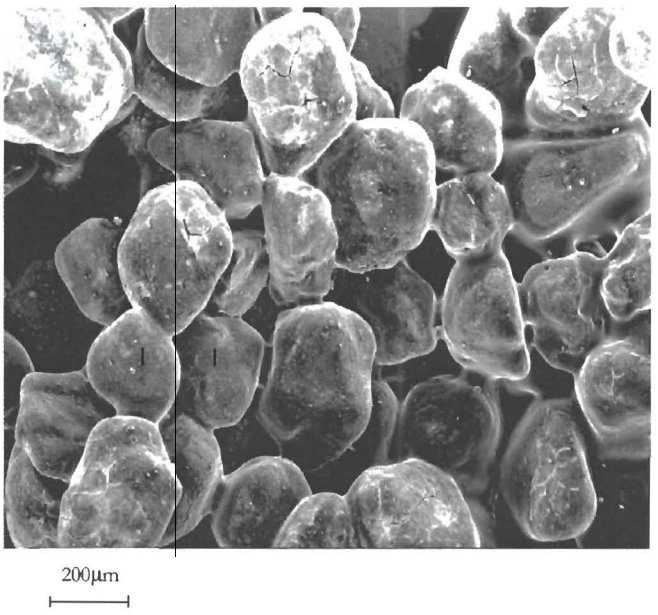

Figure 6.15: SEM pellet sample

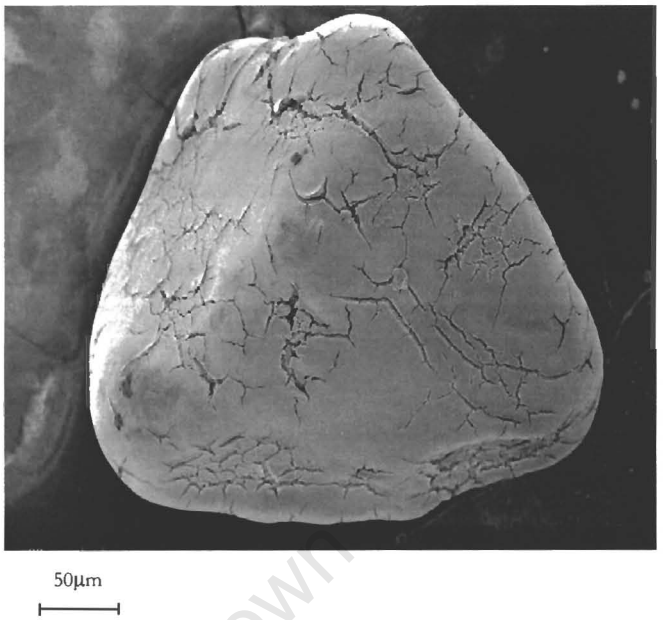

Figure 6.16: SEM view of a pellet

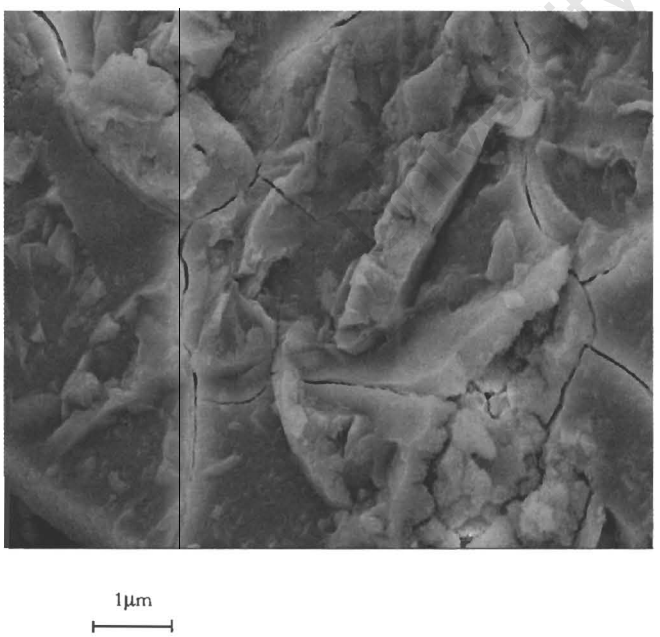

Figure 6.17: SEM pellet surface

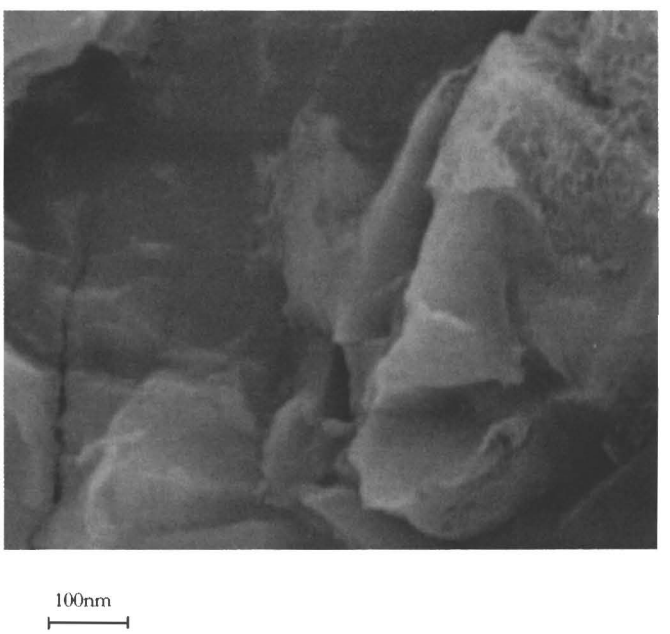

Figure 6.18: SEM Detail of the surface

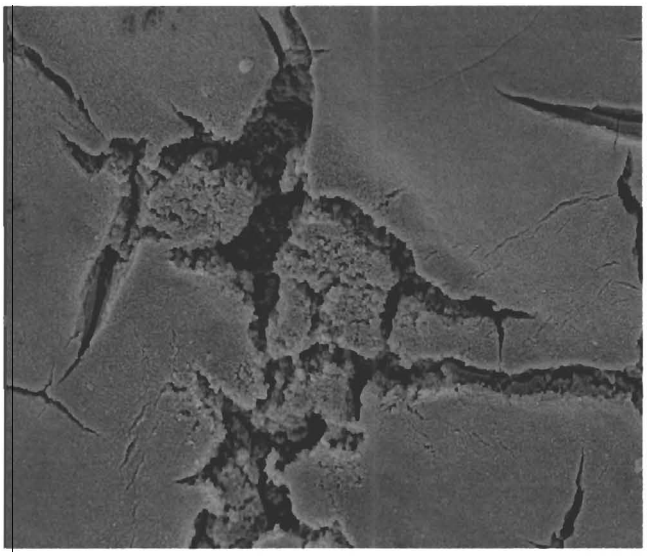

Figure 6.19: SEM view of a crack on the pellet surface

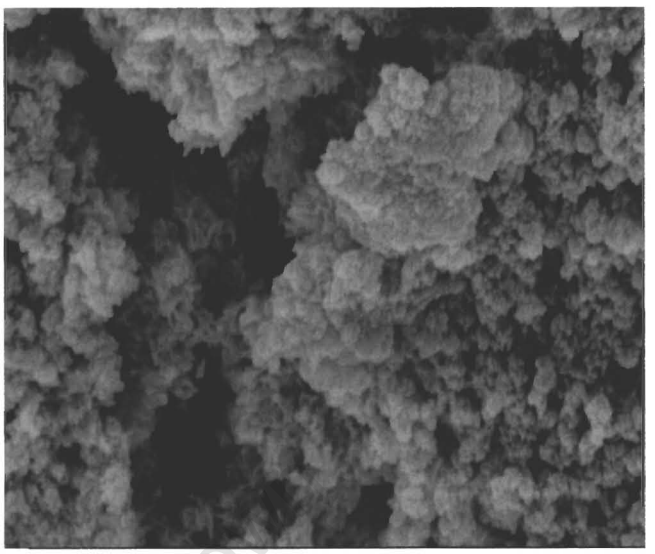

Figure 6.20: SEM detail of the crack

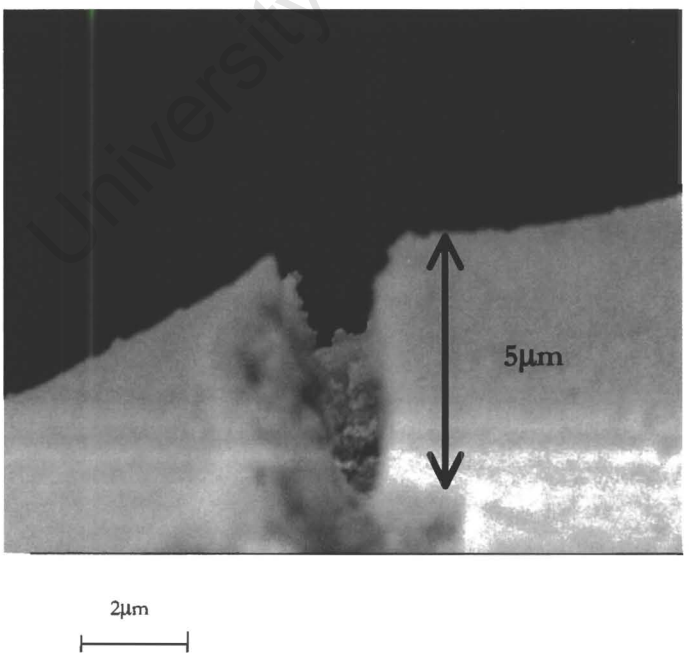

Figure 6.21: SEM measurement of the precipitate layer width on the pellet

XRD analysis was carried out using a Philips diffracto-meter X'Pert Graphics & Identity, and K-Alpha wave length on the raw sand seeds. The diffracto-graph reveals the presence of low quartz (SiO_2), aragonite ($CaCO_3$) and calcite ($CaCO_3$) in the sample (diffracto-graph in Appendix 7).

XRF analysis was carried out using a Philips X'UNIQ spectrometer with raw sand seeds as reference. Elemental analysis revealed the presence of traces of several metals: iron, manganese, magnesium, aluminium, and potassium, and the presence of calcium and silica from the sand in large amounts. The other metallic ions probably originated from the tap water used to prepare and dilute the carbonate and nickel solutions. Two large peaks of nickel were observed at a 2-Theta angle of 44° (Ni/C6, 13kcps) and 48° (Ni/Ca, 77kcps) respectively (XRF analysis in Appendix 7).

6.6.2 Quantitative analysis of the precipitate

A first set of quantitative analysis was carried out using the SEM technique XPP/ASAP on two different pellet samples from the same experiment (SEM spectrograph in Appendix 7). The elements isolated were: carbon, oxygen, silica, sulphur, calcium and nickel. The presence of the metal traces detected with XRF were not identified with the SEM technique. The analysis showed that in both cases, more than 98.2% of the metal present on the pellet was nickel.

The precipitate formed is likely to be a mixture of amorphous and crystalline material with slightly different chemical formulæ and solubilities (Seckler, 1994). For the purposes of simplification and understanding of reactor behaviour, the assumption was made that the precipitate in all its different forms (pellets, fines, and agglomerates) has one general composition with single characteristics independent of operating conditions.

An analytical technique was developed to measure the exact composition of the precipitate (see Appendix 6), using a combination of AA spectroscopy and titration. Although the reproducibility of the results was acceptable (relative error of 5.5%), a lack of accuracy in the titration method must be underlined (standard error of 15% on the nickel measurements). Thus, only a rough approximation of the composition was made. The calculations were based on the assumption that the precipitate has a chemical formula of the type: $Ni(OH)_X(CO_3)_Y$. The measured composition on average for the samples taken was:

$$Ni(OH^-)_{0.667}(CO_3^{2-})_{0.667} \qquad (6.1)$$

If a greater accuracy is required, Packter *et al* (1975) have developed different nickel hydroxy-carbonate analytical techniques.

6.7 Experimental error, a black box approach

All the measurements carried out during the experiments have some error associated with them. Some random errors came from ambiguities and uncertainties in the process measurements (Barford, 1985), as well as from human errors, like "sensing" or transcription errors (Sydenham *et al*, 1989). For the nickel carbonate precipitation in the pellet reactor, the sources of experimental error were isolated and defined as a function of the different steps within the process (Figure 6.22).

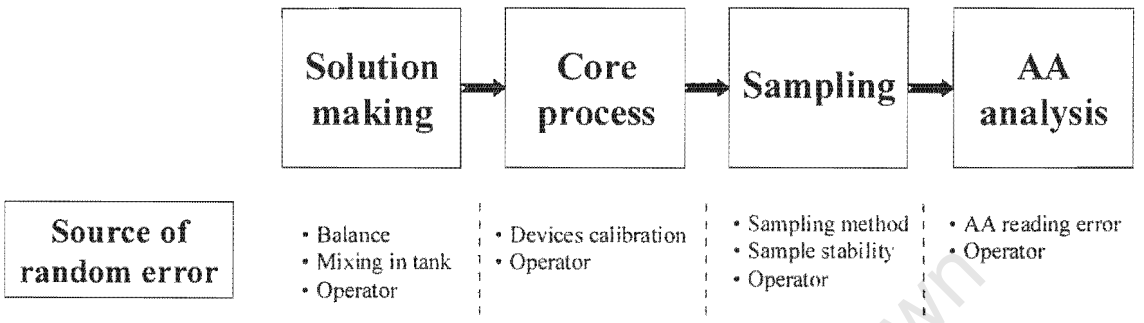

Figure 6.22: Experimental error: a black box approach

The solution make-up error, experimentally measured, introduced an error of up to 7% of the solution concentration value. The influencing factors were random error in the balance, the operator (or "human") error and non-homogeneous mixing of the solution.

The core process random error was more difficult to estimate, as many more parameters had to be taken into account. The important factors were instrumentation calibration, measuring error and operator transcription of the readings and data.

During the sampling phase, the experimental error was mostly due to the operator, even if the sampling procedure was kept constant. The samples were stabilised with five drops of hydrochloric acid, and this could introduce an error in the resulting concentration, because of the small change of sample volume. Furthermore the samples were not analysed directly after the experimental run and sometimes waited several days in a refrigerator before AA analysis. The stabilisation and conservation conditions were constant but certain variations could nevertheless have occurred. It would be necessary to run experiments on different sampling methods and on the solution stability to establish clearly the influence of random error on the concentration.

The last source of error originated from the Atomic Adsorption analyses where systematic, random and operator errors were generally observed.

It appeared from this black box analysis of the experimental error, that quantitatively estimating the random error on the whole process was not possible since many sources of error had to be identified from each of the different steps within the process. Consequently an overall estimation of the influence of random error over the process was not possible, because of the indirect interactions between the instrumentation error and the process efficiency. This overall random error on the process will be encompassed in the standard error and variation coefficient calculation during the RSM analysis.

6.8 Discussion

The "Start-up" (Figure 6.1 and Figure 6.2) and "Shut-down" (Figure 6.4) experiments were very useful to determine the conditions of stable operation of the reactor and the response time after variation of any parameter. Such information was essential to establish reproducibility and reliability during the runs. It also gave information about the stability of the operations as well as the nickel fines formation related to attrition breeding.

The $Ni_{tot\ out}$ variation at the beginning of the start-up run was due, according to Zhou *et al* (1999), to the progressive coating of the sand particles with the first layer of precipitate. A lattice structure compatibility problem seemed to be encountered while the sand was not covered by the precipitate. No easy nucleation, growth and agglomeration sites were provided on the pellets. This lattice structure problem referred to a low wetting angle, Φ, of the quartz. The high supersaturation in the reactor thus favoured homogeneous nucleation of fines in the bulk of the solution instead of heterogeneous nucleation, according to the equation 2.12.

The ratio hetero/homo nucleation then increased with the coating of the first layer of precipitate, as the wetting angle of the precipitate was more favourable to nucleation on the pellets. In addition to this phenomenon, crystal growth and agglomeration also occurred on the pellets when they were coated with the precipitate. Steady state was reached when the first layer of precipitate covered all the seeds. The removal efficiency was then linked to other factors such as the total active surface provided by the seeds, the residence time in the bed and the supersaturation. Notice that the steady state was reached much faster than in the experiments by Zhou *et al* (1999). This could be due to several factors: difference in operating conditions, more favourable wetting angle of the raw seeds or a difference in the surface area on the seeds.

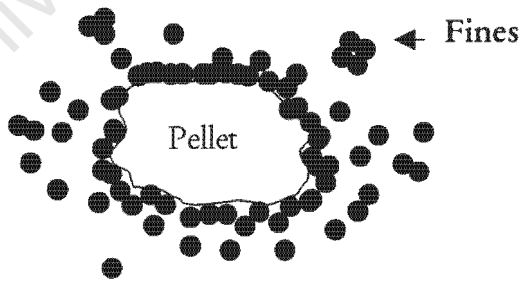

Figure 6.23: Schematic representation of nucleated recipitation and fines formation (Zhou *et al*, 1999)

The Patterson *et al* (1982) solubility model discussed in Chapter IV has to be used with caution when predicting the efficiency of the reactor for two reasons. Deviations from the theoretical solubility could be firstly observed because of a lack of information concerning the equilibrium between the phases. The presence of discrepancies between the solubility constants found in the literature, the presence of other insoluble metal hydroxides and carbonates, the lack of equilibrium conditions, ionic strength effects,

analytical inability to precisely separate the colloidal precipitate and the presence of impurities and complexing agents are the main sources of discrepancies. The second reason is due to the nature of the pellet reactor itself, as the nickel in the outlet stream can occur both as dissolved nickel and as fines. Consequently, the solubility of the product was not the only parameter that played a role in the nickel removal. Some fines were also washed out with the outlet stream, and these were not classified as being part of the nickel removal. Fines could be formed by two phenomena: attrition breeding of the precipitate already on the pellet as it was described in paragraph 6.2, and primary nucleation occurring in the bulk of the solution as it was shown in paragraph 6.5.3 and illustrated in Figure 6.23. The relative roles of these formation mechanisms were not investigated during the study. Given sufficient residence time in the reactor the fines could agglomerate onto the pellet.

The precipitation mechanisms were closely linked to the supersaturation within the bed, and particularly related to the local high supersaturation at the bottom of the bed. A low supersaturation favoured the crystal growth of the precipitate and the seeded nucleation of new crystal, i.e., the enlargement of the size of the pellets, whereas a high supersaturation lead to the formation of new crystal matter within the liquid medium, or fines, by spontaneous primary nucleation. The supersaturation was dependent both on the nickel and on the carbonate and hydroxide concentrations. The supersaturation can be calculated as a supersaturation ratio (equation 2.5) using the experimental measurements made of the composition of the precipitate, $Ni(OH)_{0.667}(CO_3)_{0.667}$.

$$\ln \beta = 0.427 \cdot \ln\left(\frac{(Ni^{2+}).(OH^{-})^{0.67}.(CO_3^{2-})^{0.67}}{Ksp}\right) \qquad (6.2)$$

Regions of high local supersaturation developed at the reactant inlets at high CO_3^{2-} concentrations and in the whole reactor at high pH. Usually the supersaturation was very high at the bottom of the reactor after the T-mixer (Figure 6.14), and decreased within the first 20 centimetres of bed to stabilise thereafter. This phenomenon led to the spontaneous nucleation of a solid phase within the liquid phase and explained the presence of the discrepancies between solubility and removal observed in Figure 6.4 and 6.5, and explains why a higher carbonate to nickel ratio did not cause an improvement in the nickel removal. Thus, at pH = 9.8, the removal of the nickel reached 99.6% for a ratio of 2 (Figure 6.7), and only 97.2% for a ratio of 4 (Figure 6.8), while the nickel conversion exceeded 99.8% in both experiments. The generation of a significant amount of fines due to high concentrations of hydroxides was illustrated by the two outliers found at high pH values (above pH = 10.5) in Figure 6.5 (ratio 2). Up to 40% of the introduced nickel exited the reactor as fines at a pH of 11.25 (Figure 6.7). The relative importance of agglomeration in the process efficiency was shown in Figure 6.11 during the experiment S28, at a pH of 9.5, where around 12% of the nickel precipitated as fines, which had already agglomerated after 20cm of bed. Nevertheless agglomeration played a secondary role in the nickel removal, in comparison to nucleation and growth of the precipitate on the pellet.

The general efficiency of the process could be improved by the addition of a post filtration stage. With filtration, the process could remove more than 99.9% of the initial nickel under optimum conditions and less than 0.1ppm was found in the treated stream when filtered (Figure 6.7 and Figure 6.8). Nevertheless, optimisation of the working pH

was necessary to avoid two problems: wastage of chemicals such as carbonates, pH regulation chemicals (sodium hydroxide, hydrochloric acid), and high costs of post-neutralisation agent. The eventual blockage of the filter was due to the nature of the fines, mostly composed of nickel hydroxide above pH=9.8, whereas below pH=9.8, fines formation was found to be negligible and no filtration problems were experienced.

Chapter VII

Response surface methodology part I. First order model fitting.

The response surface methodology (RSM) has been developed as a method of process and product optimisation using designed experiments (Myers and Montgomery, 1995). The methodology is mostly used in industry when several input variables influence the performance quality. The "response", or sometimes several responses, are analysed as functions of the input parameters (McAnally *et al*, 1981). The plot of the relationship between the response variable and the process variables lead to a graphical perspective of processing the problem, the response surface methodology.

The RSM finds some application in 3 major fields: the mapping of a response surface over a particular region of interest; the optimisation of the response; and the selection of operating conditions to achieve specifications.

The RSM is used in this chapter to optimise the nickel removal efficiency in the process. Two different responses, with different implications for the process, were investigated as functions of the process parameters for this purpose: the total nickel concentration ($Ni_{tot\ out}$) and the dissolved nickel concentration ($Ni_{dis\ out}$) of the effluent stream. 32 experiments plus 9 centre point experiments were drawn to map the response surface in the region of interest. This chapter presents an introduction to the RSM, as well as the results and interpretation of the first order model fitted to the experimental results.

7.1 Experimental design

One of the characteristics of the RSM is its sequential nature that allows rapid screening of the experiments. The main aim of the factor and experiments screening, is to reduce the list of separate variables of importance in explaining the response so that subsequent experimentation is more efficient and requires fewer runs. The time of testing is then reduced, and a response far from the hypothesised distribution can be rapidly located (Lipson, 1973). The experimental design is far more efficient than the conventional factorial matrix of experiments that involve a number of runs which is not always feasible, and no tests for reproducibility. The paragraphs below describe the RSM steps usually followed to obtain optimum results.

The phase zero of the RSM is to identify the important independent variables (Myers and Montgomery, 1995). In the case of the optimisation of the nickel carbonate precipitation in a pellet reactor, the process was assumed to be influenced by 5 main variables, although later it became apparent that there were others. They were the pH, the nickel load of the column (Ni_{feed}), the carbonate to nickel molar ratio (Ratio), the re-circulation rate (RR) and the number of multiple feed inlets used to introduce the carbonate into the reactor (MF).

Operating all the experiments under completely identical conditions is impossible for several reasons: difference of operator, utilisation of a second reactor, or any uncontrolled variation of a potentially influent parameter. In such a situation the design technique aims at arranging the factorial design in blocks containing only homogeneous parameters, and is called blocking (Hicks *et al*, 1999). The non-homogeneous parameter is therefore incorporated in the design by running a replicate design block at each of its possible levels.

Phase one determines if the current variable levels (settings) result in a value that is near the optimum of the process, or if the process is operating in a remote place from the optimum. A 2^k factorial experimental design is defined, with k, the system number of variables. Note that "2^k" represents the number of experiments to be run to analyse the surface response within the limits of the chosen variable settings. If k is large, the number of experiments to be run can be huge, and generally only half-factorial or quarter of factorial design are run. These give a reasonable approximation of the surface response. Then, a set of adjustments can be made in order to move the process toward its optimum. A first order structural model is therefore used in conjunction with the method of the steepest ascent to optimise the process (Myers and Montgomery, 1995).

The second phase starts when the process nearly reaches its optimum. A second order model incorporating a curvature is then used to approximate accurately the true response surface. The second order models are very flexible and can fit a wide range of functional forms, and parameters are easy to estimate (e.g. method of the least squares). Moreover, these models have been widely used in industry, and are known to solve real problems quite well (McAnally *et al*, 1981).

7.1.1 First order model:

The form of the true response function is unknown. The general form for five independent variables can be expressed as below:

$$y = f(\xi_1; \xi_2; \xi_3; \xi_4; \xi_5) + \varepsilon_s \tag{7.1}$$

Where y represents the response, ξ_i the natural variables and ε_s the statistical error.

For the purposes of RSM, the natural variables are encoded to x_i variables. They are dimensionless, and with a mean of 0 and also containing some spread or standard deviation. The true response function η can be expressed as below.

$$\eta = f(x_1; x_2; x_3; x_4; x_5) \tag{7.2}$$

First Order (for a k variables system):

$$\eta = \beta_0 + \beta_1 x_1 + ... + \beta_k x_k \tag{7.3}$$

Equation 7.3 represents the main effects model. The equation is the one of a plane in a k dimensional space (Muirhead, 1982).

$$\eta = \beta_0 + \beta_1 x_1 + ... + \beta_k x_k + \sum_{i \leq j} \sum \beta_{ij} x_i x_j \tag{7.4}$$

Equation 7.4 is then used when interactions between the variables are observed. A curvature is introduced in this equation which is now different from a plane.

7.2 Two level factorial design applied to nickel removal optimisation

The aim is to investigate the joint effects of the factors on a response variable (main effects and interactions). Two main levels are determined for each of the k variables in order to reduce the number of experiments. In the case of the nickel carbonate precipitation within the pellet reactor, five variables of importance have been determined and two levels chosen around the estimate maximum of nickel removal. Each variable has now a high value, encoded +1 or +, and a low value, encoded -1 or -. For the five variables of concern, the code is shown in Table 7.1.

It is necessary to impose restrictions on two of the variables. The MF variable represents the physical number of carbonate inlets and therefore must be an integer value of 1, 2 or 3. The RR variable could take any value between 30 and 70rpm. Below 30rpm, the scaling in the reactor does not allow operating under optimal conditions, and above 70rpm, the pellets are lifted up to the re-circulation outlet of the reactor and are swept out of the column.

A 2^5 factorial design, including the five factors with two levels each, is the more appropriate design to fit a first order response surface, to generate the factor estimates required to perform the method of the steepest assent and to reach the optimum in a minimum of experiments.

Variable	*Natural variable* value	*Encoded variable* level
pH	9.5	-
	10.5	+
Nifeed, ppm	50	-
	150	+
Ratio CO_3 to Ni	1	-
	4	+
RR, ppm	0.66	-
	1.67	+
MF	1	-
	3	+

Table 7.1: Encoding the variables of importance

Random order	*pH*	*Ratio*	*RR* rpm	*MF*	Ni_{feed} ppm
13	-	-	-	-	+
9	+	-	-	-	-
14	-	+	-	-	-
1	+	+	-	-	+
2	-	-	+	-	-
5	+	-	+	-	+
6	-	+	+	-	+
12	+	+	+	-	-
10	-	-	-	+	-
3	+	-	-	+	+
7	-	+	-	+	+
16	+	+	-	+	-
11	-	-	+	+	+
4	+	-	+	+	-
8	-	+	+	+	-
15	+	+	+	+	+
29	-	-	-	-	-
25	+	-	-	-	+
30	-	+	-	-	+
17	+	+	-	-	-
18	-	-	+	-	+
21	+	-	+	-	-
22	-	+	+	-	-
28	+	+	+	-	+
26	-	-	-	+	+
19	+	-	-	+	-
23	-	+	-	+	-
32	+	+	-	+	+
27	-	-	+	+	-
20	+	-	+	+	+
24	-	+	+	+	+
31	+	+	+	+	-

Table 7.2: 2^5 factorial experimental design and random order of the runs

The number of treatment combinations in a two level factorial design with five factors is: $2^5 = 32$ treatments. They are detailed with the coded notation in Table 7.2, as well as the random order in which the runs were performed.

Using the sequential nature of the RSM, and in order to achieve primary screening of the experiments, a half-factorial design was firstly carried out (first half of the Table 7.2), and the results analysed. The analyses showed that an optimal of nickel removal was reached within the region investigated. No further research of the minimal nickel response with the steepest descent was needed. The second half of the design was thereafter run to improve the accuracy of the model predictions and interpretations (second half of Table 7.2).

Addition of centre points

The replication of certain points during the 2^5 design gives information about the independent estimate of error. The additional points, usually located at the centre of the design have the coordinates $x_i=0$. For the factors studied, the centre points settings are described in Table 7.3.

pH	*Ratio*	*RR* rpm	*MF*	Ni_{feed} ppm
10	2.5	50	2	100

Table 7.3: 2^5 factorial central points natural coordinates

For a 2^5 factorial design with y_f the average of the runs and y_c the averages of the centre points, if y_f-y_c is large, then curvature of the surface is present and the fitting of a first order model is not appropriate.

7.3 Search for a minimal region of nickel concentration in outlet: first order model approach.

The experimental design to be run was firstly set as half of a 2^5 factorial design, for purposes of economising on time for the optimal response region search. Sixteen experiments with nine additional centre points were run. Analysis of the data rapidly showed that the region investigated contained a response minimum for $Ni_{dis\ out}$ and $Ni_{tot\ out}$ within its perimeter. However, an uncontrolled variation in the response (Table 7.6) was noticed. Consequently the full 2^5 factorial design was run with four additional centre points, in order to increase the reliability of the model predictions.

The data collected experimentally are displayed in Table 7.4 and Table 7.5 (random points) and Table 7.6 (central points). To prevent any kind of systematic error, the runs

and central points were carried out in a random order. $Ni_{dis\ out}$ corresponds to the dissolved nickel concentration (ppm) of the outlet of the reactor, and $Ni_{tot\ out}$ to the total nickel concentration (ppm). The data analyses are presented in part 7.5 and the experiments are listed in Appendix 3 and 8.

Experiment Number	$Ni_{tot\ out}$ ppm	*%Nickel* removal	$Ni_{dis\ out}$ ppm	*%Nickel* removal	*Temperature* °C
S19	18.42	82.1	2.92	97.2	27.4
S15	8.55	77.4	0.33	99.1	26
S20	3	91.9	2.36	93.6	27.1
S01	1.81	98.3	0.42	99.6	23.7
S03	4.79	87	1.82	95.1	24.9
S09	28.64	74.7	0.54	99.5	24.9
S10	3.95	96.3	2.86	97.3	23.3
S18	5.46	85.3	0.43	98.8	25.5
S16	10.88	73.7	0.45	98.9	22.8
S05	30.73	72.3	0.77	99.3	25.4
S11	3.49	96.8	3.06	97.2	25.1
S22	5.09	86.2	0.41	98.9	24.4
S17	19.74	81.7	2.9	97.3	22.8
S07	7.47	80.9	0.44	98.9	25.9
S13	4.33	89.1	2.75	93.1	25.5
S21	2.8	97.3	0.28	99.7	23.8

Table 7.4: First half of the 2^5 factorial design experimental points

Experiment Number	$Ni_{tot\ out}$ ppm	*%Nickel* removal	$Ni_{dis\ out}$ ppm	*%Nickel* removal	*Temperature* °C
S35	5.24	85.6	1.62	95.5	29
S31	47.66	57.1	0.23	99.8	23
S36	5.65	94.3	4.3	95.6	26
S23	8.2	77.9	0.13	99.7	24
S24	9.88	89.5	1.83	98	24.8
S27	6.91	80.9	0.15	99.6	25.6
S28	1.79	95.1	0.89	97.5	25.5
S34	7.68	93.2	0.69	99.4	27
S32	10.01	91.2	3.09	97.3	25.6
S25	10.98	70.4	0.12	99.7	24.8
S29	1.14	96.9	0.79	97.8	27.2
S38	1.81	98.3	0.32	99.7	24.6
S33	5.34	86	2.09	94.5	26.4
S26	48.8	49.2	0.2	99.8	25.1
S30	3.71	96	2.36	97.5	28.2
S37	6.2	83.6	0.06	99.8	28.5

Table 7.5: Second half of the 2^5 factorial design experimental points

Experiment Number	$Ni_{tot\ out}$ ppm	*%Nickel* removed	$Ni_{dis\ out}$ ppm	*%Nickel* removed	*Temperature* °C
SC02	1.65	97.7	1.01	98.5	26.6
SC04	1.67	97.7	1.14	98.4	26.2
SC05	9.31	86.5	0.81	98.8	23.7
SC06	3.89	94.5	1.08	98.5	24.2
SC07	4.79	92.6	0.53	99.2	24.7
SC08	4.44	93.5	0.93	98.6	21.9
SC09	8.18	86.9	1.07	98.3	28.5
SC11	9	85.6	0.9	98.6	27.6
SC12	5.35	91.4	0.74	98.8	25.2
SC13	4.62	93.3	0.94	98.6	25.8
SC14	5.19	92.4	1.33	98.1	24.2
SC15	4.08	94.1	0.92	98.7	24.2
SC16	5.83	91.5	1.15	98.3	24.5

Table 7.6: Response surface method experimental results: centre points

7.4 Analysis of the data and discussion

In the following analyses, the different factors were labelled as follows: X_1 is pH. X_2 is the carbonate to nickel ratio (RATIO). X_3 is the re-circulation rate in rpm (RR). X_4 is the number of inlet points of the carbonate (MF). X_5 is the nickel concentration of the waste flow in ppm (Ni_{feed}). The SAS statistical package was used to analyse the experimental data. First order empirical regression equations were established and provided information on the properties of the system from which the data are taken. The sign and magnitude of the coefficients and the presence or absence of interactions between variables allowed the determination of the region containing a minimum in the outlet nickel concentration.

7.4.1 Analysis of the nickel dissolved found in the outlet

7.4.1.1 First half of the factorial design:

The fitted first order model, also called linear regression model, is (Appendix 8):

$$Ni_{dis\ out} = 1.3390 - 0.96875X_1 + 0.150X_2 + 0.08125X_3 - 0.03875X_4 + 0.2975X_5 \quad (7.5)$$

The parameters defined for each variable in the model are called the partial regression coefficients, and measure the expected change of the response as a function of the variation of the concerned variable, the other variables remaining constant. They thus represent a measurement of the significance of the influence of the variable on the

response, and the variable with the greatest absolute value coefficient is considered the most influential on the response. In this first order model, the most important parameter is X1 (coefficient of 0.97 coded unit). Parameters of small influence are X5 (coefficient of 0.30 coded unit) and X2 (coefficient of 0.15 coded unit). The least influential on the response is X4 (coefficient of 0.04 coded unit). The model constant (1.34 coded unit) represents the predicted response value at the centre of the model where all the X_i variables are equal to zero. The typical method used to estimate the regression parameters is the least squares method. No interactions between the parameters have been found and added to the model.

The model can be simplified by considering two different cases: MF=1 and MF=3, as the multiple feed variable can only take the finite values 1, 2 or 3. The MF variable is thereafter considered as a blocking parameter, which induces non-homogeneous operating conditions rather than a plain variable. The model studied is then a "two blocks" 2^4 factorial experimental design instead of a single 2^5. The two models will be compared in order to have an idea of the value of MF that induces the best response.

MF=1
The fitted first order model is:

$$Ni_{dis\ out} = 1.3100 - 1.030X_1 + 0.05750X_2 - 0.04750X_3 + 0.2250X_5 \quad (7.6)$$

MF=3
The fitted first order model is:

$$Ni_{dis\ out} = 1.258833 - .9075X_1 + 0.2425X_2 + 0.210X_3 + 0.370X_5 \quad (7.7)$$

The analysis of variance (Lee, 1975) for the MF=1 and MF=3 models indicated that the minimum value of $Ni_{dis\ out}$ occurs within the experimental region. Also, the sign of the coefficient for X_4 (the MF variable), indicates that increasing the value of MF at the centre of the design will decrease $Ni_{dis\ out}$, i.e. increasing MF to 3. The choice of MF=3 is also suggested since at the centre of the designs for MF=1 and MF=3, $Ni_{dis\ out}$ has the lowest value when MF=3.

7.4.1.2 Second half of the factorial design:

The fitted first order model is:

$$Ni_{dis\ out} = 1.097143 - 0.941875X_1 + 0.013125X_2 - 0.145625X_3 - 0.050625X_4 + 0.448125X_5 \quad (7.8)$$

The analysis of variance is summarised in Table 7.6.

Source of variation	*DF*	*SS*	*MS*	*F*
Model	5	17.79		
(residual	15	6.6749)		
Quadratic	1	0.4544	0.4544	10.66
Other 2nd order	10	6.0347	0.6035	14.39
Pure error	4	0.1849	0.0426	
Total	20	24.4642		

Table 7.7: Analysis of variance of the second half of the factorial design ($Ni_{dis\ out}$)

DF is the degree of freedom of the source of variation. SS is the sum of squares and MS the mean square. The F tests assesses whether or not the MS of the model is significantly greater than the one due to pure error (Napier-Munn, 1996) and gives a evaluation measurment of the fitting of the model on the data points.

As with the first experiments, the F tests calculated are significant, i.e. the first order model is not adequate, and the experimental region contains a minimum for $Ni_{dis\ out}$. The most important factor is X_1, as it has the largest coefficient. If $\$X_1$ represents the amount by which X_1 is moved from the origin, and $\$X_4$ the amount by which X_4 is moved, then $\$X_4$ can be computed as:

$$\$X_4=\$X_1\text{-}0.050625/\text{-}0.941875 \qquad (7.9)$$

This is obviously positive, and since at the centre of design, X_4 is zero and MF=2, a move from the centre means that MF>2 has to be taken, i.e. MF=3. This means that in this case, the region with MF=3 is preferred.

7.4.1.3 Combined experiments

The fitted first order model is:

$$Ni_{dis\ out} = \underset{}{1.2115122} - \underset{(0.092609)}{0.955313X_1} + \underset{(0.104826)}{0.081563X_2} - \underset{(0.104826)}{0.032188X_3} - \underset{(0.104826)}{0.044688X_4} + \underset{(0.104826)}{0.372813X_5} \qquad (7.10)$$

The R squared value is 73%, indicating that the variables X_1 to X_5 account for 73% of the variation in $Ni_{dis\ out}$. The values in brackets are the standard errors of the coefficients. The analysis of variance (ANOVA) table is shown in Appendix 8. Its interpretation confirms the results obtained from the separate experiments. The first order model appears inadequate for a proper fitting of the surface, because of the presence of a minimum for $Ni_{dis\ out}$ within the experimental region investigated.

MF=1
The fitted first order model is:

$$Ni_{dis\ out} = 1.18920 - 0.980X_1 + 0.1650X_2 - 0.19375X_3 - 0.37870X_5$$
$$(0.10873)\ (0.13592)\ (0.13592)\ (0.13592)\ (0.13592)$$

(7.11)

(The analysis of variance can be found in Appendix 8)
The R squared value is 76%, indicating that the model accounts for 76% of the variation in $Ni_{dis\ out}$.

MF=3
The fitted first order model is:

$$Ni_{dis\ out} = 1.1320 - 0.93062X_1 - 0.001875X_2 + 0.12938X_3 + 0.36688X_5$$
$$(0.11241)\ (0.14052)\ (0.14052)\ (0.14052)\ (0.14052)$$

(7.12)

The R squared value is 72%, indicating that the variables account for 72% of the variation in $Ni_{dis\ out}$.

At the centre of this design, the yield of $Ni_{dis\ out}$ is 1.19 when MF=1 and 1.13 when MF=3: The region with MF=3 produces a smaller value of $Ni_{dis\ out}$ than with MF=1. The above results confirm those from the separate experiments, namely that at the centre of the two designs the experiment with MF=3 is preferred.

7.4.2 Analysis of the nickel total found in the outlet

7.4.2.1 First half of the factorial design:

The fitted first order model is:

$$Ni_{tot\ out} = 8.78350 + 1.37188X_1 - 6.20502X_2 - 0.29938X_3 - 0.61938X_4 + 3.75060X_5$$

(7.13)

MF=1
The fitted first order model is:

$$Ni_{tot\ out} = 7.5950 + 1.78750X_1 - 5.77250X_2 + 1.38250X_3 + 3.88750X_5$$

(7.14)

MF=3
The fitted first order model is:

$$Ni_{tot\ out} = 8.42083 + 0.95625X_1 - 6.63875X_2 - 1.98125X_3 + 3.62375X_5 \quad (7.15)$$

The analysis of variance did not give a clear indication of the nature of the response surface within the experimental region. Dropping the one large value at the centre point (8.42 coded units) did indicate that the region contained the minimum value of $Ni_{tot\ out}$. The equally high values produced in the second set of experiments nevertheless suggest that such values just reflect the magnitude of the variability in the $Ni_{tot\ out}$ variable. The models above also suggest that the region at MF=1 would produce a smaller value of $Ni_{tot\ out}$ than that at MF=3.

7.4.2.2 Second half of the factorial design:

The fitted first order model is:

$$Ni_{tot\ out} = 10.13143 + 5.96750X_1 - 6.790X_2 - 0.02375X_3 - 0.31375X_4 + 5.58750X_5 \quad (7.16)$$

There are two features of this analysis, which are different from that of the first set of experiments. Firstly, the analysis clearly indicates that the experimental region contains a minimum for $Ni_{tot\ out}$. Secondly, the sign of the coefficient for MF in the model is now negative, indicating that an increase in the value of MF will tend to minimise the value of $Ni_{tot\ out}$, i.e. it suggests that the region with MF=3 will produce a minimum.

7.4.2.3 Combined experiments

The fitted first order model is:

$$Ni_{tot\ out} = 9.47390 + 3.66969X_1 - 6.49781X_2 - 0.16156X_3 + 0.15281X_4 + 4.66906X_5$$
$$(1.27824)\quad (1.44687)\quad (1.44687)\quad (1.44687)\quad (1.44687)\quad (1.44687) \quad (7.17)$$

The R squared value is 51%, indicating that the variables X_1 to X_5 account for 51% of the variation in $Ni_{tot\ out}$. The values in brackets are the standard errors of the coefficients.

These results of the analysis of the variance indicate that the experimental region contains a minimum of $Ni_{tot\ out}$, and the region with MF=1 will produce a smaller value of $Ni_{tot\ out}$ than with MF=3, as judged by the sign of the MF coefficient in the model.

MF=1
The fitted first order model is:

$$Ni_{tot\ out} = 8.63640 + 3.88688X_1 - 5.78438X_2 - 1.83938X_3 + 4.98438X_5$$
$$(1.51793)(1.89741)\quad (1.89741)\quad (1.89741)\quad (1.89741) \qquad (7.18)$$

The R squared value is 52%, indicating that the variables account for 52% of the variation in $Ni_{tot\ out}$.

MF=3
The fitted first order model is:

$$Ni_{tot\ out} = 8.8320 + 3.45250X_1 - 7.21125X_2 - 1.1.51625X_3 + 4.35375X_5$$
$$(1.59621)\ (1.99526)\quad (1.99526)\quad (1.99526)\quad (1.99526) \qquad (7.19)$$

The R squared value is 52%, indicating that the variables account for 52% of the variation in $Ni_{tot\ out}$.

The general conclusion from this combined analysis is similar to that of the first set of experiments, namely that the region where MF=1 is preferred to that with MF=3. However, the between $Ni_{tot\ out}$ with MF=1 and MF=3 is smaller than in the first set of experiments, due to the combined effects of the first and second sets of experiments.

For the analysis of the $Ni_{tot\ out}$, the F tests were not significant in the first set of experiments. That indicates that the region of curvature around the minimum has not been found, and the path of steepest descent should be followed. However, the very large value of $Ni_{tot\ out}$ at the centre of the design (Table 7.6) was included in the calculation of the pure error above. If this value is omitted, then the MS for error is reduced, and the F tests become significant.

7.5 Conclusion

The object of this chapter was to fit a first order model to the response surface investigated in the set of 32 + 9 experiments carried out. Two different response variables were tested: total nickel ($Ni_{tot\ out}$) and dissolved nickel out ($Ni_{dis\ out}$).

The 5 variables X_1 to X_5, account for 73% of the variations in the $Ni_{dis\ out}$. The separation between the experiments using MF 1 and MF 3, indicates that MF 3 actually gives smaller outlet values. And finally, the 1st order model is inadequate for a proper fitting of the region, which means that the investigated region does contain a minimum.

For $Ni_{tot\ out}$, the 5 variables account only for 51% of the response variation, and MF 1 is preferred to MF 3. The F tests are not significant. However, the value of the pure error

on the results is significant and when outlying value was omitted, the region investigated seems to include a minimum.

Phase one of the RSM is completed when the model reaches a zone containing a maximum of nickel removal (=minimum in $Ni_{tot\ out}$ and $Ni_{dis\ out}$) in both response cases studied. In this case, there is no need to use the technique of the steepest ascent or descent to search for a region in which the minimum exists. The second phase of the RSM can start with the fitting of a second order model to the true response involving a curvature.

Chapter VIII

RSM part II, second order model

In Chapter VII five variables of influence on the process efficiency were defined, and a 1st order model was fitted for the two responses analysed, the total nickel and dissolved nickel concentration in the outlet. In both studies, a lack of fit between experimental data and the first order model was observed, due mostly to curvature of the surfaces in the region investigated. In both cases, the F-test analysis revealed the presence of a minimum in the nickel out in the region studied, and thus no further scanning of the surface response had to be made using the steepest descent technique, in order to optimise the process. The aim of this part is to define and fit a second order response surface model to the data points corresponding to each of the two responses studied. This model is then used to predict the location of the minimum response within the surface investigated, or to predict the direction on the surface towards the minimum response point. The relative importance of the five variables is also discussed, with a brief study of the temperature influence on the model.

8.1 Second order model

8.1.1 Taylor series type model

Assuming that the response function (equation 8.1) is unknown, the second order response surface model can be developed as a Taylor Series as illustrated in equation 8.2 (Myers and Montgomery, 1995).

$$y = f(x, \theta) \tag{8.1}$$

$$\eta = \beta_0 + \sum_{j=1}^{k} \beta_j x_j + \sum_{j=1}^{k} \beta_{jj} x_j^{\,2} + \sum_{i<j} \sum \beta_{ij} x_i x_j + \varepsilon \tag{8.2}$$

Equation 8.2 is used as an approximation of the true response surface in a relatively small region. Second order models are widely used because they present real advantages such as flexibility, simplicity of estimating their parameters and historical use in industry. The ε represents the random errors term. The model contains 1+2k+k(k-1)/2 parameters and

therefore the experimental design must include at least the same number of runs. Note that linear models are sometimes not adapted to the curvature type of the response and non-linear models have then to be used (Neter and Wasserman, 1974).

8.1.2 Face centred cube design

In many cases, strict constraints on the ranges of the design variables are imposed. The design has to be a cube. Thus, some variables cannot be investigated outside the region set during the 1st order model design. For example, the re-circulation could not take a value below 30rpm (point of coordinates X_3=-1), or above 70rpm (X_3= +1). The MF variable also had to be set at an integer value between 1 and 3, which corresponded to X_4 coordinates of −1, 0 or +1. The face centre cube design was then desirable as the levels taken by the variables were the same as chosen for the 1st order model design, and problems of range were then avoided.

Experiment number	*X1 pH*	*X2 Ratio*	*X3 RR*	*X4 MF*	*X5 Nifeed*
SA04	-	0	0	0	0
SA10	+	0	0	0	0
SA07	0	-	0	0	0
SA01	0	+	0	0	0
SA11	0	0	-	0	0
SA03	0	0	+	0	0
SA08	0	0	0	-	0
SA06	0	0	0	+	0
SA02	0	0	0	0	-
SA05	0	0	0	0	+

Table 8.1: Dimensionless coordinates of the axial points for the design

The coordinates of the axial points are given in Table 8.1, and Figure 8.1 gives a 3 dimensional representation of a 2^3 face centre cube design (Myers and Montgomery, 1995). This kind of cuboidal experimental region must be symmetrically covered for reliable modelling of the surface. The design has the disadvantage of not being rotatable, i.e. points on the surface equidistant from the centre do not have equal precision. Only a few centre points produced a relatively stable variance for the analysis.

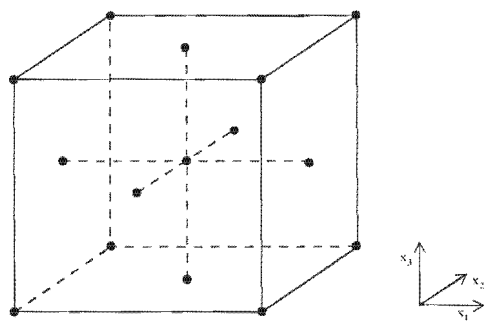

Figure 8.1: Face centre cube design, 3 variables (Myers and Montgomery, 1995)

Table 8.1 shows that to investigate the response surface it was necessary to run 10 experiments at the axial points of the cuboidal faces (encoded coordinates of each variable shown in Table 8.1). Thus, for example, for X_1, where one unit was equivalent to 0.5pH, the pH values for the axial points on the wall of the experimental cube were at a pH of 9.5 and 10.5 while all the other variables stayed at their level 0. Together with the previous 32 experiments, the new runs constituted the face centre cube central design. Four new centre points were run and added to the nine previously run for the first order model, to give a better estimate of the standard error of the points.

8.2 Experimental results

8.2.1 Axial points

All experimental results for the centre points are summarised in Table 7.6 and the axial points are summarised in Table 8.2. The responses measured were the total nickel concentration out and the dissolved nickel concentration out.

Experiment Number	*Ni tot out* ppm	*%nickel* removed	*Ni dis out* ppm	*%nickel* removed	*Temperature* Degree C
SA01	2.56	97	0.87	99	21.7
SA02	5.25	87.1	0.76	98.1	22.4
SA03	6.11	92.7	0.98	98.8	22.5
SA04	3.16	96.1	2.77	96.6	22.2
SA05	4.89	96	1.64	98.7	22.3
SA06	4.85	94.2	1.00	98.8	23.1
SA07	11.81	85.8	0.69	99.2	21.5
SA08	6.63	92.2	0.54	99.4	25.5
SA10	7.28	91.5	0.49	99.4	20.8
SA11	4.54	94.7	0.53	99.4	26.8

Table 8.2: Total results of the axial point experiments

8.2.2 Experimental variability

As a first analysis of the data from the centre points experiments, some variability can be observed, especially for the $Ni_{tot\ out}$ concentration. For the same setting of the five factors of importance, the $Ni_{tot\ out}$ concentration fluctuated from 1.65ppm to 9.31ppm. The calculation of the sample standard deviation and standard error are shown in Table 8.3, for $Ni_{tot\ out}$ and $Ni_{dis\ out}$.

Response	*Sample standard deviation*	*Standard error*
$Ni_{dis\ out}$	0.2	0.06
$Ni_{tot\ out}$	2.41	0.67

Table 8.3: Error and uncertainty on the $Ni_{tot\ out}$ and $Ni_{dis\ out}$ measurements

The calculation presented in Table 8.3, shows that the sample standard deviation and standard error were large for both $Ni_{tot\ out}$ and $Ni_{dis\ out}$. The standard deviation represents 46.1% of the mean $Ni_{tot\ out}$ value, and 21.1% of the mean $Ni_{dis\ out}$ value.

This variability is a sign of the presence of uncontrolled parameters in the process, such as the temperature, which were not taken into account during the runs, and which had an influence on the system response.

8.2.3 Second order model

Fitted second order model, dissolved nickel out:

The developed Taylor Series fitting the dissolved nickel out response is:

$$\begin{aligned} Ni_{dis\ out} = {} & 0.931386 - 0.966176X_1 + 0.082059X_2 - 0.017059X_3 - 0.028529X_4 \\ & (0.118001)\ (0.079212)\ (0.079212)\ (0.079212)\ (0.079212) \\ & + 0.376765X_5 + 0.677055X_1^2 - 0.084063X_1X_2 - 0.172945X_2^2 + 0.3593X_1X_3 \\ & (0.079212)\ (0.293615)\ (0.081649)\ (0.293615)\ (0.081649) \\ & - 0.059688X_2X_3 - 0.197945X_3^2 + 0.024688X_1X_4 - 0.083437X_2X_4 + 0.161563X_3X_4 \\ & (0.081649)\ (0.293615)\ (0.081649)\ (0.081649)\ (0.081649) \\ & - 0.182945X_4^2 - 0.286563X_1X_5 + 0.031563X_2X_5 - 0.183483X_3X_5 - 0.005937X_4X_5 \\ & (0.293615)\ (0.081649)\ (0.081649)\ (0.081649)\ (0.081649) \\ & + 0.247055X_5^2 \\ & (0.293615) \end{aligned} \qquad (8.3)$$

The values in brackets are the standard errors of the parameters. The R^2 value is 87.1%, indicating that the variables X1 to X5 accounted for 87.1% of the variation in $Ni_{dis\ out}$; the fitting of the model has largely improved since the 1st order model fitting. The model calculations are shown in Appendix 9 from the SAS statistical package.

Fitted second order model, total nickel out:

The fitted second order model is:

$$\begin{aligned}Ni_{tot\ out} = {} & 4.998550 + 3.57500X_1 - 6.387647X_2 - 0.105882X_3 + 0.091487X_4 \\ & \quad (1.371983) \quad (0.920985) \quad (0.920985) \quad (0.920985) \quad (0.920985) \\ & + 4.38382X_5 + 0.633082X_1^2 - 2.920312X_1X_2 + 2.598082X_2^2 + 0.107187X_1X_3 \\ & \quad (0.920985) \quad (3.413829) \quad (0.99330) \quad (3.413829) \quad (0.99330) \\ & + 0.519687X_2X_3 + 0.738082X_3^2 - 0.217187X_1X_4 - 0.713438X_2X_4 + 1.677812X_3X_4 \\ & \quad (0.99330) \quad (3.413829) \quad (0.99330) \quad (0.99330) \quad (0.99330) \\ & + 1.153082X_4^2 + 2.272813X_1X_5 - 4.938438X_2X_5 + 0.512813X_3X_5 - 0.315313X_4X_5 \\ & \quad (3.413829) \quad (0.99330) \quad (0.99330) \quad (0.99330) \quad (0.99330) \\ & + 0.483082X_5^2 \\ & \quad (3.413829)\end{aligned} \tag{8. 4}$$

The values in brackets are the standard errors of the parameters. The R^2 value is 82.8%, indicating that the variables X1 to X5 accounted for 82.8% of the variation in $Ni_{tot\ out}$ and the fitting of the model has largely improved.

8.3 Second order model analyses

8.3.1 Canonical analysis

The aim of the second order model fitting analysis is to localise the point of minimum response located within the limits of the investigated surface. This point is called a stationary point. Depending on the system studied, several geometries are possible for the surface structure. Elliptic or hyperbolic systems are commonly encountered. In the particular case of the hyperbolic system, the stationary point is neither an absolute maximum nor a minimum, and is called a saddle point (or local optimum). In the case of a local optimum, further searching for the absolute optimum has to be carried out on another portion of the surface. In contrast, on elliptic surfaces the stationary point is an absolute optimum and the coordinates of the stationary point give the optimal conditions of operation for the process. The characterisation of the nature of the system and the location of the stationary point are important parts of the 2nd order model analysis, and are called "canonical analysis".

The calculation relevant to this analysis is shown in Appendix 9 for the two responses studied, $Ni_{tot\ out}$ and $Ni_{dis\ out}$. The nature of the stationary point is given by the signs of the eigenvalues (λ_i) of the second order model matrix $\hat{A}$. If all the λ are negative, the stationary point is a maximal response; all λ positive, gives a minimal response, and finally λ of different signs are typical of a saddle point.

Dissolved nickel out:

As indicated in the calculations in Appendix 9 from the SAS statistical package, there was no unique value for $Ni_{dis\ out}$. The stationary point was a saddle point, which indicates that the stationary point was just a local minimum. The coordinates of the saddle point are shown in Table 8.4. The predicted response value for this point was 0.56ppm of nickel.

Variable	*Critical Value*
pH	10.3
Ratio	2.5
RR	53.7
MF	2
Nifeed	83.8

Table 8.4: Dissolved nickel out surface saddle point coordinates

The eigenvalues and eigenvectors of the matrix of the parameter estimates of the second order model, provided evidence of this saddle surface. If a unique minimum had to be found, then all eigenvalues would be positive. However three eigenvalues out of five were negative, and the eigenvector coefficients associated with these eigenvalues were interpreted to determine the relative influence of the parameters in exploring the saddle surface. The first of these eigenvalues was close to zero, and thus carried little weight in the analysis. For the eigenvectors of the other two negative eigenvalues, factors with the largest coefficients were the Ratio, RR and MF. This suggests that these were the important factors in exploring the saddle surface.

A restriction had to be made on the model prediction, as MF had to be an integer value, and was then approximated to its closest integer value for the purpose of the study.

Total nickel out:

The stationary point was again a saddle point, which indicated that there was no unique minimum value for $Ni_{tot\ out}$ in the region and the stationary point was just a local minimum. The coordinates of the saddle point are shown in Table 8.5. The predicted response value for this point was 1.37ppm of nickel.

Variable	*Critical Value*
pH	9.97
Ratio	3.5
RR	43.9
MF	2.3
Nifeed	69.5

Table 8.5: Total nickel out surface saddle point coordinates

The eigenvalues and eigenvectors of the matrix of the parameter estimates of the second order model provided evidence of this saddle surface. If a unique minimum had been found, then, all eigenvalues would be positive. However, two out of five eigenvalues

were negative, and the eigenvector coefficients associated with these eigenvalues were interpreted in order determine the relative influence of the parameters in exploring the saddle surface. If all the coefficient of the eigenvectors, except for one, are relatively small, then the vector points roughly along the axis associated with the single large coefficient. A change in the value of that factor will then have more influence on the minimum response than the other factors. The factors with the largest coefficients were pH, Ni_{feed} and Ratio. This suggests that these were the important factors in exploring the saddle surface.

8.3.2 Ridge system and analysis

The goal of this analysis is to determine the nature and shape of the surface response within the experimental region or on its perimeter. The ridge analysis, although in this case a "valley" rather than a ridge was considered, consists of a constrained optimisation algorithm, which evaluates the response of points on a sphere of a certain radius, centred on the centre of the design. In the response surface studied for the nickel analysis, the radii are studied in steps of 0.1 coded data units, from the centre of the surface of the experimental region. Note that the predicted response values at radii beyond that of the local minimum have somewhat large standard errors, indicating a lack of reliability. The aim of the study was either to anchor the stationary point inside the region or to obtain some guidelines on the direction of future experiments in order to achieve more desirable conditions (Myers and Montgomery, 1995). In the case of the saddle surface the point on the "path" at the design perimeter is the point of the minimum estimated response. It may be viewed as a reasonable candidate for optimal operating conditions.

Dissolved nickel out:

The calculation and results of the ridge analysis are provided in Appendix 9, and were carried out with the SAS statistical package. The different estimated responses corresponding to the increasing radii are plotted (Figure 8.2), together with the variation of standard error.

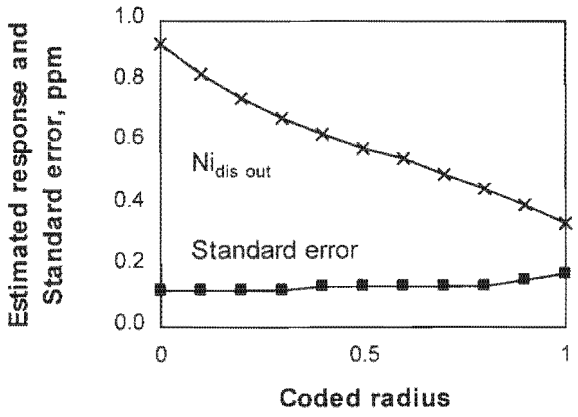

Figure 8.2: Estimated $Ni_{dis\ out}$ and standard error as a function of the coded radius

The value of $Ni_{dis\ out}$ consistently decreases with the increase in radius. The standard error did not significantly influence the reliability of the estimated response for small radii (13% of the response at the centre of the design), but its relative influence increased with the radius up to 50% of the estimated response at the unity radius.

The factors RR and MF did not appear influential until the region of the local minimum, and beyond, where the reliability was poor. The estimated MF fluctuated very close to the value of 2, and had to be fixed at this integer value for the purposes of this study. The pH and Ratio variables appeared to stabilise around the region of the local optimum, at a pH of 10.2 and a ratio of 2.3 carbonates per nickel respectively. Both RR and Ni_{feed} falling from 100rpm to 83rpm.

Total nickel out:

The ridge or "valley" analysis results are shown in Appendix 9, and Figure 8.3 shows the estimated $Ni_{tot\ out}$ response with its standard error, as a function of the distance from the centre of the design.

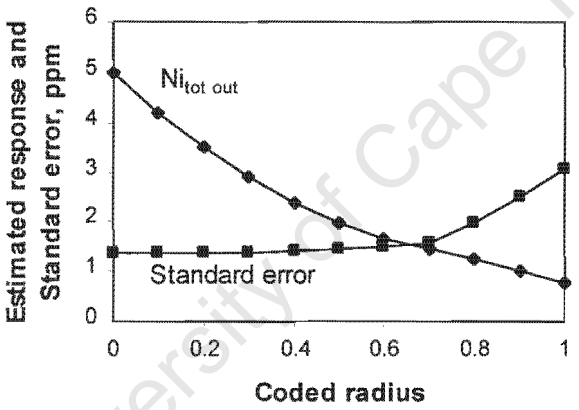

Figure 8.3: Estimated $Ni_{tot\ out}$ and standard error as a function of the coded radius

The predicted response values at radii beyond 0.6 encoded units had somewhat large standard errors (from 27% to 404% of the predicted value), indicating that the prediction is unreliable when distant from the centre of the design.

Again, MF and RR did not have a large influence, MF fluctuating around two, and so can be considered fixed at this integer value. Thereafter, the RR factor remained stable across the range of radii, slowly increasing from 50rpm to 54rpm. The pH factor appeared to stabilise at a pH of 9.85 around the region of the local optimum. The Ratio variable reached a maximum value of 3.12 at a radius of 0.6, then decreased again to 2.64 for a radius of 1. The Ni_{feed} factor showed the greatest change in value at each radius minimum, falling from 100ppm at the centre of the design to 54ppm at a radius of 1 (Appendix 9).

8.4 Influence of the temperature

The experiments were not all run under the same conditions. The temperature of the reaction for all the runs was monitored but not controlled. It varied between 21°C and 29°C. The temperature could have a potentially significant influence on the precipitation phenomena, such as the supersaturation ratio and the solubility, the nucleation rate, the growth rate and the agglomeration rate. Consequently the temperature was a potential source for the uncontrolled variation observed in the data. The overall influence was measured by including the recorded temperature as a co-variate parameter in the second order model design. This co-variate parameter was recorded as the X_6 variable, and could be defined as a "nuisance" factor. That is to say that neither did the variable have a special interest, nor had the operator any control over it, but it could account for the response data. Consequently, the results were analysed as a function of the temperature.

8.4.1 Temperature and solubility

The influence of the temperature on the solubility was modelled using ASPEN Plus™. A flow of nickel carbonate was introduced in the model reactor together with a flow of base (sodium hydroxide) to maintain the pH at 10. Then different temperatures were set and the output concentrations were used to plot the solubility of the nickel carbonate as a function of the temperature. See Figure 8.4.

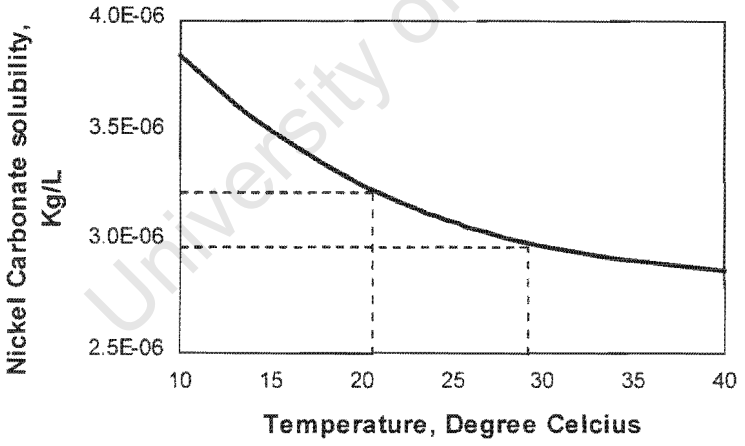

Figure 8.4: ASPEN Plus™ prediction on the nickel carbonate solubility as a function of the temperature

Figure 8.4 shows an ASPEN Plus™ model, which plots the change in nickel carbonate solubility as a function of the temperature. In the temperature range of interest, 21 to 29°C, the solubility appeared relatively constant ($3e^{-06}$ to $3.2e^{-06}$ kg/L), and consequently, the variation of temperature within these limits had little effect on the supersaturation of the solution.

8.4.2 Temperature influence on the centre points of the design

The temperature of the outlet stream was recorded for every run, and especially for the centre point of the design. The $Ni_{tot\ out}$ and $Ni_{dis\ out}$ plot as a function of the temperature is shown in Figure 8.5 for all the centre points run under the same experimental conditions.

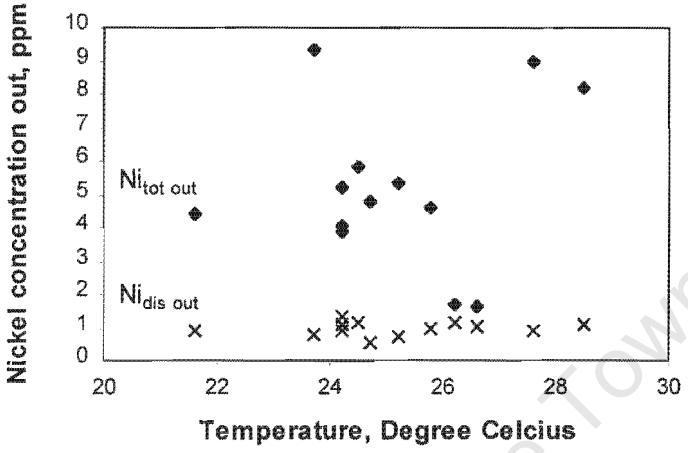

Figure 8.5: Temperature influence on the nickel total and dissolved out monitored at the centre point of the design

Figure 8.5 shows that the variation in the temperature did not affect the $Ni_{dis\ out}$ concentration. The effect on the $Ni_{tot\ out}$ does not appear clearly on the plot, and no simple model seems to link the temperature to this outlet concentration. The uncontrolled variations were therefore not directly linked to the temperature.

8.4.3 Second order model analysis including temperature

The results of the fitting of the second order model including the temperature as a nuisance parameter, are shown in Appendix 10. To sum up the analysis of the calculations, adding the temperature X_6 factor to the model, increased the R^2 of the predictions slightly in the case of the $Ni_{tot\ out}$ (from 82.8% to 83%), and had no effect on the R^2 of the $Ni_{dis\ out}$. In both cases, the coefficient of variability was slightly increased together with the standard error on the predictions (e.g. from 256 to 262 for the pH predictions on the $Ni_{tot\ out}$ surface). In other words, the inclusion of the temperature in the model made very little difference to the analysis, and therefore, the temperature did not appear to be contributing to the uncontrolled variation in the data.

8.5 Discussion

8.5.1 Second order model analysis

For the $Ni_{dis\ out}$, the response corresponding to the saddle point was 0.56ppm of dissolved nickel out of the reactor. The eigenvector coefficient pointed out that the RR and MF variables could be used in exploring the response surface, even if they did not appear influential around the region of the local minimum. The MF variable stabilised around 2, the coordinates at the design centre. The Ni_{feed}, pH and ratio stabilised at respectively 83.8, 10.2 and 2.3 around the local optimum.

The saddle point on the $Ni_{tot\ out}$ response surface corresponded to a concentration of 1.38ppm of total nickel in the reactor outlet stream. The pH, Ni_{feed} and Ratio, which had the greatest coefficient corresponding to the negative eigenvalues, could be used in exploring the response surface. Again, RR and MF were of minor influence, and stabilised around 44rpm and 2 respectively. The Ni_{feed}, pH and ratio again stabilised around the local minimum of 69.5, 9.97 and 3.5.

All the predicted variables investigated during the valley analysis fluctuated within the surface limit as a function of the radius length. The Ni_{feed} variable varied the most. The analyses in Chapter VII showed that $Ni_{dis\ out}$ and $Ni_{tot\ out}$ minima were present on the surface investigated, considering the first order model fitted to the experimental results. The present second order model proved that both stationary points were for instance only local minima, or saddle points. The optimum response points were not reached within the perimeter of the experiments for $Ni_{dis\ out}$ or for $Ni_{tot\ out}$. Several minima appeared however on different locations of the surface, when investigated with the valley analysis. The analyses of the surface were difficult because of the large standard error of the prediction, which was increased when investigating the surface far from the centre of the design, and thus the reliability of the predictions decreased simultaneously. Consequently, the large variability of the response did not allow accurate predictions of the surface optima, nor on the exact direction to optimise the process.

Figure 6.7 and Figure 6.8 presented the $Ni_{dis\ out}$ and $Ni_{tot\ out}$ as a function of the pH at fixed ratio, Ni_{feed}, RR and MF. In both cases, the $Ni_{tot\ out}$ reached a maximum in the pH range 9.5 to 10.5, whereas $Ni_{dis\ out}$ constantly increased in the same range, reaching more than 99.9% removal. These results confirm those above, that no optimisation of the $Ni_{dis\ out}$ is observed on the section of the response surface studied. In contrast, $Ni_{tot\ out}$ reached an absolute minimum around a pH of 9.8 on both Figure 6.7 and Figure 6.8, while only a local minimum was found on the second order model response surface.

8.5.2 Parameters of influence

In both surface responses investigated, the parameters of influence were the same: Ratio, pH and Ni_{feed}. The three of them influence the supersaturation, the speciation, and the composition of the precipitate, and their importance on the process has already been shown in Chapter VI, parts 4 and 5.

The RR and MF parameters appeared of secondary influence on the process efficiency. The variables stabilised around their coordinates at the centre of the design in both cases, 50rpm for the re-circulation, and 2 for the multiple inlet feed. The RR did not have a significant influence on the process efficiency and pellet attrition, since the operating range was limited. It varied between 30 and 70rpm (Table 5.3), and did not influence the hydrodynamics in the reactor significantly, since the Reynolds number increased only from 2.29 to 3.54, and the flow remained laminar. Because of the small scale of the reactor, the RR could not be increased significantly to allow a change in the state of the flow, and therefore its influence on the agglomeration and attrition mechanisms was limited. The operating height of the reactor would have to be increased to allow a broader study of the RR influence on the process efficiency, and particularly on the attrition of the pellets.

MF had to take an integer value, therefore 2, as it represented the physical number of inlet points of the carbonate stream. When increasing MF, two simultaneous phenomena occurred: firstly, the supersaturation was lowered at each inlet point and at the bottom of the column. Secondly, the supersaturation was more efficiently dispersed over the height of the reactor. According to the previous results, the variable MF did not have a large influence on the process. This result could be interpreted in two ways: firstly, the supersaturation at the bottom of the reactor within the limits of the surface investigated did not need to be dispersed to avoid high local concentration zones to develop. Also, the supersaturation did not need to be dispersed through the column, which means that agglomeration did not play an important role in the nickel removal all the way up the column. This result confirms the one previously observed in Figure 6.11, where agglomeration was only important within the first 20cm of column.

8.5.3 Variability of the measurements

Variability was monitored during the runs for both $Ni_{dis\ out}$ and $Ni_{tot\ out}$. The absolute error in the total nickel concentration measurements was larger than the one on the dissolved nickel concentration. The calculated simple standard deviations and standard errors are presented in Table 8.3. The standard deviation on the $Ni_{tot\ out}$ corresponded to 46.1% of the data mean, and 21.1% of the $Ni_{dis\ out}$ data mean. The standard error was 0.67 for the total nickel and 0.06 for the dissolved nickel. The relative errors were large, especially for the total nickel. The variation in $Ni_{tot\ out}$ therefore included the variations in $Ni_{dis\ out}$, but also the variation in the fines concentration. The fines formation rate depended on many parameters that did not influence the $Ni_{dis\ out}$, such as the attrition rate of the pellets, the supersaturation level and the agglomeration rate. These parameters were largely dependent on the experimental conditions. From the R^2 analysis of the second order model, 82.8% of the $Ni_{tot\ out}$ and 87.1% of the $Ni_{dis\ out}$ responses were accounted for by the five variables studied. The variability directly due to fines formation therefore accounted for 4.3% of the total $Ni_{tot\ out}$ measurement.

The uncontrolled variability in the results, 17.2% of the $Ni_{tot\ out}$ and 12.9% of the $Ni_{dis\ out}$, created a reliability problem as well as a large uncertainty in exploring the response surface. It was necessary to identify and include the source of variation in the model before further optimisation of the process was possible (Neter and Wasserman, 1974). The causes of variability that were identified during the runs are described in the following paragraphs.

The uncontrolled factors firstly included the experimental and analytical random errors discussed in Chapter VI. The ε error on each factor relative to operations and analyses could be included in the model calculation, but this is generally taken into account only in very accurate models, when other sources of error have been isolated. Including this variability in our model was therefore not relevant as yet.

The influence of the precipitation reaction temperature was investigated in the second order model analysis (paragraph 8.4). According to the analyses made, the temperature did not appear to contribute to the uncontrolled variation in the data and even increased the standard errors on the predictions, when included in the model (Appendix 10).

A portion of the uncontrolled variability observed could be a direct consequence of the nature of the pellet reactor processes. The dynamic behaviour of the process encompassed phenomena such as transient flow patterns, hydrodynamics and mixing, which, for this system, have not been fully characterised as yet and theoretically had an important effect on the local supersaturation and thus on all the precipitation processes.

Furthermore, such variability could be due to a lack of steady state conditions when operating the reactor. Although a steady state was observed during the start-up experiments after 48 hours of run, the equilibrium is likely to have further evolved with time during the successive runs. Zhou *et al* (1999) showed that under their operating conditions, the precipitation of nickel carbonate in a pellet reactor reached steady state only after eight days of run and needed the introduction of a co-plating agent (calcium chloride). The evolution of the experimental state after 48 hours of start-up experiment could therefore be a parameter influencing the overall stability of the process.

Finally, the process could be described as operating under cyclical steady state conditions. The period of the cycle was based on the frequency of pellet removal and the introduction of new seeds. Within each cycle, the total mass of pellets increased together with the active surface of the pellet until the next pellet removal. As a result, the operating state of the reactor depended on the location in the cycle, and could possibly be one of the parameters accounting for the uncontrolled variability.

8.5.4 Industrial relevance of the analysis

Finally, the industrial relevance of the two response functions studied could be identified. For instance, the two parameters measured did not have the same impact on the process efficiency. The $Ni_{tot\ out}$ indicated the total efficiency of the process, while the $Ni_{dis\ out}$ did not take into account the concentration of fines in the outlet. Although the $Ni_{dis\ out}$ appeared lower and the efficiency good, the local minimum occurred at a pH around 10.2-10.3, a region where fines formation was relatively high (Figure 6.7 and Figure 6.8). A large amount of fines exited the reactor with the effluent, and the overall process efficiency in this region was then reduced. The possibility of filtering the effluent could dramatically increase the process efficiency (up to 99.8% of nickel removed), but the problem of filter clogging during the sludge filtration would remain the same as the one experimented in hydroxide precipitation processes. The high pH would also increase the cost of effluent neutralisation and in conclusion, no real improvement would have been achieved. The $Ni_{tot\ out}$ response was more significant for the efficiency analysis. Moreover

the pH of the stationary point stabilised around 9.8 during the valley analysis, indicating a great reduction in the post neutralisation costs. Around this zone of pH most of the nickel, which was not recovered in the reactor, exited the column in dissolved form. Fines formation was not important, and the filtration problem would be avoided. If the process had to be run industrially, the addition of a post filtration stage would be necessary to secure the process, in case of an uncontrolled fines bloom. An interesting study on the maximum load of fines allowed on the filter could be carried out, to further reduce the concentration of nickel in the effluent.

Chapter IX

Conclusions

During this dissertation, several aspects of nickel carbonate precipitation within a pellet reactor were investigated. The first aim was the study of the nickel carbonate precipitation mechanisms within a pellet reactor. The experimental work consisted of a series of tests on the nickel removal efficiency under different operating conditions, as well as the establishment of different profiles of the bed. The conclusions are:

- The removal efficiency depends mainly on two parameters: the total nickel conversion and the degree of fines formation within the reactor.
- The fines are mostly formed by the spontaneous nucleation of solid phase in the liquid medium generated by a high supersaturation zone, often at the reactant inlets.
- The kinetics of the precipitation reaction are fast, and the soluble species reach near-equilibrium with the solid phase only after 20 centimetres of bed.
- The Patterson *et al* (1977) solubility diagram accurately predicts the nickel conversion, when two solid phases are taken into account: nickel hydroxide and nickel carbonates. The model is employed to determine the pH zone of the lowest soluble nickel concentration, i.e. the maximal conversion to solid nickel.
- Experimental nickel removal data fits the Patterson model well when a low supersaturation is employed within the bed. At high supersaturation, (pH above 9.8, or carbonate to nickel ratio above 4), a significant concentration of fines is found in the outlet stream and thus the removal of the nickel is reduced. Maximal removal efficiencies of 99.6% (ratio 2) and 97.2% (ratio 4) are found at pH = 9.8 for the synthetic stream used during the experiments. At increasing pH, the nickel conversion reaches a steady level of 100%, while the removal efficiency decreases below 80% at pH 11 for both ratios. The Patterson *et al* (1977) solubility model cannot thus be employed alone for nickel removal prediction, as it does not take into account fines formation.

The composition of the precipitate during the experiments was: $Ni(OH)_{0.667}(CO_3)_{0.667}$.

The second part of the experimental work was carried out using the response surface methodology (RSM). The five main parameters included in the statistical model were the pH, the nickel concentration of the feed, the carbonate to nickel molar ratio, the number of inlet feeds of the carbonate and the re-circulation rate. The aim of the study was to

locate the experimental point with the five variables as co-ordinates, where the total and the dissolved nickel concentration of the effluent stream were minimised.

The first result of the data analysis using the RSM was that the pH, Ni_{feed} and Ratio factors were the determining parameters on the response, while the RR and MF were of lesser importance. This result for MF is important as it proves again that agglomeration is a secondary phenomenon for nickel removal in the process. As the RR operating range was limited, the influence of the re-circulation on the efficiency cannot be clearly determined.

The data analysis showed that for both responses only a local minimum, or saddle point, was found within the boundaries of the experimental region. Further "steepest descent" experiments should help to locate the optimum nickel removal region for both responses.

Nevertheless, an uncontrolled variability of the response was observed and has to be identified before any further optimisation is possible. The variability accounted for 17.2% of the $Ni_{tot\ out}$ and 12.9% of the $Ni_{dis\ out}$. This implies that 4.3% of the variability of $Ni_{tot\ out}$ was due to fines formation. The effect of influence of temperature was examined but the standard errors were increased by the inclusion of temperature as a factor, and the importance of the temperature was consequently found to be negligible. The other possible origins of such variability were:

- The random experimental and analytical errors
- The lack of steady state conditions, i.e. the dynamic behaviour of the reactor, and the cycling behaviour of the process.

Finally of the two responses investigated, the $Ni_{tot\ out}$ minimisation appeared the more significant for industrial purposes even if the nickel removal as measured by $Ni_{dis\ out}$ was superior, reaching a value of 99.9%. The predicted pH of optimal response for $Ni_{tot\ out}$ stabilised 0.35 pH units below the predicted optimal pH for $Ni_{dis\ out}$. The optimal removal point was thus situated in a pH zone where fines formation and thus the fines outlet concentration was negligible. The two major problems experienced with the hydroxide precipitation of metals were thus reduced: the difficulty of solid-liquid separation of nickel hydroxide and the post neutralisation cost of the effluent.

Nevertheless the process variability experienced proved that a post filtration stage is essential to reduce any massive discharge of nickel carbonate fines in the environment due to unpredictable variation in the process efficiency.

References

Baes.C.F. and Mesmer.R.E., *The hydrolysis of cations*, New York: Wiley, ISBN 0-471-03985-3, 1976.

Baldyga.J., Bourne.J.R. and Yang.Y., "Influence of feed pipe diameter on mesomixing in stirred tank reactors", *Chem. Eng. Science*, Vol. 48, No. 19, pp. 3383-3390, 1993.

Baltpurvins.K.A., Burns.R.C., Lawrance.G.A. and Stuart.A.D., "Use of the solubility domain approach for the modelling of the hydroxide precipitation of heavy metals from wastewater", *Environ. Sci. Technol.*, vol. 30, pp. 1493-1499, 1996.

Baltpurvins.K.A., Burns.R.C., Lawrance.G.A. and Stuart.A.D., "Effect of electrolyte composition on zinc hydroxide precipitation by lime", *Wat. Res.*, No. 5, vol. 31, pp. 973-980, 1997.

Barford.N.C., *Experimental measurements: precision, error and truth*, London: Addison-Wesley, 2nd ed., ISBN 0-471-90701-4, 1985.

Brooks.C.S., "Metal recovery by selective precipitation part I. Hydroxide precipitation", *Metal finishing*, pp. 21-26, 1990.

Brooks.C.S., "Selective precipitation of mixed metal hydroxides", 45th Proc. Ind. Waste Conf., pp. 691-694, 1991.

Clesceri.L.S., Greenberg.A.E. and Eaton.A.D., *Standard methods for the examination of water and wastewater*, Washington DC: American public Health association, 20th ed., ISBN 0-87553-235-7, 1998.

Coulson.J.M. and Richardson.J.F., *Chemical engineering*, vol 2, Oxford: Butterworth-Heinemann, 4th edition, 1991.

Davidson.J., Clift.R. and Harrison.D., *Fluidization*, London Academic Press, 2nd ed., ISBN 0-1220-5552-7, 733p., 1985.

Habashi.F., *Handbook of extractive metallurgy*, vol. 2, Germany: Wiley-VCH, ISBN 3-527-28792-2, 1997.

Hartman.P., *Crystal growth, an introduction*, New York: American Elsevior, ISBN 0-7204-1821-6, 1973.

Hatakka.H., Oinas.P., Reunanen.J. and Palosaari.S., "The effect of supersaturation on agglomeration", http://www.lut.fi/~hhatakka/docit/agglo.html, 1999.

Heffels.S.K. and Kind.M., "Seeding technology: an underestimated critical success factor for crystallization", Proceedings of 14th International Symposium on Industrial Crystallization, 1999.

Hicks.C.R. and Turner.K.V., *Fundamental concepts in the design of experiments*, New York: Oxford University Press, 5th ed., ISBN 0-19-512273-9, 1999.

Hounslow.M.J., Mumtaz.H.S., Collier.J.P., Barrick.J.P. and Bramley.A.S., "Aggregation during precipitation - putting the pieces of the puzzle together", Proceedings of 14th International Symposium on Industrial Crystallization, 1999.

Impala Platinum Limited, Personal communication, 2000.

Jeffery.G.H., Bassett.J., Mendham.J. and Denney.R.C., *Vogel's. Textbook of quantitative chemical analysis*, New York: Wiley, 5th ed., ISBN 0-582-44693-7, 1989.

Jenkins.S.H., Keight.D.G. and Humphreys.R.E., "The solubility of heavy metal hydroxides in water, sewage and sewage sludge I. The solubility of some metal hydroxides.", *Int. J. Air Wat. Poll.*, vol. 8, pp. 537-556, 1964.

Kind.M., "Precipitation phenomena and their relevance to precipitation technology", Proceedings of 14th International Symposium on Industrial Crystallization, 1999.

Kramer.H., Personal communication, 2001.

Kunii.D., *Fluidization engineering*, Boston: Butterworth-Heinemann, 2nd ed., ISBN 0-4099-0233-0, 491p., 1991.

Kurz.W. and Fisher.D.J., *Fundamentals of solidification*, Switzerland: Trans Tech Publications, 3rd ed., ISBN 0-87849-522-3, 1989.

Lee.W., *Experimental design and analysis*, San Fransisco: W.H.Freeman, ISBN 0-7167-0772-1, 1975.

Lipson.C., *Statistical design and analysis of engineering experiments*, New York: McGraw-Hill, ISBN 0-070-37991-2, 518p., 1973.

Lowenthal.R., Personal communication, 2000.

McAnally.S., Benefield.L. and Reed.R.B., "Nickel removal from synthetic and actual nickel plating wastewater using sulfide and carbonate for precipitation and coprecipitation", Proc. Ind. Waste Conf. (1985), 39th, 1981.

McAnally.S., Benefield.L. and Reed.R.B., "Nickel removal from a synthetic nickel-plating waste water using sulfide and carbonate for precipitation and co-precipitation", *Separation science and technology*, vol. 19, pp. 191-217, 1984.

Moosa.S., "A kinetic study on anaerobic sulphate reduction", Doctoral thesis, University of Cape Town, South Africa, 2000.

Muirhead.R.J., *Aspects of multivariate statistical theory*, New York: Wiley, ISBN 0-471-09442-0, 1982.

Mullin.J.W., *Crystallisation*, London: Butterworth, 2nd ed., ISBN 0-40870-349-0, 480p, 1972.

Myers.H. and Montgomery.D.C., *Response surface methodology. Process and product optimization using designed experiments*, New York: Wiley, ISBN 0-471-58100-3, 1995.

Napier-Munn.T.J., "An introduction to Comparative Statistics and Experimental Design for Minerals Engineers", Course notes, University of Queensland, 2nd ed version 2.2, 1996.

Neter.J., *Applied linear statistical models: regression, analysis of variance, and experimental designs*, Homewood: Irwin, ISBN 0-256-01498-1, 842p., 1974.

Nielsen.A.E., *Industrial Crystallisation*, Amsterdam: Jong and Jancic, 1979.

Othmer.D.F., *Fluidisation*, New York: Reinbold, 231p., 1956.

Packter.A. and Uppaladinni.S.C., "The precipitation of basic carbonate powders from aqueous solution. Crystallite numbers, composition and final size", *Cryst. Res. and Tech.*, vol. 10, pp. 985-994, 1975.

Patterson.J.W., "Effect of carbonate ion on precipitation treatment of cadmium, copper, lead and zinc", Proc. Inc. Waste Conf., 36th, 1982.

Patterson.J.W., Allen.H.E., Scala.J.J., "Carbonate precipitation for heavy metals pollutants", *J. Water Pollut. Control Fed.*, vol. 49, 2397-410, 1977.

Perry.R.H and Green.D., *Perry's chemical engineers handbook*, Singapore: McGraw-Hill Book Company, 7th ed., ISBN: 0-07049-841-5, 1997.

Randolph.A.D. and Larson.M.A., *Theory of particulate processes: analysis and techniques of continuous crystallisation*, San Diego: Academic Press, 2nd ed., ISBN 0125796528, 1988.

Seckler.M.M., "Calcium phosphate precipitation in a fluidized bed", Doctoral thesis, Delft University of Technology, The Netherlands, 1994.

Skousen.J., Hilton.T. and Faulkner.B., "Overview of acid mine drainage treatment with chemicals", www.wvu.edu/~agexten/landrec/chemtn.htm, 1997.

Söhnel.O. and Garside.J., *Precipitation, basic principles and industrial application*, Oxford: Butterworth Heinemann, ISBN 0 7506 1107 3, 1992.

Sohnel.O. and Mullin.J.W., "Agglomeration in batch precipitated suspensions", AIChE Symposium, series no. 284, vol. 87, p182-188, 1987.

Stumm.W. and Morgan.J.J., *Aquatic chemistry, chemical equilibria and rates in natural waters*, New York: Wiley, ISBN 0-471-51184-6, 1022 p, 1996.

Sydenham.P.H., Hancock.N.H. and Thorn.R., *Introduction to measurement science and engineering*, New York: Wiley, ISBN 0-471-92223-4, 1989.

Torbacke.M. and Rasmuson.A.C., "Influence of different scales of mixing in reaction crystallisation", *Chem. Eng. Sci*, 56(7), 2459-2473, 2001.

Toyokura.K., Tanaka.H. and Tanahashi.J., "Size distribution of crystals from classified bed type crystallizer", *J.Chem. Eng. Jap.*, vol. 6, pp. 325-331, 1973

Tunay.O., Tasli.R. and Orhon.D., "Factors affecting the performance of hydroxide precipitation of metals", Proc. Ind. Waste Conf., 46th, 1992.

Uhl.W.V. and Gray.J.B., *Mixing: theory and practice*, New York: Academic Press, 1966.

Van Dijk.J.C., Scholler.M. and Wilms.D., "Recovery of metals by crystallization in the pellet reactor", *Envir. Tech.*, Prod. Env. Conf, 2nd, pp.294-303, 1987.

Van Dijk.J.C., Van Ammers.M., Graveland.A. and Nuhn.P.A.N.M., "State of the art of pellet softening in the Netherlands", *Wat Supply*, vol 4, pp. 223-235, 1986.

Van Rosmalen.G.M., "Crystallisation and precipitation workshop", Glenburn Lodge, South Africa, 10th to 12th of June, 1998.

Van Rosmalen.G.M., Lewis.A. and Kramer.H., "Controlling precipitation processes", Glenburn Lodge, South Africa, 22nd to 24th of March, 2001.

Van Weert.G. and Van Dijk.J.C., "The production of nickel carbonate spheroids from dilute solutions in a pellet reactor", Paul Queneau International Symposium on Extractive Metallurgy of Copper, Nickel and cobalt, vol 1, pp. 1133-1144, 1993.

Wang.Y. and Anderson.P.R., "Effect of the surface characteristics of seed on copper precipitation", *Wat. Sci. Tech.*, vol. 26, No. 9-11, pp. 2141-2143, 1992.

Walton.A.G., *The formation and Properties of precipitates*, Huntington, New York: Krieger, ISBN 0-88275-990-6, 1967.

Wilms.D.A., "Recovery of nickel by crystallisation of nickel carbonates in a fluidised bed reactor", VTT Symposium on Non-Waste Tech., Espoo, Finland, 1988.

Wojcik.J.A., "Modelling of fluidised bed crystallizers", Proceedings of 14th International Symposium on Industrial Crystallization, 1999.

Zenz.F.A. and Othmer.D.F., *Fluidization and fluid part systems*, New York: Reinbold, 513p., 1960.

Zhou.P., Huang.J.C., Li A.W.F. and Wei.S., "Heavy metal removal from wastewater in fluidized bed reactor", *Wat. Res.*, vol. 33, no. S, pp. 1918-1924, 1999.

Appendices

Appendix 1: Nickel data sheet

Property	*Value*	*Unit*
Molar mass	58.71	$g.mol^{-1}$
Density	8.91	
mp	1455	deg.C
bp	2730	deg.C
Electronegativity	1.9	
Volume increase on melting	4.5	%
Heat of fusion	302	$J.g^{-1}$
Heat of sublimation	7317	$J.g^{-1}$
Heat of vaporisation	6375	$J.g^{-1}$
Standard entropy	29.81	$J.K^{-1}$
Surface tension	1778-0.38(T-1455)	$mN.m^{-1}$
Viscosity	$0.1663e^{-(855/RT)}$	$mPa.s^{-1}$
Thermal conductivity	88.5	$W.m^{-1}.K^{-1}$
Heat capacity	0.452	$J.g^{-1}.K^{-1}$
Electrical resistivity	6.9	$mW.cm^{-1}$
Temperature coeff of electrical resistivity	$6.8.10^{-03}$	K^{-1}
Thermal expansion coefficient	$13.3.10^{-06}$	K^{-1}
Modulus of elasticity	199.5	GPa
Brinell hardness	85	

TableA1.1: Nickel physical properties

Appendix 2: Chemicals safety sheet

SODIUM CARBONATE ANHYDROUS

MSDS Number: S3242 --- *Effective Date: 05/17/01*

Product Identification

Synonyms: Carbonic acid, disodium salt; disodium carbonate; soda ash
CAS No.: 497-19-8
Molecular Weight: 105.99
Chemical Formula: Na2CO3
Product Codes:
J.T. Baker: 3602, 3604, 3605, 4502, 4923, 5198, 5834
Mallinckrodt: 1338, 7468, 7521, 7527, 7528, 7698

Hazards Identification

Emergency Overview

DANGER! MAY CAUSE EYE BURNS. HARMFUL IF SWALLOWED OR INHALED. CAUSES IRRITATION TO SKIN AND RESPIRATORY TRACT.

J.T. Baker SAF-T-DATA(tm) Ratings (Provided here for your convenience)

Health Rating: 1 - Slight
Flammability Rating: 0 - None
Reactivity Rating: 1 - Slight
Contact Rating: 2 - Moderate
Lab Protective Equip: GOGGLES; LAB COAT; VENT HOOD; PROPER GLOVES
Storage Color Code: Orange (General Storage)

Potential Health Effects

Inhalation:
Inhalation of dust may cause irritation to the respiratory tract. Symptoms from excessive inhalation of dust may include coughing and difficult breathing. Excessive contact is known to cause damage to the nasal septum.
Ingestion:
Sodium carbonate is only slightly toxic, but large doses may be corrosive to the gastro-intestinal tract where symptoms may include severe abdominal pain, vomiting, diarrhea, collapse and death.
Skin Contact:
Excessive contact may cause irritation with blistering and redness. Solutions may cause severe irritation or burns.
Eye Contact:
Contact may be corrosive to eyes and cause conjuctival edema and corneal destruction. Risk of serious injury increases if eyes are kept tightly closed. Other symptoms may appear from absorption of sodium carbonate into the bloodstream via the eyes.
Chronic Exposure:

Prolonged or repeated skin exposure may cause sensitization.
Aggravation of Pre-existing Conditions:
No information found.

Physical and Chemical Properties

Appearance:
White powder or granules.
Odor:
Odorless.
Solubility:
45.5 g/100 ml water @ 100C (212F)
Specific Gravity:
2.53
pH:
11.6 Aqueous solution
% Volatiles by volume @ 21C (70F):
0
Boiling Point:
Decomposes.
Melting Point:
851C (1564F)
Vapor Density (Air=1):
No information found.
Vapor Pressure (mm Hg):
No information found.
Evaporation Rate (BuAc=1):
No information found.

Toxicological Information

For Sodium Carbonate:
Oral rat LD50: 4090 mg/kg; inhalation rat LC50: 2300 mg/m3/2H; irritation eye rabbit: 50 mg severe; investigated as a mutagen, reproductive effector.

--------\Cancer Lists\----------

Ingredient	---NTP Carcinogen--- Known	Anticipated	IARC Category
Sodium Carbonate (497-19-8)	No	No	None

SODIUM HYDROXIDE

MSDS Number: S4034 ***--Effective Date: 08/20/98***

Product Identification

Synonyms: Caustic soda; lye; sodium hydroxide solid; sodium hydrate
CAS No.:1310-73-2
Molecular Weight:40.00
Chemical Formula: NaOH
Product Codes:
J.T. Baker: 3718, 3721, 3722, 3723, 3728, 3734, 3736, 5045, 5565
Mallinckrodt: 7001, 7680, 7708, 7712, 7772, 7798

Hazards Identification

Emergency Overview

POISON! DANGER! CORROSIVE. MAY BE FATAL IF SWALLOWED. HARMFUL IF INHALED. CAUSES BURNS TO ANY AREA OF CONTACT. REACTS WITH WATER, ACIDS AND OTHER MATERIALS.

J.T. Baker SAF-T-DATA(tm) Ratings (Provided here for your convenience)

Health Rating: 3 - Severe (Poison)
Flammability Rating: 0 - None
Reactivity Rating: 2 - Moderate
Contact Rating: 4 - Extreme (Corrosive)
Lab Protective Equip: GOGGLES; LAB COAT; VENT HOOD; PROPER GLOVES
Storage Color Code: White Stripe (Store Separately)

Potential Health Effects

Inhalation:
Severe irritant. Effects from inhalation of dust or mist vary from mild irritation to serious damage of the upper respiratory tract, depending on severity of exposure.

Symptoms may include sneezing, sore throat or runny nose. Severe pneumonitis may occur.

Ingestion:
Corrosive! Swallowing may cause severe burns of mouth, throat, and stomach. Severe scarring of tissue and death may result. Symptoms may include bleeding, vomiting, diarrhea, fall in blood pressure. Damage may appears days after exposure.

Skin Contact:
Corrosive! Contact with skin can cause irritation or severe burns and scarring with greater exposures.

Eye Contact:
Corrosive! Causes irritation of eyes, and with greater exposures it can cause burns that may result in permanent impairment of vision, even blindness.

Chronic Exposure:
Prolonged contact with dilute solutions or dust has a destructive effect upon tissue.

Aggravation of Pre-existing Conditions:
Persons with pre-existing skin disorders or eye problems or impaired respiratory function may be more susceptible to the effects of the substance.

Physical and Chemical Properties

Appearance:
White, deliquescent pellets or flakes.

Odor:
Odorless.

Solubility:
111 g/100 g of water.

Specific Gravity:
2.13

pH:
13 - 14 (0.5% soln.)

% Volatiles by volume @ 21C (70F):
0

Boiling Point:
1390C (2534F)

Melting Point:
318C (604F)

Vapor Density (Air=1):
> 1.0

Vapor Pressure (mm Hg):
Negligible.

Evaporation Rate (BuAc=1):
No information found.

Toxicological Information

Irritation data: skin, rabbit: 500 mg/24H severe; eye rabbit: 50 ug/24H severe; investigated as a mutagen.

--------\Cancer Lists\----------

Ingredient	---NTP Carcinogen--- Known	Anticipated	IAR
Sodium Hydroxide (1310-73-2)	No	No	

HYDROCHLORIC ACID, 33 - 40%

MSDS Number: H3880 ***---Effective Date: 11/17/99***

Product Identification

Synonyms: Muriatic acid; hydrogen chloride, aqueous
CAS No.:7647-01-0
Molecular Weight:36.46
Chemical Formula:HCl
Product Codes:
J.T. Baker: 5367, 5537, 5575, 5800, 5814, 5839, 6900, 7831, 9529, 9530, 9534, 9535, 9536, 9537, 9538, 9539, 9540, 9544, 9548
Mallinckrodt: 2062, 2612, 2624, 2626, 5587, H611, H613, H987, H992, H999, V078, V628

Hazards Identification

Emergency Overview

POISON! DANGER! CORROSIVE. LIQUID AND MIST CAUSE SEVERE BURNS TO ALL BODY TISSUE. MAY BE FATAL IF SWALLOWED OR INHALED. INHALATION MAY CAUSE LUNG DAMAGE.

J.T. Baker SAF-T-DATA(tm) Ratings (Provided here for your convenience)

Health Rating: 3 - Severe (Poison)
Flammability Rating: 0 - None
Reactivity Rating: 2 - Moderate
Contact Rating: 3 - Severe (Corrosive)
Lab Protective Equip: GOGGLES & SHIELD; LAB COAT & APRON; VENT HOOD; PROPER GLOVES
Storage Color Code: White (Corrosive)

Potential Health Effects

Inhalation:
Corrosive! Inhalation of vapors can cause coughing, choking, inflammation of the nose, throat, and upper respiratory tract, and in severe cases, pulmonary edema, circulatory failure, and death.
Ingestion:
Corrosive! Swallowing hydrochloric acid can cause immediate pain and burns of the mouth, throat, esophagus and gastrointestinal tract. May cause

nausea, vomiting, and diarrhea. Swallowing may be fatal.
Skin Contact:
Corrosive! Can cause redness, pain, and severe skin burns. Concentrated solutions cause deep ulcers and discolor skin.
Eye Contact:
Corrosive! Vapors are irritating and may cause damage to the eyes. Contact may cause severe burns and permanent eye damage.
Chronic Exposure:
Long-term exposure to concentrated vapors may cause erosion of teeth. Long term exposures seldom occur due to the corrosive properties of the acid.
Aggravation of Pre-existing Conditions:
Persons with pre-existing skin disorders or eye disease may be more susceptible to the effects of this substance.

Physical and Chemical Properties

Appearance:
Colorless, fuming liquid.
Odor:
Pungent odor of hydrogen chloride.
Solubility:
Infinite in water with slight evolution of heat.
Density:
1.18
pH:
For HCL solutions: 0.1 (1.0 N), 1.1 (0.1 N), 2.02 (0.01 N)
% Volatiles by volume @ 21C (70F):
100
Boiling Point:
53C (127F) Azeotrope (20.2%) boils at 109C (228F)
Melting Point:
-74C (-101F)
Vapor Density (Air=1):
No information found.
Vapor Pressure (mm Hg):
190 @ 25C (77F)
Evaporation Rate (BuAc=1):
No information found.

Toxicological Information

Inhalation rat LC50: 3124 ppm/1H; oral rabbit LD50: 900 mg/kg (Hydrochloric acid concentrated); investigated as a tumorigen, mutagen, reproductive effector.

--------\Cancer Lists\----------

Ingredient	---NTP Carcinogen--- Known	Anticipated	IARC Cate
Hydrogen Chloride (7647-01-0)	No	No	3
Water (7732-18-5)	No	No	None

NICKEL SULFATE

MSDS Number: N3122 ***--Effective Date: 04/15/99***

Product Identification

Synonyms: Nickel (II) sulfate hexahydrate (1:1:6); sulfuric acid, nickel (2+) salt, hexahydrate
CAS No.:7786-81-4
Molecular Weight:262.88
Chemical Formula: NiSO4 6H2O
Product Codes:
J.T. Baker: 2808
Mallinckrodt: 6400

Hazards Identification

Emergency Overview

WARNING! HARMFUL IF SWALLOWED OR INHALED. CAUSES IRRITATION TO SKIN, EYES AND RESPIRATORY TRACT. MAY CAUSE ALLERGIC SKIN OR RESPIRATORY REACTION. CANCER HAZARD. CAN CAUSE CANCER. Risk of cancer depends on duration and level of exposure.

J.T. Baker SAF-T-DATA(tm) Ratings (Provided here for your convenience)

Health Rating: 3 - Severe (Cancer Causing)
Flammability Rating: 0 - None
Reactivity Rating: 0 - None
Contact Rating: 3 - Severe (Life)
Lab Protective Equip: GOGGLES; LAB COAT; VENT HOOD; PROPER GLOVES
Storage Color Code: Blue (Health)

Potential Health Effects

Inhalation:
Causes irritation to the respiratory tract. Symptoms may include coughing, sore throat, and shortness of breath. Lung damage may result from a single high exposure or lower repeated exposures. Lung allergy occasionally occurs, with asthma type symptoms.
Ingestion:
Toxic. Symptoms may include abdominal pain, diarrhea, nausea, and

vomiting. Absorption is poor, but should it occur, symptoms may include giddiness, capillary damage, myocardial weakness, central nervous system depression, and kidney and liver damage.

Skin Contact:
Causes irritation. May cause skin allergy with itching, redness or rash. Some individuals may become sensitized to the substance and suffer "nickel itch", a form of dermatitis.

Eye Contact:
Causes irritation, redness, and pain.

Chronic Exposure:
Prolonged or repeated exposure to excessive concentrations may affect lungs, liver and kidneys. Chronic exposure to nickel and nickel compounds is associated with cancer.

Aggravation of Pre-existing Conditions:
Persons with pre-existing skin disorders, impaired respiratory or pulmonary function, or with a history of asthma, allergies, or sensitization to nickel compounds may be at an increased risk upon exposure to this substance.

Physical and Chemical Properties

Appearance:
Blue-green crystals.

Odor:
Odorless.

Solubility:
75.6 g/100 cc water @ 15.5C

Specific Gravity:
2.03

pH:
ca. 4.5

% Volatiles by volume @ 21C (70F):
0

Boiling Point:
103C (217F) (Loses 6H2O)

Melting Point:
100C (212F) Loses water

Vapor Density (Air=1):
No information found.

Vapor Pressure (mm Hg):
No information found.

Evaporation Rate (BuAc=1):
No information found.

Toxicological Information

No LD50/LC50 information found relating to normal routes of

occupational exposure. Investigated as a tumorigen and mutagen.

--------\Cancer Lists\----------

Ingredient	---NTP Carcinogen--- Known	Anticipated	IARC Cate
Nickel Sulfate (7786-81-4)	No	Yes	1

PHOSPHORIC ACID,10%

MSDS Number: P3976 ***---Effective Date: 08/24/00***

Product Identification

Synonyms: Ortho-phosphoric acid
CAS No.:7664-38-2
Molecular Weight: Not applicable to mixtures.
Chemical Formula:H3PO4 in H2O
Product Codes:5683

Hazards Identification

Emergency Overview

DANGER! CORROSIVE. CAUSES SEVERE IRRITATION AND BURNS TO EVERY AREA OF CONTACT. HARMFUL IF SWALLOWED OR INHALED.

J.T. Baker SAF-T-DATA(tm) Ratings (Provided here for your convenience)

Health Rating: 2 - Moderate
Flammability Rating: 0 - None
Reactivity Rating: 2 - Moderate
Contact Rating: 2 - Moderate
Lab Protective Equip: GOGGLES & SHIELD; LAB COAT & APRON; VENT HOOD; PROPER GLOVES
Storage Color Code: White (Corrosive)

Potential Health Effects

The hazards on this data sheet apply to concentrated (85%) phosphoric acid. The hazards of the 10% solution are expected to be reduced, but no information for the dilute solution is available.

Inhalation:
Inhalation is not an expected hazard unless misted or heated to high temperatures. Mist or vapor inhalation can cause irritation to the nose, throat, and upper respiratory tract. Severe exposures can lead to a chemical pneumonitis.
Ingestion:

Corrosive. May cause sore throat, abdominal pain, nausea, and severe burns of the mouth, throat, and stomach. Severe exposures can lead to shock, circulatory collapse, and death.
Skin Contact:
Corrosive. May cause redness, pain, and severe skin burns.
Eye Contact:
Corrosive. May cause redness, pain, blurred vision, eye burns, and permanent eye damage.
Chronic Exposure:
No information found.
Aggravation of Pre-existing Conditions:
Persons with pre-existing skin disorders or eye problems, or impaired respiratory function may be more susceptible to the effects of the substance.

Physical and Chemical Properties

Appearance:
Clear, colorless liquid.
Odor:
Odorless.
Solubility:
Miscible in all proportions in water.
Specific Gravity:
1.05 @ 25C
pH:
1.5 (0.1 N aqueous solution)
% Volatiles by volume @ 21C (70F):
No information found.
Boiling Point:
158C (316F)
Melting Point:
21C (70F)
Vapor Density (Air=1):
3.4
Vapor Pressure (mm Hg):
0.03 @ 20C (68F)
Evaporation Rate (BuAc=1):
No information found.

Toxicological Information

Oral rat LD50: 1530 mg/kg; investigated as a mutagen.

--------\Cancer Lists\----------

Ingredient	---NTP Carcinogen--- Known	Anticipated	IARC Cate

Phosphoric Acid (7664-38-2)	No	No	None
Water (7732-18-5)	No	No	None

quirements.

Appendix 3: Experiment listing

Experiment name	*Number*	*Date*	*Note*
Exp 1	A01	12/07/00	
Exp 2	A02	14/07/00	
Exp 3	A03	14/07/00	
Exp 4	A04	14/07/00	
Exp 5	A05	08/08/00	
Exp 6	A06	09/08/00	
Exp 7	A07	11/08/00	
Exp 8	A08	13/08/00	
Exp 9	A09	15/08/00	
Exp 1bis	G01	09/10/00	Start-up column
Exp 2bis	G02	11/10/00	Ni profile, pH 9.2
Exp 3bis	G03	11/10/00	Ni profile, pH 8.4
Exp 4bis	G04	11/10/00	
Exp 5bis	G05	17/10/00	Ni profile, pH 9.4
Exp 6bis	G06	23/10/00	Ni profile, pH 9.15
Exp 7bis	G07	24/10/00	Ni and carbonate profiles, pH 9.75
Exp 8bis	G08	30/10/00	Blank run: no carbonate injected, only hydroxides
Exp 9bis	G09	31/10/00	Start-up 2 column, Ni and carbonate profiles, pH 9.15
Exp 10bis	G10	20/11/00	Comparaison solubilities
Exp 11bis	G11	20/11/00	Comparaison solubilities
Exp Stat 01	S01	29/11/00	
Exp Stat 02	S02	29/11/00	
Exp Stat 02bis	S03	11/01/01	
Exp Stat 03	S04	01/12/00	
Exp Stat 03bis	S05	22/01/01	
Exp Stat 04	S06	01/12/00	
Exp Stat 04bis	S07	22/01/01	
Exp Stat 05	S08	04/12/00	
Exp Stat 05bis	S09	23/01/01	
Exp Stat 06	S10	06/12/00	
Exp Stat 07	S11	06/12/00	
Exp Stat 08	S12	07/12/00	
Exp Stat 08bis	S13	23/01/01	
Exp Stat 09	S14	07/12/00	
Exp Stat 09bis	S15	23/01/01	
Exp Stat 10	S16	08/12/00	
Exp Stat 11	S17	11/12/00	
Exp Stat 12	S18	09/01/01	
Exp Stat 13	S19	09/01/01	

Exp Stat 14	S20	09/01/01	
Exp Stat 15	S21	11/02/01	
Exp Stat 16	S22	11/02/01	
Exp Stat 17	S23	13/02/01	
Exp Stat 18	S24	13/02/01	
Exp Stat 19	S25	13/02/01	
Exp Stat 20	S26	14/02/01	
Exp Stat 21	S27	14/02/01	
Exp Stat 22	S28	15/02/01	Ni profile, pH 9.5
Exp Stat 23	S29	15/02/01	
Exp Stat 24	S30	15/02/01	
Exp Stat 25	S31	20/02/01	Ni profile, pH 10.5
Exp Stat 26	S32	26/02/01	
Exp Stat 27	S33	26/02/01	
Exp Stat 28	S34	26/02/01	Ni and carbonate profile, pH 10.5. Ni shut down
Exp Stat 29	S35	28/02/01	
Exp Stat 30	S36	01/03/01	
Exp Stat 31	S37	01/03/01	
Exp Stat 32	S38	02/03/01	
Stat Central 01	SC01	04/12/00	
Stat Central 01bis	SC02	22/01/01	
Stat Central 02	SC03	07/12/00	
Stat Central 02bis	SC04	23/01/01	
Stat Central 03	SC05	8/12/00	
Stat Central 04	SC06	10/01/01	
Stat Central 05	SC07	15/02/01	
Stat Central 06	SC08	20/02/01	
Stat Central 07	SC09	28/02/01	
Stat Central 08	SC10	01/03/01	
Stat Central 08bis	SC11	01/03/01	Ni profile, pH 10
Stat Central 09	SC12	02/03/01	
Stat Central 10	SC13	26/03/01	
Stat Central 11	SC14	27/03/01	Ni shut down
Stat Central 12	SC15	27/03/01	
Stat Central 13	SC16	28/03/01	
Stat Axial 01	SA01	02/04/01	
Stat Axial 02	SA02	02/04/01	
Stat Axial 03	SA03	02/04/01	
Stat Axial 04	SA04	03/04/01	
Stat Axial 05	SA05	03/04/01	
Stat Axial 06	SA06	03/04/01	
Stat Axial 07	SA07	04/04/01	
Stat Axial 08	SA08	05/04/01	
Stat Axial 09	SA09	05/04/01	
Stat Axial 09bis	SA10	26/04/01	
Stat Axial 10	SA11	05/04/01	
Start-up 1	SU01	25/04/01	Start-up 1 column

Table A3.1: Experiments numbering

Appendix 4: Experimental Results

Experiment	*G01*				*SU01*			
Time	*outlet pH*	*Nitot out*	*idis ou*	*bed H*	*outlet p*	*Nitot out*	*idis ou*	*bed H*
h	pH	ppm	ppm	cm	pH	ppm	ppm	cm
0	9.2			72				
0.0017					10.3	3.1	1.68	79.9
0.0033				72.1	10.3	10.7	0.85	
0.0083					10.27	12.2	1.1	
0.17					10.17	9.8	1.4	80.5
0.25					10.2	5.4	1.37	80.5
0.33	9.03	9.41	6.3		10.22	3.4	1.31	80.5
0.5	9.11	6.7	5.42		10.18	3.25	1.36	81
0.66	9.16	5.14	4.66		10.15	3.4	1.42	
1	9.23	4.2	3.91	72.2	10.08	4.41	1.33	81
2	9.28	5.13	4.4	72.4	9.99	4.15	1.46	81
3	9.25	4.89	4.42		9.85	4.76	1.37	82
4	9.22	5.31	4.32	72.5				
5	9.21	5.18	4.32	72.1				
6	9.13	5.4	4.62					
7	9.19	5.25	4.78					
7.5					9.95	4.5	1.42	82.5
8	9.18	5.45	4.92	72.8	9.94	5.02	1.45	83.2
17				75.8	9.98	4.70	1.48	84
17.5					9.98	4.16	1.52	84
21					9.92	4.89	1.95	83.9
23	9.14	5.2	4.82		10	4.57	1.55	85
24	9.16	5	4.76		10.02	4.12	1.49	85.1
27	9.16	5.34	4.88		10.02	4.8	1.57	
30	9.09	5.76	5.14	75.2	10	4.7	1.45	
32	9.05	5.61	5.44	76.2				
47	9.18	5.65	5.41	79	9.97	4.21	1.56	
48	9.22	5.8	5.2	79	9.96	5.01	1.62	

Table A4.1: Start up results (G01, SU01)

Experiment	*S34*		*SC14*	
Time	*Nidis out*	*Nitot out*	*Nidis out*	*Nitot out*
min	ppm	ppm	ppm	ppm
-5	0.37	1.74	0.75	2.23
0	0.59	2.21	0.6	3.02
1	0.73	18.79	1.32	5.85
2		15.12		
3		17.5		7.58
4		15.32		
5	1.04	11.88	1.26	12.34
6		10.19		
7		7.63	0.74	6.57
8		6.51		4.35
9		5.79		4.08
10	0.69	5.84	0.77	3.14
15		5.31		2.08
20		4.46		1.75
30	0.8	2.61	0.74	1.79
60	0.56	2.21	0.69	2.7
120	0.45	1.8	0.56	1.45

Table A4.2: Nickel feed shut down results (S34, SC14)

Experiment	*pH*	*Ni/CO3* ratio	*Nitot out* mol/L	*log[Ni]* mol/L
G02	9.37	2	1.07E-05	-4.97
G02	9.24	2	1.45E-05	-4.84
G03	9	2	7.50E-05	-4.12
G03	8.87	2	9.45E-05	-4.02
G03	8.6	2	2.18E-04	-3.66
G05	9.86	2	3.24E-06	-5.49
G05	9.7	2	5.74E-06	-5.24
G06	11.25	2	2.78E-04	-3.56
G06	10.49	2	7.09E-05	-4.15
G06	9.45	2	2.88E-05	-4.54
G06	9.16	2	5.07E-05	-4.29
G07	10	2	7.94E-06	-5.10
G07	10.19	2	1.26E-05	-4.90
A01	9.78	4	3.94E-06	-5.40
A02	9.37	4	4.36E-05	-4.36
A03	9.99	4	4.53E-06	-5.34
A04	9.98	4	5.01E-06	-5.30
A09	8.39	4	1.76E-04	-3.75
A07	10.58	4	1.03E-04	-3.99
G07	8.22	4	9.05E-04	-3.04
G08	8.57	4	5.05E-04	-3.30
G09	9.13	4	1.17E-04	-3.93
G10	9.28	4	8.86E-05	-4.05
G11	9.74	4	1.98E-05	-4.70
G12	10.1	4	7.43E-05	-4.13
G13	10.22	4	6.12E-05	-4.21

Table A4.3: Nickel hydroxy-carbonate experimental solubility

Experiment	pH	Nickel Removal %	Conversion %	Fines Concentration %
Ratio 2				
G03	8.6	65.2	65.7	0.5
G03	8.87	84.9	85.2	0.3
G03	9	88	90	2
G06	9.16	92.7	93.3	0.6
G02	9.24	97.7	98	0.3
G02	9.37	98.3	99.1	0.8
G06	9.45	95.9	97.6	1.7
G05	9.7	99.2	99.8	0.6
G05	9.86	99.6	100	0.4
G06	10.49	89.8	100	10.2
G06	11.25	60	100	40
Ratio 4				
G11	8.56	17.24	26.15	8.91
G12	8.92	60.46	62.15	1.7
G13	9.15	79.54	80.04	0.5
G14	9.27	84.5	85.46	0.96
G15	9.39	91.48	95.17	3.7
G16	9.58	94.98	94.52	-0.46
G17	9.61	85.83	94.43	8.61
G18	9.75	93.37	96.8	3.43
G19	9.84	92.37	96.96	4.59
G20	9.97	88.7	97.65	8.96
G21	10.02	97.13	99.41	2.28
G22	10.08	85.13	98.09	12.96
G23	10.17	87.15	99.2	12.04
G24	10.18	84.28	98.65	14.37
G25	10.36	84.63	99.15	14.52
G26	10.47	83.72	99.48	15.76
G27	10.54	85.35	98.57	13.22
G28	10.7	82.04	99.74	17.7
G29	10.82	83.52	99.93	16.41
G30	10.92	79.76	99.89	20.13

Table A4.4: Nickel removal efficiency versus pH

Experiment	*G07*	*G09*	*S34*	*S31*
pH	*9.75*	*9.15*	*10.5*	*10.5*
H from bottom cm	$Ni_{dis\ out}$ ppm	$Ni_{dis\ out}$ ppm	$Ni_{dis\ out}$ ppm	$Ni_{dis\ out}$ ppm
0			19.72	15.5
10	9.15	13.72	1.62	1.2
20	1.75	4.94	1.01	0.21
30	0.95	4.3	0.7	0.2
40	0.83	4.75	0.72	0.23
50	0.8	4.63	0.69	0.22
60	0.83	4.41	0.75	0.22
70	0.87	4.75	0.71	0.2
90	0.86	4.88	0.76	0.23

Experiment	*G02*	*G07*	*G09*	*S34*	*SC11*
pH	*9.2*	*9.75*	*9.15*	*10.5*	*9.7*
H from bottom cm	$Ni_{tot\ out}$ ppm	$Ni_{tot\ out}$ ppm	$Ni_{tot\ out}$ ppm	$Ni_{tot\ out}$ ppm	$Ni_{tot\ out}$ ppm
0				60.62	40.28
10	11.97	10.55	15.02	6.67	6.97
20	1.82	7.6	5.03	4.98	2.01
30	2.76	5.47	4.79	5.07	2.31
40	1.6	3.82	4.09	3.05	1.73
50	1.31	2.5	4.98	2.63	1.25
60	2.15	1.75	4.91	2.3	1.51
70	0.94	1.3	4.68	1.1	1.82
90	0.78	1.04	5.84	9.05	6.38

Table A4.5: $Ni_{tot\ out}$ and $Ni_{dis\ out}$ profiles of the reactor (G02, G07, G09, S34 and SC11)

Experiment		*SC11*								
pH		*9.7*								
H from bottom	$Ni_{tot\ out}$	$Ni_{tot\ out}$	$Ni_{dis\ out}$	$Ni_{dis\ out}$	Ni_{fines}	Ni_{fines}	Ni_{in}	Ni_{in}	$Ni_{removal}$	$Ni_{removal}$
cm	ppm	%	ppm	%	ppm	%	ppm	%	ppm	%
0	40.28	100.0	30.1	74.7	10.18	25.3	60.62	100	20.34	0.0
10	6.97	17.3	4.49	11.1	2.48	6.2	60.62	100	53.65	82.7
20	2.01	5.0	1.97	4.9	0.04	0.1	60.62	100	58.61	95.0
30	2.31	5.7	1.1	2.7	1.21	3.0	60.62	100	58.31	94.3
40	1.73	4.3	1.05	2.6	0.68	1.7	60.62	100	58.89	95.7
50	1.25	3.1	1.1	2.7	0.15	0.4	60.62	100	59.37	96.9
60	1.51	3.7	0.98	2.4	0.53	1.3	60.62	100	59.11	96.3
70	1.82	4.5	1.01	2.5	0.81	2.0	60.62	100	58.8	95.5
90	6.38	15.8391	1.09	2.70606	5.29	13.1331	60.62	100	54.24	84.160874

Table A4.6: Nickel concentration profiles of the reactor (SC11)

Experiment	*G07*	*G09*
H from bottom	*Supersaturation*	
cm	beta	
0	916.6	873.2
10	377.2	452.3
20	0.0	58.7
30	0.0	54.4
40	0.0	107.6
50	0.0	116.9
60	0.0	135.5
70	0.1	154.8
90	0.1	164.8

Table A4.7: Supersaturation profile of the reactor (G07 and G09)

Experiment	*G02*	*G03*	*G05*	*G09*	*G07*
H from bottom cm	*pH at sampling point*				
10	8.58	8.36	8.85	8.79	8.63
20	9.3	8.71	9.54	9.2	9.86
30	9.23	8.64	9.53	9.27	9.89
40	9.21	8.57	9.49	9.29	9.84
50	9.2	8.5	9.43	9.2	9.8
60	9.17	8.45	9.41	9.16	9.78
70	9.16	8.36	9.36	9.15	9.74
90	9.2	8.36	9.39	9.15	9.75

Table A4.8: pH profiles of the reactor (G02, G03, G05, G07 and G09)

Experiment	*G07*	*G09*	*S34*
H from bottom cm	*[CO3]* mol/L	*[CO3]* mol/L	*[CO3]* mol/L
0	0.0232	0.0126	0.0659
10	0.0081	0.0051	0.0256
20	0.0046	0.0039	0.018
30	0.0043	0.0037	0.0171
40	0.004	0.0035	0.017
50	0.0035	0.0036	0.0159
60	0.0037	0.0034	0.0175
70	0.0035	0.0035	0.0165
90	0.0034	0.0031	0.0163

Table A4.9: Carbonate profiles of the reactor (G07, G09 and S34)

Appendix 5: Carbonate titration
(Lowenthal, 2000)

The best accuracy when measuring the carbonate concentration was obtained by a pH-metric titration, using a 0.1molar hydrochloric acid standard, aiming at measuring the total alkalinity of the solution. A Hanna pH-metre pH212 was used.

The titration procedure was the following: 100mL of the solution to be titrate was poured in conical flask, and the pH was measured: pHs. Then, 3 drops of mixed indicator (methyl orange – indigo carmine) were added. HCl solution was dropped in the solution energetically stirred with a magnetic bar, until the change of colour of the indicator (green to purple). Then, 5 pH values where taken, adding each time 1mL of HCl to the solution: pH_i corresponding to Vx_i. Then, we can plot Fx=f(Vx), called "Gram function" considering the following equations:

$$alk_x = -[H^+]_x$$

$$alk_x = \frac{(Ve - Vx)\,\overline{C}_a}{Vs + Vx}$$

$$Fx = (Ve - Vx)\,\overline{C}_a$$

With: Ve equivalent volume to be calculated; Vs the sample volume; Vx the volume dropped for each pHx.

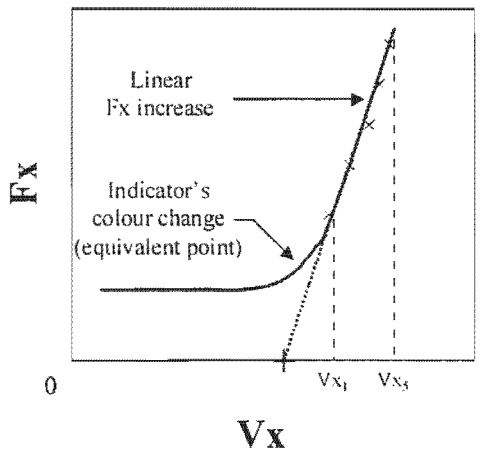

Figure A5.1: Carbonate titration curve: Fx=f(Vx)

We see graphically that Fx increases linearly after the equivalent point. The intercept of the Vx axes with the linear Vxi extrapolation gives the exact volume dropped at the equivalent point. From this value, the exact carbonate concentration of the solution can be calculated with the following equations:

$$T_{alk} = \frac{Ve.\overline{C_a}}{Vs}$$

$$T_{alk[} = 2[CO_3^{2-}] + [HCO_3^-] + [OH^-] - [H^+]$$

This method gives very accurate results in comparison with the simple, and quickly made colourimetric titration, as the equivalent point volume is measured as the result of 5 different pH measurements, and not related to the subjectivity of a pH-indicator colour change.

Nevertheless, the carbonate titration is used to check the mother liquor concentration, but does not give other exploitable results. It was just measured as an indicator of the precipitation of nickel carbonate, when achieving the carbonate molar balance of the system (considered closed to the atmosphere). The following equation was used for the mass balances:

$$C_{mother\_CO3} \times Q_{CO3} + C_{tap\_water\_CO3} \times Q_{Ni} = n_{CO3\_ppt} + C_{effluent\_CO3} \times (Q_{CO3} + Q_{Ni})$$

Appendix 6: Pellets analysis

A method to analyse the precipitate composition was developed coupling AA spectroscopy, and the titration of phosphoric acid used to dissolve the precipitate. The experimental procedure is based on the dissolving reaction of the nickel hydroxy-carbonate by the phosphoric acid:

$$2nYH_3PO_4 + nYCO_3^{2-} \longrightarrow 2nYH_2PO_4^- + nYCO_2 + nYH_2O$$

$$nXH_3PO_4 + nXOH^- \longrightarrow nXH_2PO_4^- + nXH_2O$$

$$2nH_3PO_4 + nYCO_3^{2-} + nXOH^- \longrightarrow 2nH_2PO_4^- + nYCO_2 + n(X + Y)H_2O$$

The precipitate composition is assumes to be of the type: $Ni(OH)_X(CO_3)_Y$, with thus the electroneutrality relationship:

$$X + 2Y = 2$$

The procedure below has been followed and gives relatively reproductive results:

- Dry some pellets (EcoTherm 24h, 150°C), and weight 0.5g exactly for 3 samples, Med_i
- Pour each sample in a clean dry beaker, then weight exactly, $Mebd_i$
- Take 3ml of phosphoric acid in a syringe, and weight the whole accurately, Msd_i
- Drop exactly 200ml of distilled water in each beaker
- Drop the phosphorus acid in the beaker, and weight exactly the syringe afterwards, Msf_i. The dissolution is made in large excess of acid.
- Knowing the density of the acid, we have the exact volume dropped in each beaker: Va_i

$$Va_i = \frac{Ma_i}{d_{H_3PO_4}}$$

As the pellets dissolve, the carbon dioxide escapes as a gas, and some bubbles are released in the atmosphere.

- When the dissolving is total, and the solution homogeneous, draw 2 samples of 20ml of the concentrated solution for AA analysis, on the total nickel concentration (further dilution of the samples is possible to facilitate the AA analysis).
- Draw 2 times 5ml of the solution (for each sample) and titrate the excess of phosphoric acid with a standard 0.1M OH^- solution. The pH indicator used is a mix of phenolphthalein (2parts) and 1-naphtolphtalein (1part) which changes from pale rose through green to violet at pH 9.6 (Jeffery, 1989), corresponding to the second equivalent point of the phosphoric acid. The volume of OH^- drop to the equivalent point are averaged Veq_i. The number of mole of phosphoric acid present in the sample is then determined by:

$$n_{H_3PO_4} = \frac{C_{OH^-} Veq_i}{2} \times \frac{200 + Va_i}{5}$$

As the change of colour of the precipitate is not instantaneous and subject to eyes perception errors, the accuracy of this titration technique is relatively low. When estimating the titration random error to two drops of the hydroxide solution, the standard error increases up to 15% of the nickel concentration measured.

- The sand left over is then rinsed 3 times with distilled water, filtrated (0.45µm membrane), and dried (EcoTherm 24h, 150°C). When dry, the sand is weighted accurately, Mef_i, and the exact mass of precipitate originally present on the pellet can be calculated:

$$Mpptt_i = Med_i - Mef_i$$

Making the assumption that the precipitate is pure (containing n moles of Ni, X moles of OH^-, and Y moles of CO_3^{2-}, and using the previous relationships, the system of equations can be drawn:

$$Mpptt_i = n \times M_{Ni} + n \times X \times M_{OH^-} + n \times Y \times M_{CO_3^{2-}}$$
$$2n = n_{H_3PO_4\_init} - n_{H_3PO_4}$$
$$X + 2Y = 2$$

With: M_{Ni} = 58.7g/mol; M_{CO3} = 60.01g/mol; M_{OH} = 17.01g/mol.

As we know the amount of nickel in the sample, the amount of phosphorus acid consumed in the reaction, and the total mass of precipitate, this system with 2 unknowns, X and Y can be resolved easily, giving the composition of the precipitate (see calculations).

[H3PO4] molar (mol/l)	15.40	(mol/kg) 9.01
[NaOH] (mol/l)	0.1095	

	Sample 1	*Sample 2*	*Sample 3*
M syringe full	7.0895	6.7506	7.0023
M syringe empty	1.7368	1.7423	1.8133
M H3PO4 injected	5.3527	5.0083	5.189
V H3PO4 injected	0.03130234	0.0292883	0.03034503
Nb moles H3PO4 injected (=p)	0.48218947	0.45116475	0.46744282
M beaker	100.4001	101.1692	98.9202
M beaker+sample	103.0095	104.4577	102.219
M sample	2.6094	3.2885	3.2988
Dilution (de-ionized water) (ml)	200	200	200
Sample for titration (ml)	5	5	5
Dilution for titration (ml)	50	50	50
Titration equivalent 1 (ml)	21.3	19.85	20.55
Titration equivalent 2 (ml)	21.25	19.9	20.6
Average (ml)	21.275	19.875	20.575
CbVb	0.0233	0.0218	0.0225
Nb moles H3PO4 in sample	0.01164806	0.01088156	0.01126481
Nb moles H3PO4 post react	0.47321473	0.44163655	0.45742912
Nb moles H3PO4 consummed	0.0090	0.0095	0.0100
nNi	0.0045	0.0048	0.0050

Mass dry filter	0.0927	0.093	0.0931
Mass dry filter+sand	2.211	2.8523	2.8398
Mass sand	2.1183	2.7593	2.7467
Masse precipitate g	0.4911	0.5292	0.5521
Precipitate Mass % sample	18.8	16.1	16.7

Ni AA analysis (sample number)	Ni comp 2	Ni comp 3	Ni comp 4
Ni AA analysis ([C]ppm)	0.96384	1.13186	1.09862
Ni mass in sample (mg)	1.93E-01	2.26E-01	2.20E-01
Ni moles in sample (moles)	3.28E-03	3.86E-03	3.74E-03

NB: all masses in g

The general chemical formula of the precipitate is assumed to be: $Ni(OH)_X(CO_3)_Y$

X	0.71	0.59	0.65
Y	0.64	0.71	0.68

Table A6.1: Calculation of the nickel hydroxy-carbonate pellets composition

Appendix 7: XRD, XRF and SEM analysis of the precipitate and raw sand

[A N A L Y S I S R E P O R T]

GENERAL CONDITIONS

Result File	: DAMIEN_PELLETS
File Version	: 1
Background Method	: Fit
Decon Method	: Gaussian
Decon ChiSquared	: 1.53
Analysis Date	: 10-NOV-2000
Microscope	: SEM
Comments	:

ANALYSIS CONDITIONS

Quant. Method	: XPP/ASAP
Acquire Time	: 100 secs
Normalization Factor	: 100.0

SAMPLE CONDITIONS

kV	: 15.0
Beam Current	: 2000.0 picoAmps
Working Distance	: 25.0 mm
Tilt Angle	: 0.0 Degrees
TakeOff Angle	: 35.0 Degrees
Solid Angle*BeamCurrent	: 12.2

Element	Line	Weight%	Error	K-Ratio	Atomic%
C	Ka	44.87	1.695	0.1504	67.63
O	Ka	18.21	0.237	0.0517	20.61
Si	Ka	0.40	0.014	0.0027	0.26
S	Ka	0.65	0.017	0.0053	0.37
Ca	Ka	0.46	0.017	0.0042	0.21
Ni	Ka	35.41	0.316	0.2925	10.92
Total		100.00			

} → 99,11 % des métaux.

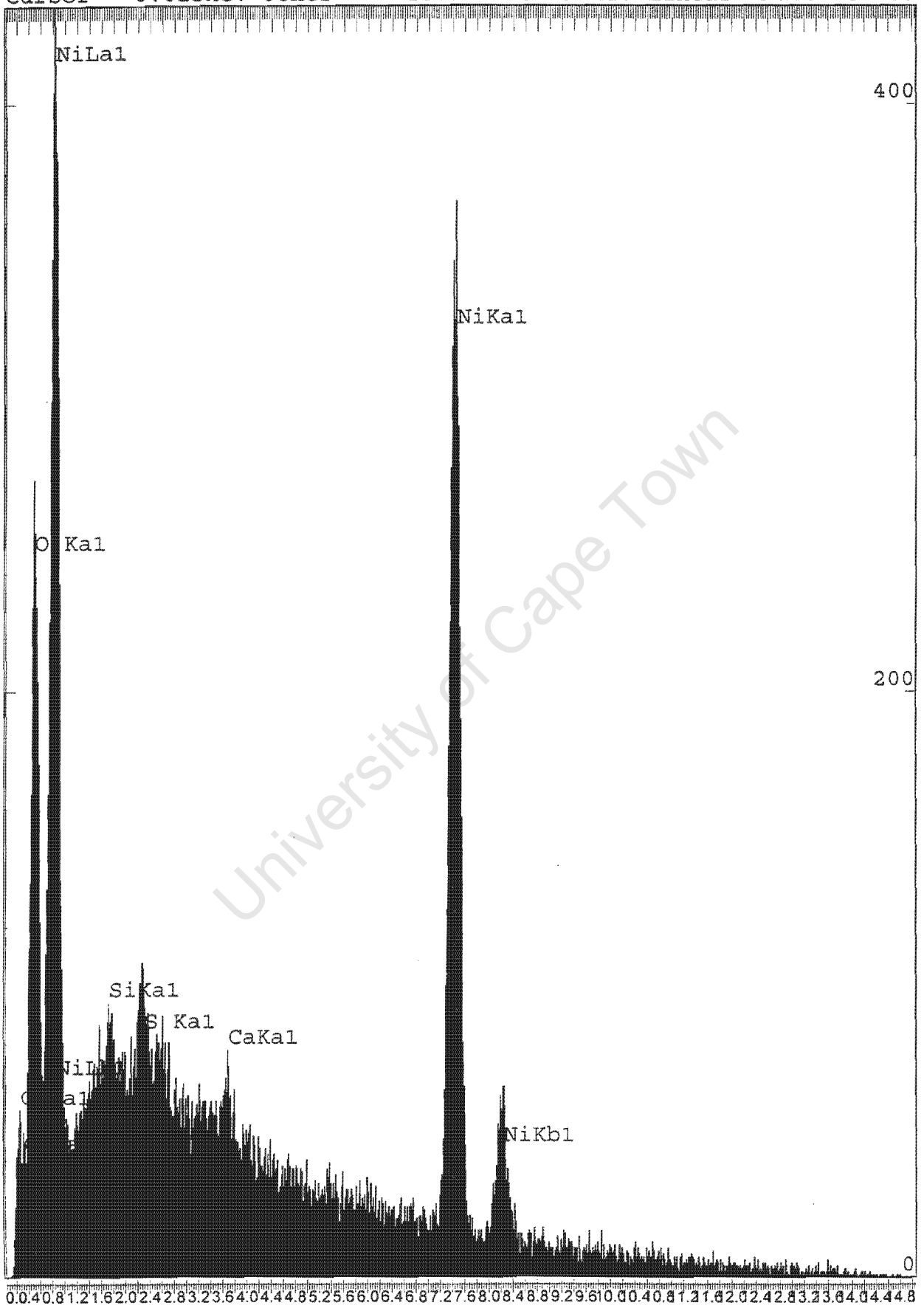

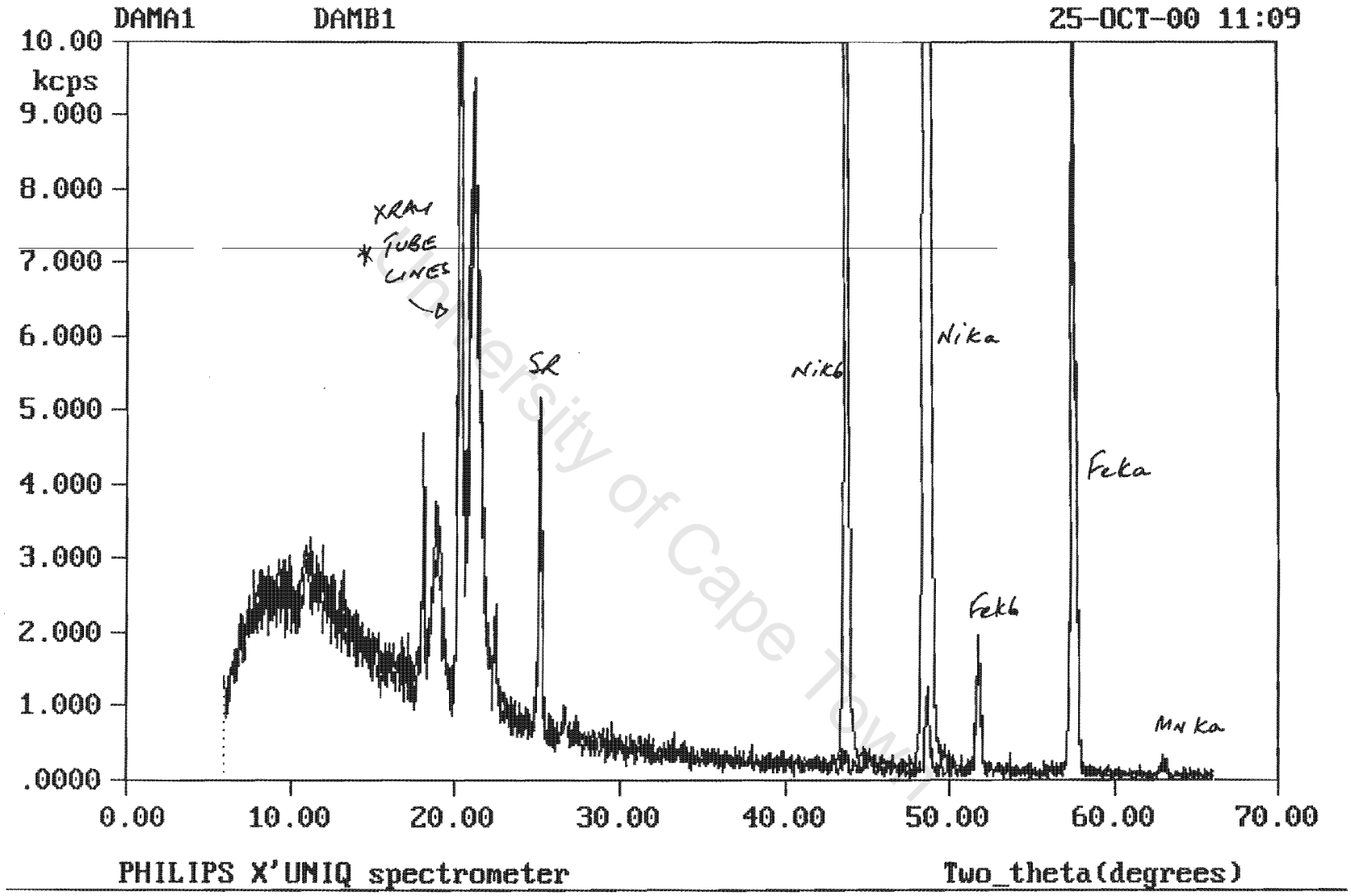

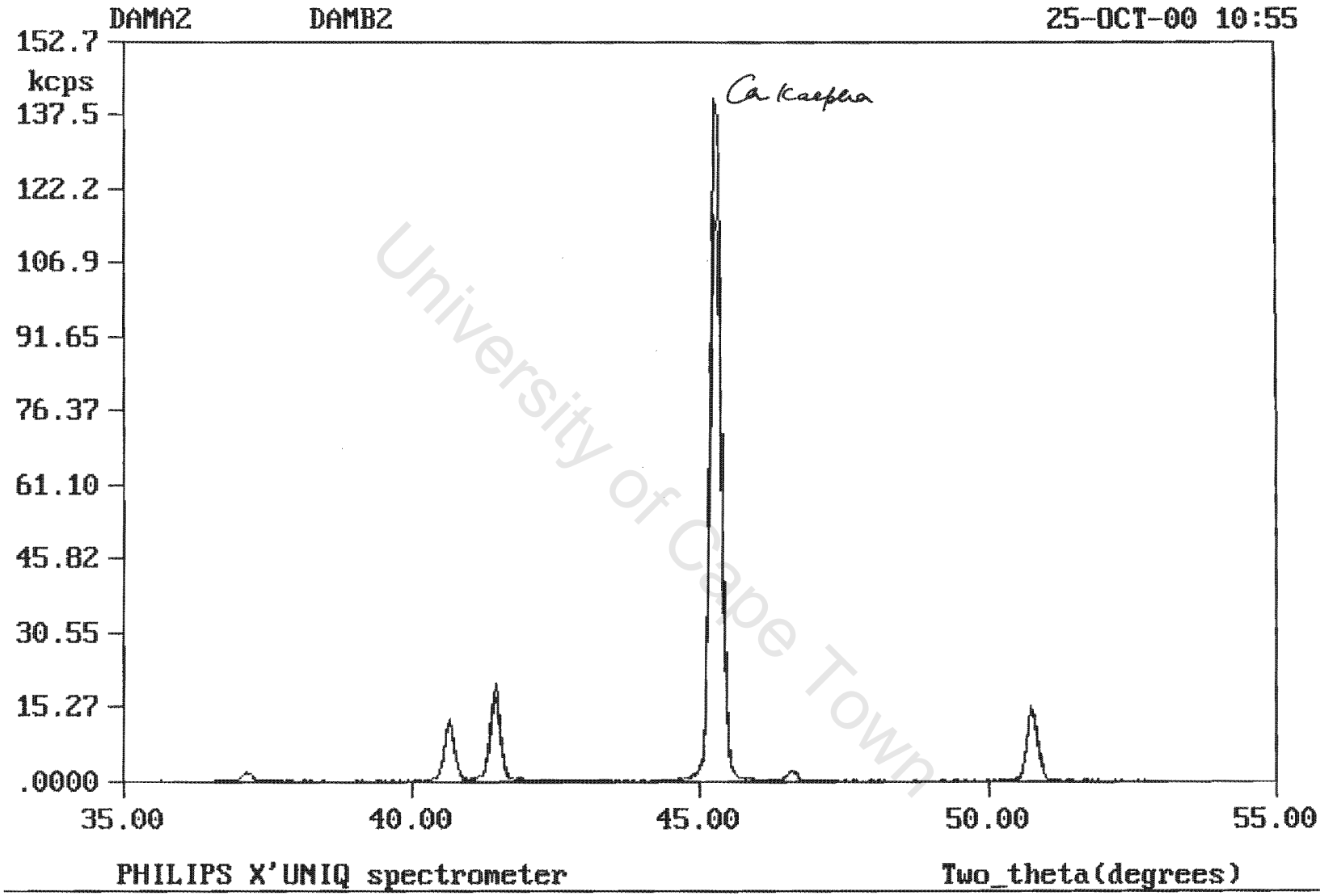

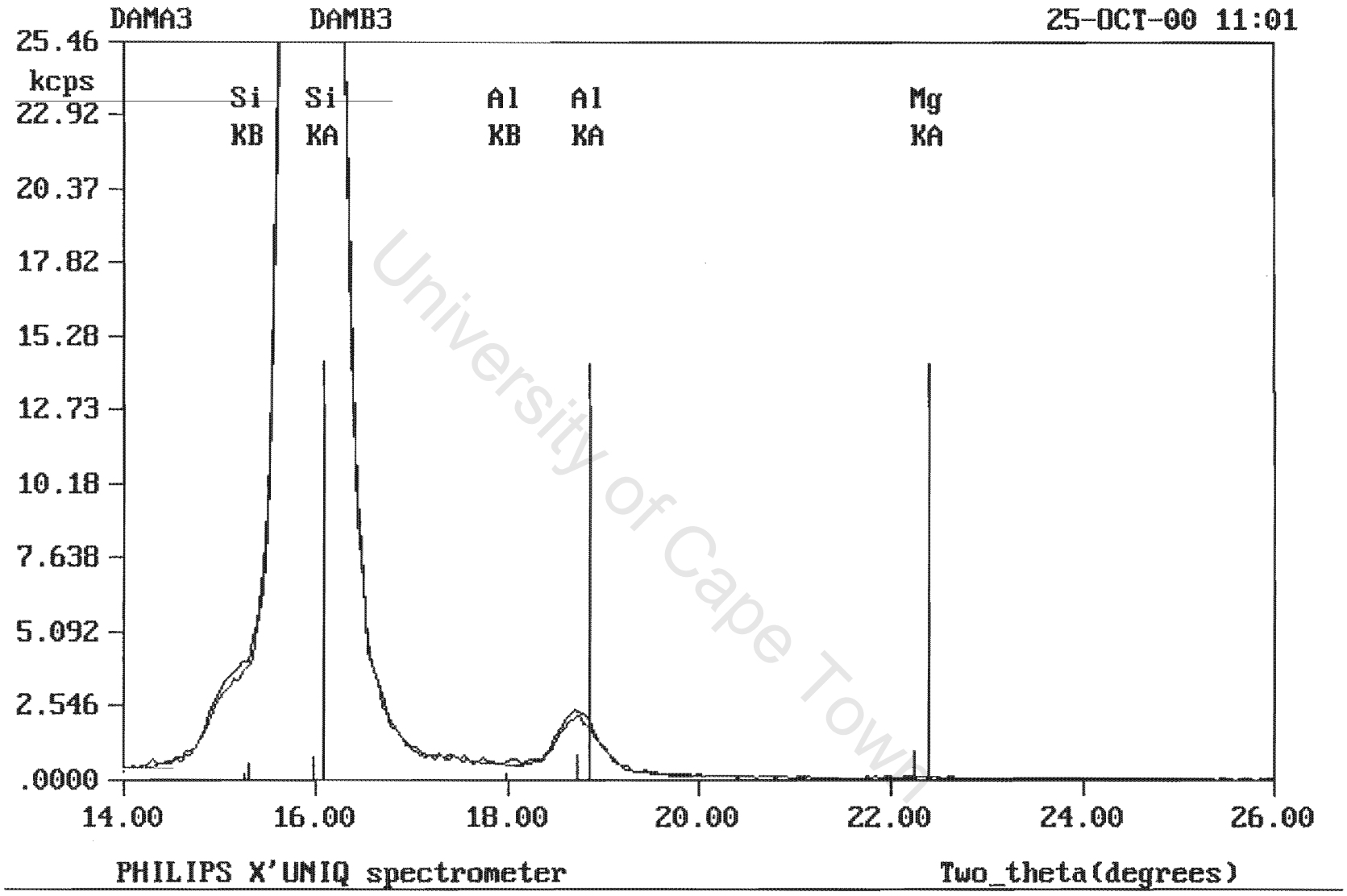

Original scan: Ni-carbonate Date: 26/10/2000 14:24
Description of scan:

Used wavelength: K-Alpha

K-Alpha1 wavelength (Å):	1.54056
K-Alpha2 wavelength (Å):	1.54439
K-Alpha2/K-Alpha1 intensity ratio :	0.50000
K-Alpha wavelength (Å):	1.54056
K-Beta wavelength (Å):	1.39222

d-spacing (Å)	Relative Intensity (%)
10.14042	0.90
7.28909	0.87
4.26114	15.38
3.86099	2.06
3.78639	2.22
3.35033	100.00
3.24348	19.20
3.03852	26.69
2.87400	3.26
2.70706	18.69
2.49293	11.20
2.45652	7.84
2.37750	10.12
2.33843	6.63
2.28402	10.29
2.23905	5.62
2.19358	3.73
2.12888	7.81
2.09520	6.76
1.97975	12.19
1.91331	7.97
1.87789	9.83
1.81859	15.59
1.74558	9.09
1.72733	4.57
1.67288	4.97
1.62432	1.65
1.60388	3.11
1.54204	11.50
1.52235	5.40
1.46693	2.72
1.45387	2.53
1.43858	1.99
1.41426	2.75
1.38294	6.28
1.37318	9.33
1.36058	1.65

d-spacing (Å)	Relative Intensity (%)
1.29740	0.63
1.28799	1.35

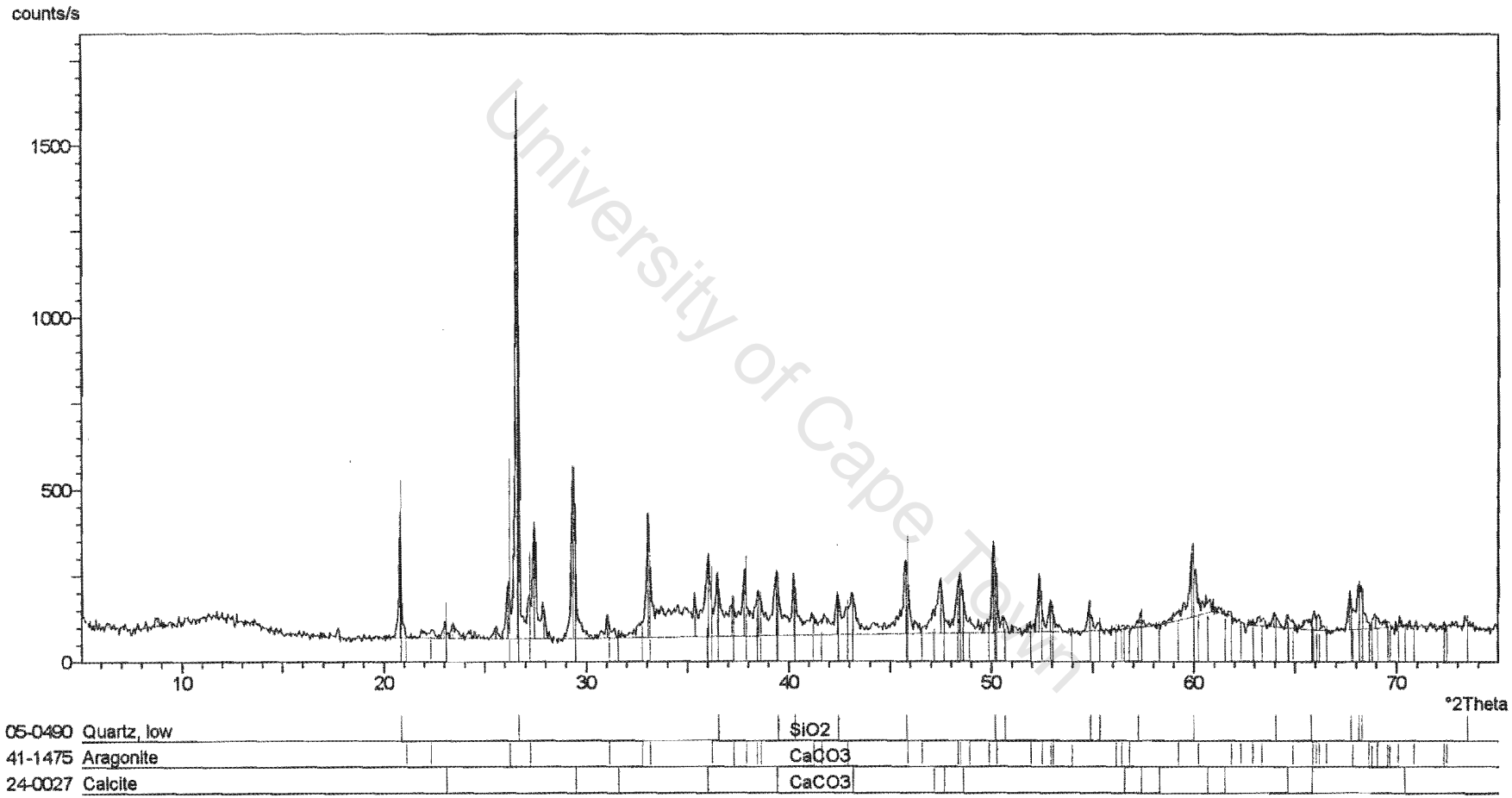

Appendix 8: Variance analysis, First order model

Nickel dissolved out

Second experiment

Source of variation	DF	SS	MS	F
Model	5	17.79018		
(residual	15	6.67495)		
Quadratic	1	0.45441	0.45441	10.66
Other 2nd order	10	6.03472	0.60347	14.39
Pure error	4	0.18492	0.04263	
Total	20	24.46423		

Combined experiments

Source of variation	DF	SS	MS	F
Model	5	33.96149		
(residual	35	12.30713		
Quadratic	1	1.05797	1.05797	28.1
Other 2nd order	26	10.948	0.42108	11.19
Pure error	8	0.30116	0.03764	
Total	40	46.26862		

Combined experiments when MF = 1

Source of variation	DF	SS	MS	F
Model	4	18.69785		
(residual	20	5.91133)		
Quadratic	1	1.07883	1.07883	28.66
Other 2nd order	11	4.53134	0.41194	10.94
Pure error	8	0.30116	0.03764	
Total	24	24.60918		

Combined experiments when MF = 3

Source of variation	DF	SS	MS	F
Model	4	16.27843		
(residual	20	6.31837)		
Quadratic	1	0.67925	0.67925	18.05
Other 2nd order	11	5.33796	0.48527	12.89
Pure error	8	0.30116	0.03764	
Total	24	22.5968		

Nickel total out

Second experiment

Source of variation	DF	SS	MS	F
Model	5	1808.54905		
(residual	15	1548.22141		
Quadratic	1	93.73928	93.73938	21.48
Other 2nd order	10	1437.0283	143.70283	32.93
Pure error	4	17.45308	4.36327	
Total	20	3356.77046		

Combined experiments

Source of variation	DF	SS	MS	F
Model	5	2481.20872		
(residual	35	2344.63186)		
Quadratic	1	194.73562	194.73562	23.07
Other 2nd order	26	2082.3794	80.09151	9.49
Pure error	8	67.51682	8.4396	
Total	40	4825.84058		

Combined experiments when MF = 1

Source of variation	DF	SS	MS	F
Model	4	1228.70538		
(residual	20	1152.04920)		
Quadratic	1	150.54884	150.54884	17.84
Other 2nd order	11	933.95354	84.90487	10.06
Pure error	8	67.51682	8.4396	
Total	24	2380.75458		

Combined experiments when MF = 3

Source of variation	DF	SS	MS	F
Model	4	1362.81658		
(residual	20	1273.93883)		
Quadratic	1	169.08671	169.08671	20.03
Other 2nd order	11	1037.3353	94.30321	11.17
Pure error	8	67.51682	8.4396	
Total	24	2636.7554		

Appendix 9: Variance and ridge analyses, second order model

esponse Surface for Variable NITOTOUT

esponse Mean	8.458727
oot MSE	5.049431
-Square	0.8285
oef. of Variation	59.6949

egression	Degrees of Freedom	Type I Sum of Squares	R-Square	F-Ratio	Prob > F
inear	5	2475.884985	0.4898	19.421	0.0000
uadratic	5	365.475588	0.0723	2.867	0.0290
rossproduct	10	1347.111931	0.2665	5.283	0.0001
otal Regress	20	4188.472505	0.8285	8.214	0.0000

esidual	Degrees of Freedom	Sum of Squares	Mean Square	F-Ratio	Prob > F
ack of Fit	22	797.153814	36.234264	6.235	0.0011
ure Error	12	69.735692	5.811308		
otal Error	34	866.889506	25.496750		

arameter	Degrees of Freedom	Parameter Estimate	Standard Error	T for H0: Parameter=0	Prob > |T|
NTERCEPT	1	191.552400	1272.203728	0.151	0.8812
H	1	-42.758919	256.714671	-0.167	0.8687
ATIO	1	35.568621	14.065368	2.529	0.0163
R	1	-0.560117	1.209602	-0.463	0.6463
F	1	-2.563866	22.236285	-0.115	0.9089
IFEED	1	-0.708747	0.444726	-1.594	0.1203
H*PH	1	2.544243	12.830155	0.198	0.8440
ATIO*PH	1	-3.893750	1.190162	-3.272	0.0025
ATIO*RATIO	1	1.156027	1.425573	0.811	0.4231
R*PH	1	0.010719	0.089262	0.120	0.9051
R*RATIO	1	0.017323	0.029754	0.582	0.5643
R*RR	1	0.001853	0.008019	0.231	0.8187
F*PH	1	-0.434375	1.785243	-0.243	0.8092
F*RATIO	1	-0.475625	0.595081	-0.799	0.4297
F*RR	1	0.083891	0.044631	1.880	0.0687
F*MF	1	1.156061	3.207539	0.360	0.7208
IFEED*PH	1	0.090913	0.035705	2.546	0.0156
IFEED*RATIO	1	-0.065846	0.011902	-5.533	0.0000
IFEED*RR	1	0.000513	0.000893	0.575	0.5694
IFEED*MF	1	-0.006306	0.017852	-0.353	0.7261
IFEED*NIFEED	1	0.000194	0.001283	0.152	0.8804

arameter	Parameter Estimate from Coded Data
NTERCEPT	4.984358
H	3.575000
ATIO	-6.387647
R	-0.105882
F	0.091471
IFEED	4.383824
H*PH	0.636061
ATIO*PH	-2.920313
ATIO*RATIO	2.601061
R*PH	0.107188
R*RATIO	0.519688
R*RR	0.741061
F*PH	-0.217187
F*RATIO	-0.713437
F*RR	1.677812
F*MF	1.156061
IFEED*PH	2.272813
IFEED*RATIO	-4.938438
IFEED*RR	0.512813
IFEED*MF	-0.315313
IFEED*NIFEED	0.486061

actor	Degrees of Freedom	Sum of Squares	Mean Square	F-Ratio	Prob > F
H	6	875.625837	145.937639	5.724	0.0003
ATIO	6	2482.290333	413.715056	16.226	0.0000
R	6	109.249209	18.208201	0.714	0.6407
F	6	114.657052	19.109509	0.749	0.6141
IFEED	6	1611.314078	268.552346	10.533	0.0000

anonical Analysis of Response Surface
based on coded data)

actor	Critical Value Coded	Uncoded
H	-0.049707	9.975146
ATIO	0.693199	3.539799
R	-0.305746	43.885090
F	0.308269	2.308269
IFEED	-0.610558	69.472096

redicted value at stationary point 1.373546

Eigenvalues	Eigenvectors PH	RATIO	RR	MF	NIFEED
5.014336	0.387316	-0.765146	-0.003405	0.038142	0.512905
1.815638	-0.057113	-0.004017	0.609265	0.790701	-0.017619
0.338556	0.370732	0.286838	0.698694	-0.505896	0.190206
-0.232177	0.840031	0.262723	-0.283006	0.274180	-0.264684
-1.316050	-0.060248	0.513066	-0.246007	0.205504	0.793966

tationary point is a saddle point.

stimated Ridge of Minimum Response for Variable NITOTOUT

Coded adius	Estimated Response	Standard Error
0.0	4.984358	1.148756
0.1	4.181053	1.149740
0.2	3.477780	1.154231
0.3	2.874416	1.166602
0.4	2.370740	1.193210
0.5	1.966292	1.240306
0.6	1.659872	1.308557
0.7	1.441715	1.404628
0.8	1.236157	1.794741
0.9	1.006904	2.296255
1.0	0.752132	2.848185

Coded adius	Uncoded Factor Values PH	RATIO	RR	MF	NIFEED
0.0	10.000000	2.500000	50.000000	2.000000	100.000000
0.1	9.978847	2.611930	50.025884	1.999153	97.431114
0.2	9.957156	2.722925	50.054179	1.998828	94.861431
0.3	9.934639	2.832431	50.085508	1.999155	92.290052
0.4	9.910755	2.939321	50.121362	2.000268	89.713414
0.5	9.884372	3.040855	50.167416	2.002149	87.112489
0.6	9.852826	3.126885	50.261442	2.003303	84.306217
0.7	9.825555	3.055245	51.138445	1.970904	76.168939
0.8	9.829581	2.878872	52.294938	1.922902	66.799055
0.9	9.833892	2.751363	53.116735	1.888646	60.160775
1.0	9.837855	2.641417	53.822919	1.859184	54.459336

esponse Surface for Variable NIDISOUT

esponse Mean	1.171455
oot MSE	0.440164
-Square	0.8711
oef. of Variation	37.5742

egression	Degrees of Freedom	Type I Sum of Squares	R-Square	F-Ratio	Prob > F
inear	5	36.831765	0.7208	38.021	0.0000
uadratic	5	2.481022	0.0486	2.561	0.0453
rossproduct	10	5.196581	0.1017	2.682	0.0155
otal Regress	20	44.509368	0.8711	11.487	0.0000

esidual	Degrees of Freedom	Sum of Squares	Mean Square	F-Ratio	Prob > F
ack of Fit	22	6.090993	0.276863	6.694	0.0008
ure Error	12	0.496323	0.041360		
otal Error	34	6.587316	0.193745		

arameter	Degrees of Freedom	Parameter Estimate	Standard Error	T for H0: Parameter=0	Prob > |T|
NTERCEPT	1	274.038482	110.899357	2.471	0.0186
H	1	-54.414747	22.378092	-2.432	0.0205
ATIO	1	1.743340	1.226093	1.422	0.1642
R	1	0.021526	0.105442	0.204	0.8395
F	1	-0.016769	1.938361	-0.0087	0.9931
IFEED	1	0.111287	0.038767	2.871	0.0070
H*PH	1	2.681521	1.118418	2.398	0.0221
ATIO*PH	1	-0.112083	0.103748	-1.080	0.2876
ATIO*RATIO	1	-0.079831	0.124269	-0.642	0.5249
R*PH	1	0.003594	0.007781	0.462	0.6471
R*RATIO	1	-0.001990	0.002594	-0.767	0.4483
R*RR	1	-0.000512	0.000699	-0.732	0.4693
F*PH	1	0.049375	0.155622	0.317	0.7530
F*RATIO	1	-0.055625	0.051874	-1.072	0.2911
F*RR	1	0.008078	0.003891	2.076	0.0455
F*MF	1	-0.189620	0.279605	-0.678	0.5023
IFEED*PH	1	-0.011462	0.003112	-3.683	0.0008
IFEED*RATIO	1	0.000421	0.001037	0.406	0.6876
IFEED*RR	1	-0.000183	0.000077811	-2.357	0.0243
IFEED*MF	1	-0.000119	0.001556	-0.0763	0.9396
IFEED*NIFEED	1	0.000096152	0.000112	0.860	0.3960

arameter	Parameter Estimate from Coded Data
NTERCEPT	0.963188
H	-0.966176
ATIO	0.082059
R	-0.017059
F	-0.028529
IFEED	0.376765
H*PH	0.670380
ATIO*PH	-0.084063
ATIO*RATIO	-0.179620
R*PH	0.035937
R*RATIO	-0.059688
R*RR	-0.204620
F*PH	0.024688
F*RATIO	-0.083437
F*RR	0.161563
F*MF	-0.189620
IFEED*PH	-0.286563
IFEED*RATIO	0.031563
IFEED*RR	-0.183438
IFEED*MF	-0.005937
IFEED*NIFEED	0.240380

actor	Degrees of Freedom	Sum of Squares	Mean Square	F-Ratio	Prob > F
H	6	35.767373	5.961229	30.768	0.0000
ATIO	6	0.903687	0.150615	0.777	0.5933
R	6	2.181043	0.363507	1.876	0.1137
F	6	1.195467	0.199245	1.028	0.4240
IFEED	6	8.707117	1.451186	7.490	0.0000

anonical Analysis of Response Surface
based on coded data)

Factor	Critical Value Coded	Uncoded
H	0.644771	10.322385
ATIO	0.007565	2.511348
R	0.180548	53.610955
F	0.047170	2.047170
IFEED	-0.330387	83.480637

redicted value at stationary point 0.587566

Eigenvalues	Eigenvectors PH	RATIO	RR	MF	NIFEED
0.718634	0.951841	-0.052438	0.051545	0.020900	-0.296910
0.213964	0.303299	0.024367	-0.200342	-0.040187	0.930411
-0.098674	-0.020343	-0.497963	0.515569	0.678388	0.159990
-0.209720	0.038252	0.863481	0.354524	0.352223	0.056468
-0.287303	0.011471	-0.055583	0.752135	-0.643177	0.131890

tationary point is a saddle point.

Appendix 10: 2nd order model including influence of temperature

esponse Surface for Variable NITOTOUT

esponse Mean	8.458727
oot MSE	5.102717
-Square	0.8300
oef. of Variation	60.3249

egression	Degrees of Freedom	Type I Sum of Squares	R-Square	F-Ratio	Prob > F
ovariates	1	27.556416	0.0055	1.058	0.3111
inear	5	2462.895873	0.4872	18.918	0.0000
uadratic	5	352.747666	0.0698	2.710	0.0370
rossproduct	10	1352.917215	0.2676	5.196	0.0001
otal Regress	21	4196.117169	0.8300	7.674	0.0000

esidual	Degrees of Freedom	Sum of Squares	Mean Square
otal Error	33	859.244842	26.037722

arameter	Degrees of Freedom	Parameter Estimate	Standard Error	T for H0: Parameter=0	Prob > |T|
NTERCEPT	1	101.005096	1296.444267	0.0779	0.9384
H	1	-21.589581	262.349122	-0.0823	0.9349
ATIO	1	36.248899	14.269139	2.540	0.0160
R	1	-0.834948	1.323421	-0.631	0.5325
F	1	-5.663517	23.187660	-0.244	0.8086
IFEED	1	-0.698643	0.449806	-1.553	0.1299
H*PH	1	1.438322	13.125215	0.110	0.9134
ATIO*PH	1	-3.926730	1.204261	-3.261	0.0026
ATIO*RATIO	1	1.043807	1.455428	0.717	0.4783
R*PH	1	0.025035	0.093994	0.266	0.7916
R*RATIO	1	0.019497	0.030334	0.643	0.5248
R*RR	1	0.003050	0.008400	0.363	0.7188
F*PH	1	-0.324940	1.815353	-0.179	0.8590
F*RATIO	1	-0.415161	0.611627	-0.679	0.5020
F*RR	1	0.087976	0.045728	1.924	0.0630
F*MF	1	1.551182	3.322400	0.467	0.6436
IFEED*PH	1	0.090343	0.036097	2.503	0.0175
IFEED*RATIO	1	-0.065796	0.012028	-5.470	0.0000
IFEED*RR	1	0.000487	0.000903	0.539	0.5937
IFEED*MF	1	-0.005901	0.018056	-0.327	0.7459
IFEED*NIFEED	1	0.000165	0.001298	0.127	0.8994
EMP	1	-0.239858	0.442666	-0.542	0.5916

arameter	Parameter Estimate from Coded Data
NTERCEPT	10.789160
H	3.498104
ATIO	-6.351668
R	-0.124224
F	0.062547
IFEED	4.294935
H*PH	0.359581
ATIO*PH	-2.945048
ATIO*RATIO	2.348566
R*PH	0.250353
R*RATIO	0.584899
R*RR	1.220132
F*PH	-0.162470
F*RATIO	-0.622741
F*RR	1.759514
F*MF	1.551182
IFEED*PH	2.258571
IFEED*RATIO	-4.934690
IFEED*RR	0.486578
IFEED*MF	-0.295075
IFEED*NIFEED	0.413460
EMP	-0.239858

actor	Degrees of Freedom	Sum of Squares	Mean Square	F-Ratio	Prob > F
H	6	854.074424	142.345737	5.467	0.0005
ATIO	6	2457.583274	409.597212	15.731	0.0000
R	6	116.746621	19.457770	0.747	0.6158
F	6	119.557260	19.926210	0.765	0.6024
IFEED	6	1551.157542	258.526257	9.929	0.0000

anonical Analysis of Response Surface
based on coded data)

actor	Critical Value Coded	Uncoded
H	-0.100657	9.949671
ATIO	0.715561	3.573342
R	-0.073258	48.534842
F	0.105729	2.105729
IFEED	-0.567986	71.600715

redicted value at stationary point 1.155398

Eigenvalues	Eigenvectors PH	RATIO	RR	MF	NIFEED
4.809069	0.383529	-0.759817	-0.003644	0.038363	0.523545
2.279020	-0.013671	0.020257	0.639471	0.768326	-0.012435
0.654530	0.202069	0.184046	0.728642	-0.604972	0.168477
-0.459616	0.899972	0.309243	-0.161365	0.138573	-0.221760
-1.390082	-0.044008	0.541076	-0.184678	0.151688	0.805099

tationary point is a saddle point.

stimated Ridge of Minimum Response for Variable NITOTOUT

Coded adius	Estimated Response	Standard Error
0.0	4.815830	1.201821
0.1	4.020927	1.198890
0.2	3.321935	1.201476
0.3	2.718716	1.214027
0.4	2.210998	1.243640
0.5	1.798137	1.299427
0.6	1.477957	1.398110
0.7	1.233826	1.651982
0.8	1.001437	2.009546
0.9	0.748175	2.341029
1.0	0.469532	2.668797

Coded adius	Uncoded Factor Values PH	RATIO	RR	MF	NIFEED
0.0	10.000000	2.500000	50.000000	2.000000	100.000000
0.1	9.979033	2.612924	50.030148	1.999485	97.464505
0.2	9.957495	2.725584	50.061403	1.999500	94.963474
0.3	9.935057	2.837903	50.092959	2.000200	92.523043
0.4	9.911082	2.949868	50.122551	2.001830	90.203855
0.5	9.884169	3.062087	50.142299	2.004887	88.184763
0.6	9.850946	3.181511	50.104180	2.011402	87.296828
0.7	9.816130	3.362988	49.610756	2.035669	92.564207
0.8	9.803782	3.537358	48.880894	2.066457	100.662419
0.9	9.797659	3.671603	48.289268	2.091002	107.170353
1.0	9.793189	3.788154	47.768780	2.112505	112.877115

esponse Surface for Variable NIDISOUT

esponse Mean	1.171455
oot MSE	0.446565
-Square	0.8712
oef. of Variation	38.1206

egression	Degrees of Freedom	Type I Sum of Squares	R-Square	F-Ratio	Prob > F
ovariates	1	0.638837	0.0125	3.203	0.0827
inear	5	36.321039	0.7108	36.427	0.0000
uadratic	5	2.430057	0.0476	2.437	0.0550
rossproduct	10	5.125877	0.1003	2.570	0.0201
otal Regress	21	44.515810	0.8712	10.630	0.0000

esidual	Degrees of Freedom	Sum of Squares	Mean Square
otal Error	33	6.580874	0.199420

arameter	Degrees of Freedom	Parameter Estimate	Standard Error	T for H0: Parameter=0	Prob > |T|
NTERCEPT	1	276.666935	113.458534	2.438	0.0203
H	1	-55.029262	22.959527	-2.397	0.0224
ATIO	1	1.723593	1.248766	1.380	0.1768
R	1	0.029504	0.115819	0.255	0.8005
?	1	0.073209	2.029272	0.0361	0.9714
IFEED	1	0.110994	0.039365	2.820	0.0081
H*PH	1	2.713624	1.148655	2.362	0.0242
ATIO*PH	1	-0.111126	0.105391	-1.054	0.2994
ATIO*RATIO	1	-0.076573	0.127372	-0.601	0.5518
R*PH	1	0.003178	0.008226	0.386	0.7017
R*RATIO	1	-0.002053	0.002655	-0.773	0.4449
R*RR	1	-0.000546	0.000735	-0.743	0.4626
?*PH	1	0.046198	0.158871	0.291	0.7730
?*RATIO	1	-0.057380	0.053527	-1.072	0.2915
?*RR	1	0.007960	0.004002	1.989	0.0551
?*MF	1	-0.201090	0.290760	-0.692	0.4940
IFEED*PH	1	-0.011446	0.003159	-3.623	0.0010
IFEED*RATIO	1	0.000419	0.001053	0.398	0.6929
IFEED*RR	1	-0.000183	0.000079056	-2.311	0.0272
IFEED*MF	1	-0.000130	0.001580	-0.0826	0.9347
IFEED*NIFEED	1	0.000096995	0.000114	0.854	0.3992
EMP	1	0.006963	0.038740	0.180	0.8585

arameter	Parameter Estimate from Coded Data
NTERCEPT	0.794684
H	-0.963944
ATIO	0.081014
R	-0.016526
F	-0.027690
IFEED	0.379345
H*PH	0.678406
ATIO*PH	-0.083344
ATIO*RATIO	-0.172290
R*PH	0.031782
R*RATIO	-0.061580
R*RR	-0.218527
F*PH	0.023099
F*RATIO	-0.086070
F*RR	0.159191
F*MF	-0.201090
IFEED*PH	-0.286149
IFEED*RATIO	0.031454
IFEED*RR	-0.182676
IFEED*MF	-0.006525
IFEED*NIFEED	0.242488
EMP	0.006963

actor	Degrees of Freedom	Sum of Squares	Mean Square	F-Ratio	Prob > F
H	6	34.950535	5.825089	29.210	0.0000
ATIO	6	0.907815	0.151303	0.759	0.6073
R	6	2.147782	0.357964	1.795	0.1306
F	6	1.192586	0.198764	0.997	0.4439
IFEED	6	8.656301	1.442717	7.235	0.0001

anonical Analysis of Response Surface
based on coded data)

actor	Critical Value Coded	Uncoded
H	0.633603	10.316801
ATIO	0.011889	2.517834
R	0.164504	53.290072
F	0.035736	2.035736
IFEED	-0.346677	82.666128

redicted value at stationary point 0.595574

Eigenvalues	Eigenvectors PH	RATIO	RR	MF	NIFEED
0.725698	0.953278	-0.051938	0.047727	0.019422	-0.293101
0.216227	0.298822	0.025382	-0.194016	-0.038648	0.933234
-0.104249	-0.022603	-0.576147	0.480776	0.643464	0.149506
-0.210037	0.036155	0.814135	0.389959	0.423788	0.064902
-0.298652	0.012175	-0.043552	0.759518	-0.635992	0.128848

tationary point is a saddle point.

stimated Ridge of Minimum Response for Variable NIDISOUT

Coded adius	Estimated Response	Standard Error
0.0	0.968081	0.105178
0.1	0.871321	0.105556
0.2	0.788903	0.106650
0.3	0.720665	0.109285
0.4	0.666062	0.114209
0.5	0.622250	0.118860
0.6	0.580788	0.119241
0.7	0.535741	0.120603
0.8	0.485600	0.126912
0.9	0.429926	0.140222
1.0	0.368537	0.161191

Coded	Uncoded Factor Values				
adius	PH	RATIO	RR	MF	NIFEED
0.0	10.000000	2.500000	50.000000	2.000000	100.000000
0.1	10.046173	2.487486	50.013620	2.002862	98.133323
0.2	10.091808	2.472436	49.966938	2.006433	96.158393
0.3	10.136390	2.452129	49.777404	2.011973	94.019790
0.4	10.177893	2.419120	49.149607	2.025469	91.625572
0.5	10.206008	2.367678	47.201430	2.075139	89.133092
0.6	10.214377	2.336199	44.534643	2.161366	87.397429
0.7	10.216665	2.324415	42.205565	2.245706	86.191703
0.8	10.217443	2.320185	40.130400	2.324595	85.199699
0.9	10.217656	2.319445	38.204895	2.399718	84.313342
1.0	10.217598	2.320638	36.373834	2.472304	83.488372